TECHNICAL REPORT BRL-TR-3341

BRL

A TWO-DIMENSIONAL MODEL FOR THE COMBUSTION CHAMBER/GUN TUBE OF A CONCEPT VIC REGENERATIVE LIQUID PROPELLANT GUN

TERENCE P. COFFEE

MAY 1992

U.S. ARMY LABORATORY COMMAND

BALLISTIC RESEARCH LABORATORY
ABERDEEN PROVING GROUND, MARYLAND

NOTICES

Destroy this report when it is no longer needed. DO NOT return it to the originator.

Additional copies of this report may be obtained from the National Technical Information Service, U.S. Department of Commerce, 5285 Port Royal Road, Springfield, VA 22161.

The findings of this report are not to be construed as an official Department of the Army position, unless so designated by other authorized documents.

The use of trade names or manufacturers' names in this report does not constitute indorsement of any commercial product.

REPORT DOCUMENTATION PAGE

Form Approved
OMB No. 0704-0188

1. AGENCY USE ONLY (Leave blank)	2. REPORT DATE	3. REPORT TYPE AND DATES COVERED
	May 1992	Final, January 1990 - October 1991

4. TITLE AND SUBTITLE

A Two-Dimensional Model for the Combustion Chamber/Gun Tube of a Concept VIC Regenerative Liquid Propellant Gun

5. FUNDING NUMBERS

PR: 1L162618AH80

DA30 6709

6. AUTHOR(S)

Terence P. Coffee

7. PERFORMING ORGANIZATION NAME(S) AND ADDRESS(ES)

8. PERFORMING ORGANIZATION REPORT NUMBER

9. SPONSORING/MONITORING AGENCY NAME(S) AND ADDRESS(ES)

U.S. Army Ballistic Research Laboratory
ATTN: SLCBR-DD-T
Aberdeen Proving Ground, MD 21005-5066

10. SPONSORING/MONITORING AGENCY REPORT NUMBER

BRL-TR-3341

11. SUPPLEMENTARY NOTES

12a. DISTRIBUTION/AVAILABILITY STATEMENT

Approved for public release; distribution is unlimited.

12b. DISTRIBUTION CODE

13. ABSTRACT *(Maximum 200 words)*

Standard interior ballistics models are generally lumped parameter models. This type of model has proven quite successful in modeling overall behavior in both solid and liquid propellant guns. However, some phenomena of interest cannot be reduced to lumped parameter form. One such phenomenon is high frequency pressure oscillations in liquid propellant guns. Pressure oscillations occur in almost all liquid propellant gun firings, and modeling requires at least a two-dimensional space. There is major uncertainty concerning the cause of these oscillations.

In order to examine this problem, a two-dimensional fluid dynamics model of the combustion chamber and the gun tube of a liquid propellant gun has been developed. The code was run for a variety of test cases and gives reasonable results. Models were implemented with chamber dimensions and injection rates similar to actual Concept VIC guns. Oscillations were created that were very similar in magnitude to the experimental data, although the frequency structure was somewhat simpler. However, frequencies higher than the expected low-order acoustic modes were generated. A discussion is given concerning the causes of the oscillations in the model and the implications for reducing the oscillations in the actual guns.

14. SUBJECT TERMS

computational fluid dynamics, two-dimensional model, liquid gun propellants, regenerative gun, pressure oscillations, fluid dynamics

15. NUMBER OF PAGES

111

16. PRICE CODE

17. SECURITY CLASSIFICATION OF REPORT	18. SECURITY CLASSIFICATION OF THIS PAGE	19. SECURITY CLASSIFICATION OF ABSTRACT	20. LIMITATION OF ABSTRACT
UNCLASSIFIED	UNCLASSIFIED	UNCLASSIFIED	SAR

INTENTIONALLY LEFT BLANK.

TABLE OF CONTENTS

INTENTIONALLY LEFT BLANK.

LIST OF FIGURES

1. INTRODUCTION

Regenerative liquid propellant gun (RLPG) technology is being considered in the development of the next U.S. Army artillery weapon. Test fixtures in 30-mm, 105-mm, and 155-mm sizes have been built and fired. The data from all these fixtures have been extensively analyzed to better understand the RLPG process (Coffee, Wren, and Morrison 1989, 1990; Wren, Coffee, and Morrison 1990; Coffee et al. 1991). Previous reports describe the design of the Concept VIC gun fixtures and the modeling modifications pertinent to this design. Agreement between the interior ballistics simulations and the experimental data is quite good. Details of the lumped parameter gun code used for these past simulations have been described in previous publications (Coffee 1985, 1988; Morrison and Coffee 1990).

A Concept VIC RLPG is shown in Figure 1. An external solid or liquid propellant igniter venting into the combustion chamber initiates the ballistic cycle. The chamber pressure forces both the control and injection pistons rearward. Liquid propellant is then injected from the liquid reservoir through the annulus between the pistons into the combustion chamber where it burns. The motion of the control piston is modulated by the damper assembly.

Almost all firings of liquid propellant guns have shown high frequency oscillations. As an example, Figure 2 shows pressures from shot 65 of a first generation 155-mm Concept VIC regenerative liquid propellant gun. The top figure shows the pressure measured at the combustion chamber wall. The bottom figure (moved down 100 MPa) shows the pressure at a gauge 1.7 m downbore. Note that large pressure oscillations persist for a long distance down the gun tube.

Figure 3 shows the Fourier transforms of the two pressures over a time window from 14 to 15 ms. One would normally expect the frequencies to be near the natural acoustic frequencies of the chamber. However, for such a large chamber, the acoustic frequencies are small (first radial = 4.0 kHz). It is not clear what causes the high frequency oscillations.

The barrel gauge shows frequencies similar to the chamber gauge, although the higher frequencies are missing. Pressure oscillations are driven by the energy released by the

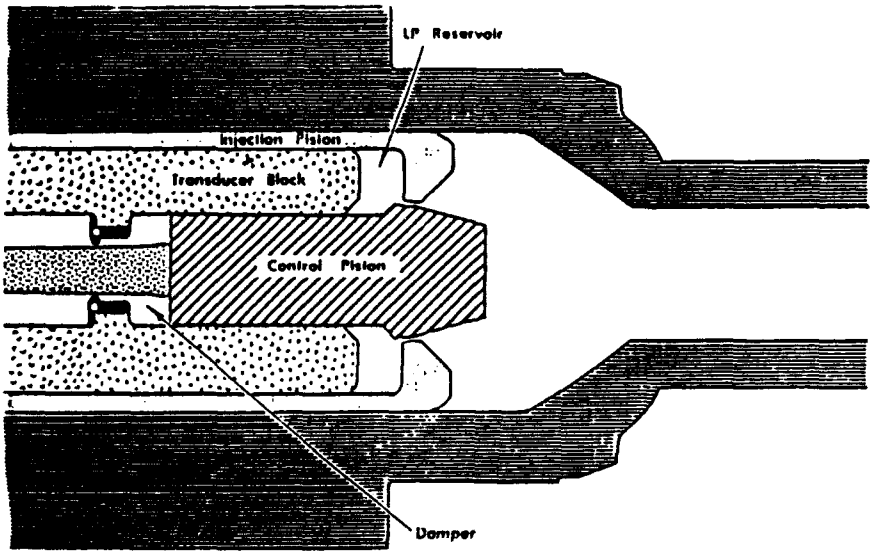

MIDSTROKE POSITION

Figure 1. A Concept VIC Regenerative Liquid Propellant Gun.

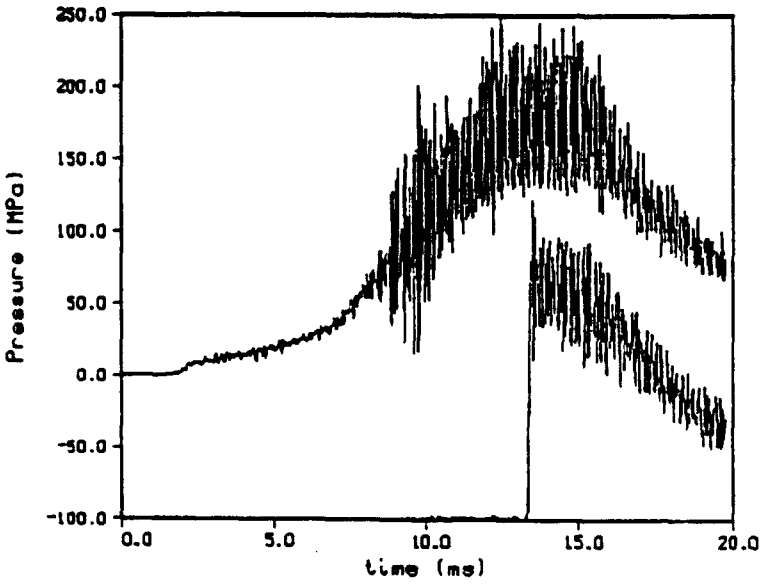

Figure 2. Experimental Result From a 155-mm VIC, Shot 65. Gauge E222 (top). Barrel Gauge B3 (bottom).

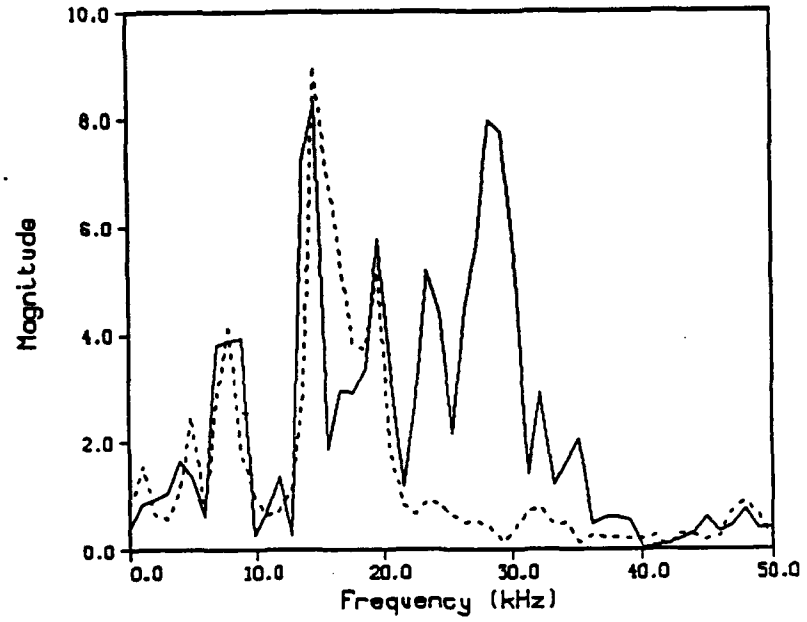

Figure 3. Fourier Transform of the Experimental Data From 14 to 15 ms. E222 (line). B3 (dot).

combustion process. Since most of the combustion is expected to occur in the chamber (based on analysis of experimental data), it is also unclear why there are still large magnitude pressure oscillations so far downstream.

2. MODEL ASSUMPTIONS

To study these problems, a two-dimensional computational fluid dynamic model of the combustion chamber/gun tube has been created. At the present, no attempt has been made to model the liquid reservoir or the damper.

In the Concept VIC regenerative liquid, the propellant is initially behind two pistons. The inner or control piston moves first, opening up an annular vent. The outer or injection piston then slightly trails the inner piston. Propellant is injected into the combustion chamber. Most of the combustion takes place in the combustion chamber. The gas then flows into the gun tube. There is a large area change from the chamber to the tube. In the 30-mm and 105-mm fixtures, there is a sharp corner. In the 155-mm fixtures, there is a taper from the chamber to the gun tube.

In the two-dimensional model, the combustion chamber is idealized as a cylinder. The left wall is allowed to move in an arbitrary fashion, roughly mimicking the motion of the pistons that inject liquid into the chamber. The grid is attached to the left wall and stretches as the wall moves. The individual grid points are moved so as to keep the grid uniform in the axial direction. There is a circular hole in the center of the right-hand wall corresponding to the entrance to the gun tube.

The injection process is simplified. Liquid droplets of a specified size are injected at a specified rate through an annulus in the left wall. The size of the annulus may vary with time. Infinite drag is assumed, so the gas and liquid at a given point have the same velocity, and only one set of momentum equations is required. The droplets then burn and release hot gas, according to a pressure dependent burning rate.

The chamber may be run in isolation, with exit conditions specified at the gun tube entrance. However, a gun tube model is available. The gun tube is also considered to be a cylinder, with the projectile at the right end. The standard equations of motion for the projectile are implemented. As the projectile moves, the grid stretches. Since the gun tube length increases dramatically during the course of the firing cycle, additional grid points are also added as the projectile moves. Values on the new grid are found by interpolation.

One option allows the use of the output from the lumped parameter gun code (Coffee 1985, 1988) as an input into the two-dimensional code. That is, the velocity of the left wall (piston velocity), the injector area, the propellant injection rate, and the injected droplet size are all read in as a function of time from the lumped parameter code output. This allows the two-dimensional code to mimic a gun firing cycle. In addition, a primer model is required. This causes hot gas to be injected through an annulus in the right-hand wall of the chamber at a specified rate at the start of the integration.

3. NUMERICAL PROCEDURE

An orthogonal grid is set up in the combustion chamber. This divides the chamber into annular control volumes. The scalar quantities (pressure, temperature, and density) are assumed to be uniform within a control volume. The axial and radial velocities are defined on

the vertices of the control volumes. The position of the vertices may be arbitrarily specified as a function of time. This type of mesh is called an arbitrary Lagrangian-Eulerian (ALE) mesh (Hirt, Amsden, and Cook 1974; Cloutman et al. 1982; Amsden et al. 1985) and is useful for representing moving boundaries. In this case, the vertices only move axially with the left wall, and the procedure is somewhat simplified from a general ALE formulation. The governing equations are cast in integral form. The procedure is inherently conservative. That is, if mass, momentum, or energy leaves one control volume through a boundary, it automatically enters the neighboring control volume.

An explicit numerical integration scheme is used. Implicit methods improve the stability of the integration and allow larger time steps to be used. However, the purpose here is to actually track pressure waves. This implies that very small time steps must be taken to accurately resolve the motion of the pressure waves. Therefore, the additional overhead of an implicit method is not useful.

Turbulent transport processes are described by a k-ε turbulence model (Jones and Launder 1972; Jones and Whitelaw 1982). This introduces two new partial differential equations for the turbulent kinetic energy and the dissipation rate. The turbulent viscosity is computed from these quantities. There are much simpler turbulence models. However, the k-ε model is the simplest model that allows for transient effects. That is, the turbulent viscosity can start out negligibly small and grow during the firing cycle. More complicated Reynold's stress models are judged not to be worth the additional effect. All of the turbulence models involve empirical parameters that must be set by comparison with experiment. Since these parameters have been chosen based on incompressible flow experiments near atmospheric pressure, extrapolating to gun conditions is only an approximation in any case.

Physically, the gas velocity at the wall should exactly match the wall velocity (no slip condition). The flow very near to the wall is laminar. Further away from the wall, the flow will become turbulent. But there will be a boundary layer where the flow is primarily parallel to the wall. Particularly for the large pressure gradients in a gun simulation, boundary layers at the walls will be very thin. It is impractical to use enough grid points to actually resolve the boundary layers. Boundary layer theory (law of the wall) is used to set the boundary conditions (Bradshaw 1978). That is, the expected velocity at the edge of the boundary layer

is used as the wall velocity in the code. Much of the turbulence is generated near the wall, and this can also be computed using boundary layer theory.

3.1 Governing Equations - Laminar Flow. The governing equations are given in Cartesian coordinates. While cylindrical coordinates might seem more appropriate for the problems of interest, it is more convenient to consider the geometry when the equations are recast into finite volume form. The continuity equation for two dimensions is (Bird, Stewart, and Lightfoot 1960)

$$\partial\rho/\partial t + \partial(\rho v_x)/\partial x + \partial(\rho v_y)/\partial y = 0 . \qquad (1)$$

Now consider some volume in three-dimensional space. By the divergence theorem, the above equation can be written as

$$\partial/\partial t \int_V \rho \, dV = -\int_V [\partial(\rho v_x)/\partial x + \partial(\rho v_y)/\partial y] \, dV$$

$$= -\int_S (\rho v_x \mathbf{I} + \rho v_y \mathbf{J}) \, \mathbf{n} \, dS .$$

The first two integrals are volume integrals. The last integral is a surface integral. The vectors $\mathbf{I}$ and $\mathbf{J}$ are the unit vectors in the x and y direction, and $\mathbf{n}$ is the unit outward normal vector to the surface. So any change in the mass in the control volume is due to mass flux across a boundary.

The energy equation can be written as (Bird, Stewart, and Lightfoot 1960)

$$\rho c_v \partial T/\partial t = -\rho c_v v_x \partial T/\partial x - \rho c_v v_y \partial T/\partial y$$

$$- T(\partial p/\partial T)_\rho (\partial v_x/\partial x + \partial v_y/\partial y) .$$

The viscous heating term, which is almost always small, is eliminated. The thermal conductivity term is also not included. For the problems of interest, the temperature is fairly

constant, and the thermal conductivity term is much smaller than the convection terms. For the Noble-Abel equation, the derivative of p with respect to T with the density constant is just pressure over temperature. Making this substitution and dividing by the specific heat,

$$\rho\,\partial T/\partial t = -\rho\, v_x \partial T/\partial x - \rho\, v_y \partial T/\partial y - p/c_v(\partial v_x/\partial x + \partial v_y/\partial y).$$

Using the continuity equation, this can be written as

$$\partial(\rho\, T)/\partial t = -\partial(\rho\, v_x T)/\partial x - \partial(\rho\, v_y T)/\partial y - p/c_v(\partial v_x/\partial x + \partial v_y/\partial y). \qquad (2)$$

The divergence theorem is applied. The pressure is assumed to be constant in the control volume and can be taken outside the integral. Then

$$\partial/\partial t \int_v (\rho\, T)\, dV = -\int_s (\rho\, v_x T I + \rho\, v_y T J)\, n\, dS - (p/c_v) \int_s (v_x I + v_y J)\, n\, dS.$$

The basic variable is the product of the mass and the temperature. This can, as before, be changed by convection (first right-hand term). Hot or cold gas can enter through a boundary. The temperature can also be changed through work (second right-hand term). Note that in the last term the pressure is not evaluated at the boundary but is the pressure in the control volume.

The momentum equation in the axial direction is (Bird, Stewart, and Lightfoot 1960)

$$\rho\,\partial v_x/\partial t = -\rho\, v_x \partial v_x/\partial x - \rho\, v_y \partial v_x/\partial y - \partial p/\partial x - \partial \tau_{xx}/\partial x - \partial \tau_{yx}/\partial y.$$

Using the continuity equation, this can be rewritten as

$$\partial(\rho v_x)/\partial t = -\partial(\rho v_x^2)/\partial x - \partial(\rho v_x v_y)/\partial y - \partial p/\partial x$$
$$- \partial\tau_{xx}/\partial x - \partial\tau_{yx}/\partial y.$$

For a Newtonian fluid, the shear stresses can be written as

$$\tau_{xx} = -4/3\,\mu\,\partial v_x/\partial x + 2/3\,\mu\,\partial v_y/\partial y$$
$$\tau_{yy} = -4/3\,\mu\,\partial v_y/\partial y + 2/3\,\mu\,\partial v_x/\partial x$$
$$\tau_{xy} = \tau_{yx} = -\mu(\partial v_x/\partial y + \partial v_y/\partial x),$$

so

$$\partial(\rho v_x)/\partial t = -\partial(\rho v_x^2)/\partial x - \partial(\rho v_x v_y)/\partial y - \partial p/\partial x$$
$$+ \partial/\partial x(4/3\,\mu\,\partial v_x/\partial x - 2/3\,\mu\,\partial v_y/\partial y)$$
$$+ \partial/\partial y(\mu\,\partial v_x/\partial y + \mu\,\partial v_y/\partial x). \qquad (3)$$

Applying the divergence theorem,

$$\partial/\partial t\int_V(\rho v_x)\,dV = -\int_S(\rho v_x v_x I + \rho v_x v_y J + pI)\,n\,dS$$
$$+ \int_S\Big[(4/3\,\mu\,\partial v_x/\partial x - 2/3\,\mu\,\partial v_y/\partial y)I$$
$$+ (\mu\,\partial v_x/\partial y + \mu\,\partial v_y/\partial x)J\Big]n\,dS.$$

Similarly, the momentum equation in the radial direction is

$$\rho \partial v_y/\partial t = - \rho v_x \partial v_y/\partial x - \rho v_y \partial v_y/\partial y - \partial p/\partial y$$
$$- \partial \tau_{xy}/\partial x - \partial \tau_{yy}/\partial y .$$

Using the continuity equation and replacing the shear stresses,

$$\partial(\rho v_y)/\partial t = - \partial(\rho v_x v_y)/\partial x - \partial(\rho v_y v_y)/\partial y - \partial p/\partial y$$
$$+ \partial/\partial x(\mu \partial v_x/\partial y + \mu \partial v_y/\partial x)$$
$$+ \partial/\partial y(4/3 \mu \partial v_y/\partial y - 2/3 \mu \partial v_x/\partial x) . \qquad (4)$$

Applying the divergence theorem,

$$\partial/\partial t \int_V (\rho v_y)\, dV = - \int_S (\rho v_x v_y I + \rho v_y v_y J + p J)\, n\, dS$$
$$+ \int_S \left[(\mu \partial v_x/\partial y + \mu \partial v_y/\partial x)\, I \right.$$
$$\left. + (4/3 \mu \partial v_y/\partial y - 2/3 \mu \partial v_x/\partial x)\, J \right] n\, dS .$$

Values for the viscosity of the fluid are required. The liquid is assumed to have a negligible effect on viscosity, and only the gas viscosity is computed. The most common propellants used are LGP1845 and LGP1846 (Decker et al. 1987). For simplicity, the assumption is made that LGP1845 goes completely to the major species CO_2, N_2, and H_2O (no minor species). The viscosity of these species as a function of temperature can be found using Lennard-Jones (Reid and Sherwood 1966) (non-polar) or Stockmayer (Monchick and Mason 1981) (polar) parameters. For the mixture viscosity, the Wilke formula is used (Bird, Stewart, and Lightfoot 1960). This formulation is for the low density limit, and ignores the pressure dependence of the viscosity. Fortunately, for high temperatures the pressure dependence is very small (Bird, Stewart, and Lightfoot 1960). Finally, a least-squares fit of the viscosity is

made between 300 K and 3,000 K, covering the temperature range of interest. The values for LGP1845 and LGP1846 are almost the same. The expression used is

$$\mu = 9.53\ 10^{-7}\ T^{0.862}\ .$$

3.2 Grid. Figure 4 shows the grid used in the chamber. The lower boundary is the center line of the chamber, and the upper boundary is the wall. The solid lines represent the vector grid. The grid is labeled from 1 to nx in the axial direction and from 1 to nr in the radial direction. The grid points are evenly spaced. The coordinates of the point labeled (i,j) are denoted by $[xv(i),yv(j)]$. The axial velocity $v_x(i,j)$ and the radial velocity $v_y(i,j)$ are defined at the point $[xv(i),yv(j)]$.

The vector grid splits the chamber into annular scalar control volumes. The scalar grid is defined by the dotted lines. The scalar grid is labeled from 1 to nx-1 in the axial direction and from 1 to nr-1 in the radial direction. The scalar grid coordinates are defined by

$$xs(i)= [xv(i) + xv(i+1)]/2 \quad ys(j)= [yv(j) + yv(j+1)]/2\ .$$

The scalar quantities are assumed to be constant within each scalar volume (between solid lines). There is a discontinuity in the scalar quantities at each solid line. Each scalar volume has a volume (V), divided up into a liquid volume (V_L) and a gas volume (V_G). Similarly, each volume has a mass (M), divided into a liquid mass (M_L) and a gas mass (M_G). The gas volume fraction $\varepsilon = V_G/V$. The gas has a temperature (T). The liquid is assumed to be isothermal, and heat transfer to the liquid is ignored. The gas has density ρ_G, and the liquid density is ρ_L. The liquid is in the form of drops with a Sauter mean diameter (d) and a total surface area (S). The pressure (p) is assumed to be the same for both the gas and the liquid.

The dotted lines split the chamber into vector control volumes. The velocities are assumed to be the same within each vector control volume, and there is a jump in velocity at the dotted lines. Note that each vector control volume is made up of parts of four scalar control volumes.

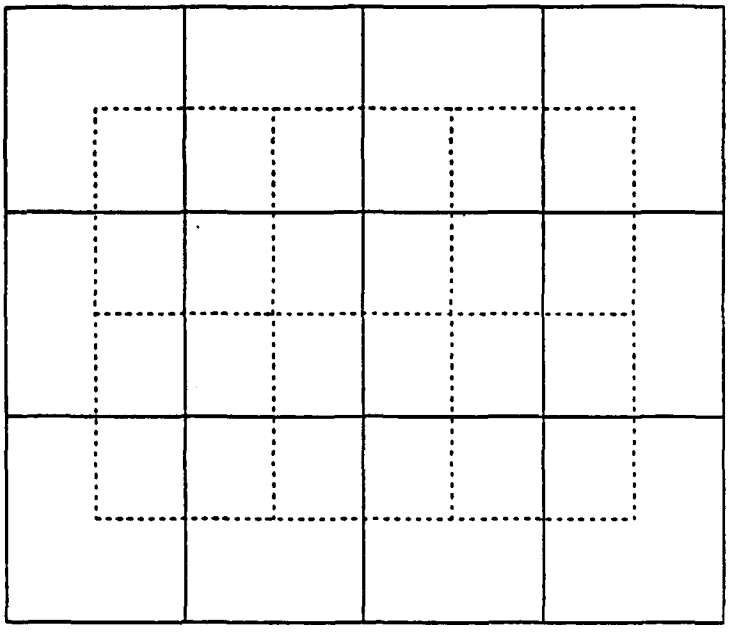

Figure 4. Combustion Chamber Grid.

There are additional scalar control volumes around the physical chamber to assist in setting the boundary conditions (see below).

3.3 Governing Equations - Combustion. The code takes a time step in two stages. First, a Lagrangian calculation is made. That is, the grid is assumed to move with the fluid. The advection terms are considered in the second stage, and the grid is returned to the desired location.

Consider a scalar control volume (V). Since all four vertices can have different velocities, the Lagrangian volume (V') is no longer defined by a simple rectangle rotated about the center line. A general formula for a quadrilateral of rotation is required. Consider first one line segment from (x_1,y_1) to (x_2,y_2). The volume under this line segment after it is rotated about the center line is given by

$$(\pi/3)(x_2 - x_1)(y_1^2 + y_1 y_2 + y_2^2) .$$

To find the volume of the entire figure, apply this formula to the four line segments going in the clockwise direction. Bottom boundaries will then generate a negative volume, and the total signed volume will be correct.

For the Lagrangian portion of the integration, there is no motion across the boundaries. Each scalar control volumes can then be integrated using the ordinary differential equations derived for lumped parameter models (Gough 1983; Coffee 1985, 1988), with the added simplification that there are no inflow or outflow terms.

In the scalar control volumes, the densities are given by

$$\rho_L = M_L / V_L \text{ and } \rho_G = M_G / V_G .$$

The density of the mixture is given by

$$\rho = M/V = (1 - \varepsilon_G)\, \rho_L + \varepsilon_G\, \rho_G ,$$

where $\varepsilon_G = V_G/V$. The Noble-Abel equation of state is used for the gas

$$p = \rho_G\, R_s\, T / (1 - b\, \rho_G),$$

where R_s is the specific gas constant and b is the covolume. The liquid equation of state is

$$p = (K_1 / K_2) \left[(\rho_L / \rho_o)^{K2} - 1 \right],$$

where K_1 is the adiabatic bulk modulus at zero pressure, K_2 is the derivative of the bulk modulus with respect to pressure, and ρ_o is the density at zero pressure. The pressure is assumed to be the same in both the liquid and the gas. The speed of sound in the liquid is given by

$$c_L = \sqrt{g_o(K_1 + K_2 p)/\rho_L} \ ,$$

where g_o is a conversion constant, and in the gas by

$$c_G = \sqrt{g_o \gamma p/[\rho_G(1 - b\rho_G)]} \ .$$

The speed of sound in the mixture (assumed to be homogeneous) is

$$c = \sqrt{(1/\rho)\{1/[\varepsilon_G/(\rho_G c_G^2) + (1 - \varepsilon_G)/(\rho_L c_L^2)]\}} \ .$$

The enthalpy of the liquid is

$$h_L = e_L + p/\rho_L ,$$

where the constant e_L is the chemical energy of the liquid, and the enthalpy of the gas is

$$h_G = c_p T + b p ,$$

where c_p is the specific heat at constant pressure.

Now the governing ordinary differential equations can be written. Let m be the combustion rate (g/s). Then

$$dM_L/dt = -\dot{m}$$

and

$$dM_G/dt = \dot{m} \ .$$

The total mass M does not change. The rate of change of the volume is given by

$$dV/dt = (V' - V)/dt ,$$

where dt is the time step. The rate of change of the pressure is

$$dp/dt = \left(\rho\, c^2 / g_o V\right)\left\{-dV/dt - \dot{m}/\rho_L + \dot{m}/\rho_G + \dot{m}\, g_o (h_L - h_G)(\gamma - 1)/\left[\rho_G c_G^2 (1 - b\rho_G)\right]\right\}.$$

The liquid density is found from the equation of state. The mixture density $\rho = M/V'$. The new liquid volume is $V_L = M_L/\rho_L$, and the new gas volume is $V_G = V' - V_L$. The new gas density is then $\rho_G = M_G/V_G$. The gas temperature is found from the equation of state.

The pressure equation is the only equation that is integrated implicitly. Because of the large velocities in the system, the volume can change noticeably in a single time step. The explicit integration may not be accurate enough. To advance from time t_n to time t_{n+1}, the derivative of pressure is found using the known quantities at time t_n. Then a first estimate of the pressure at time t_{n+1} is from the explicit equation

$$p_{n+1} = p_n + (dp/dt)_n\, dt.$$

Then new values are found for the densities and sound speeds. The new Lagrangian volume is used. The same values are used for the rate of volume change, the enthalpies, and the combustion rate. Then the time derivative of pressure is found at the new time and

$$p_{n+1} = p_n + 0.5\left[\,(dp/dt)_n + (dp/dt)_{n+1}\,\right] dt.$$

This will converge after a couple of iterations.

To close the system, the rate $\dot{m}$ at which the liquid droplets are combusting must be known. The rate of surface regression is assumed to be of the form Ap^B. The rate of combustion is

$$\dot{m} = \rho_L\, S\, A\, p^B.$$

In general, there will be different sized droplets in each control volume. In this code, only the Sauter mean diameter is tracked. If all the drops are assumed to have the same diameter (d), this is the diameter that will preserve the surface area. For one droplet,

$$V_1 = \pi\, d^3 / 6 \text{ and } S_1 = \pi\, d^2 .$$

So the total liquid surface is given by

$$S = 6\, V_L / d,$$

and the total number of drops is

$$N = V_L / V_1 = V_L\, 6 / \pi\, d^3 .$$

The quantity of interest is the surface area, S. This can also be written as

$$S = N \pi\, d^2 .$$

Then

$$\begin{aligned} dS/dt &= N \pi\, 2\, d\, dd/dt \\ &= N \pi\, 2\, d\, (-2\, A\, p^B) \\ &= -(V_L\, 6 / \pi\, d^3)\, \pi\, 2\, d\, (2\, \dot{m} / \rho_L\, S) \\ &= -V_L\, (24 / d^2)\, (\dot{m} / \rho_L)\, (d / 6 V_L) \\ &= -4\, \dot{m} / d \rho L . \end{aligned}$$

The new Sauter mean diameter can then be found from the surface area.

If there is no influx or outflux, mass and energy conservation should hold. The energy in a scalar control volume is given by

$$I = M_L\, e_L + M_G\, c_v\, T + M\, v^2 / 2\, g_o ,$$

where v is the average magnitude of the velocity in the control volume. The last term is, in practice, found in four parts. The magnitude of the velocity at each vertex of the control volume is found, and this is multiplied by the appropriate mass.

3.4 Time Step. Now we can consider the procedure for advancing a time step. Consider the axial velocity equation. The integration is performed over a vector control volume (bounded by dotted lines). The velocity $v_x(i,j)$ is assumed constant over the control volume, so it can be taken outside the integral. The density can take on four different values, since the vector control volume is made up of parts of four scalar control volumes. Let $V_l(j)$ be half the volume of the lower section of the scalar volume $V(j)$ and $V_u(j)$ be half the volume of the upper half. Then, if M_v is the mass in the vector control volume,

$$M_v = \int_v \rho \, dV = \rho(i,j) * V_l(j) + \rho(i-1,j) * V_l(j)$$
$$+ \rho(i,j-1) * V_u(j-1) + \rho(i-1,j-1) * V_u(j-1) .$$

The advection terms (first two terms on the right) disappear for the Lagrangian step. The momentum equations have actually been given for a fixed grid. In general, the advection terms are given by the momentum ρv_x times the velocity across the control volume boundary. For a Eulerian calculation (fixed grid), the velocity across the axial boundaries is v_x, and the velocity across the radial boundaries is v_y. For a Lagrangian calculation, there is no flow across the boundary.

There are pressure terms on the right and left boundaries. Let $A_l(j)$ be the lower axial area of a scalar control volume and $A_u(j)$ be the upper area. Then

$$\partial(M_v v_x)(i,j)/\partial t = p(i-1,j) * A_l(j) + p(i-1,j-1) * A_u(j-1)$$
$$- p(i,j) * A_l(j) - p(i,j-1) * A_u(j-1) + \ldots$$

The viscosity term is more complicated. Let

$$dv1_{xx}(i,j) = \partial v_x/\partial x \text{ on left boundary of the vector volume } (i,j)$$

$$= [v_x(i,j) - v_x(i-1,j)]/[xv(i-1)];$$

$$dv1_{yy}(i,j) = \partial v_y/\partial y \text{ on left boundary of the vector volume } (i,j)$$

$$= 0.5[v_y(i,j+1) - v_y(i,j-1) + v_y(i-1,j+1)$$

$$- v_y(i-1,j-1)]/[yv(j+1) - yv(j-1)];$$

$$dvb_{xy}(i,j) = \partial v_x/\partial x \text{ on bottom boundary of the vector volume } (i,j)$$

$$= [v_x(i,j) - v_x(i,j-1)]/[yv(j) - yv(j-1)];$$

$$dvb_{yx}(i,j) = \partial v_y/\partial x \text{ on bottom boundary of the vector volume } (i,j)$$

$$= 0.5*[v_y(i+1,j) - v_y(i-1,j) + v_y(i+1,j-1)$$

$$- v_y(i-1,j-1)]/[xv(i+1) - xv(i-1)].$$

The axial viscosity term becomes

$$\partial(M_v v_x)(i,j)/\partial t = \ldots - [4/3\, dvl_{xx}(i,j) - 2/3\, dvl_{yy}(i,j)]$$

$$[\mu(i-1,j) A_l(j) + \mu(i-1,j-1) A_u(j-1)]$$

$$+ [4/3\, dvl_{xx}(i+1,j) - 2/3\, dvl_{yy}(i+1,j)]$$

$$[\mu(i,j) A_l(j) + \mu(i,j-1) A_u(j-1)].$$

There is an added complication in the radial viscosity term. On each boundary, we want the viscosity term times the radial unit vector times the normal vector. But since the area of a control volume increases in the radial direction, this term is not zero on the axial sides of the control volume. Under the assumption that the viscosity term varies linearly from the bottom to the top boundary, a little algebra shows that the total contribution is the difference between the two sides times the area halfway from the bottom to the top side. Call this area $A_m(j)$ (area in the middle of the vector control volume j or at the bottom of the scalar control volume j). Then

$$\begin{aligned}\partial(M_v v_x)(i,j)/\partial t = \ldots &- [dvb_{xy}(i,j) + dvb_{yx}(i,j)]\,0.5 \\ &[\mu(i-1,j-1) + \mu(i,j-1)]\,A_m(j) \\ &+ [dvb_{xy}(i,j+1) + dvb_{yx}(i,j+1)]\,0.5 \\ &[\mu(i-1,j) + \mu(i,j)]\,A_m(j+1)\,.\end{aligned}$$

For the radial momentum equation, we also need to define

$$\begin{aligned}dvl_{xy}(i,j) &= \partial v_x/\partial y \text{ on left boundary of the vector volume } (i,j) \\ &= 0.5[v_x(i,j+1) - v_x(i,j-1) + v_x(i-1,j+1) \\ &\quad - v_x(i-1,j-1)]/[yv(j+1) - yv(j-1)];\end{aligned}$$

$$\begin{aligned}dvl_{yx}(i,j) &= \partial v_y/\partial x \text{ on left boundary of the vector volume } (i,j) \\ &= [v_y(i,j) - v_y(i-1,j)]/[xv(i) - xv(i-1)];\end{aligned}$$

$$\begin{aligned}dvb_{yy}(i,j) &= \partial v_y/\partial y \text{ on bottom boundary of the vector volume } (i,j) \\ &= [v_y(i,j) - v_y(i,j-1)]/[yv(j) - yv(j-1)];\end{aligned}$$

$$dvb_{xx}(i,j) = \partial v_x/\partial x \text{ on bottom boundary of the vector volume } (i,j)$$

$$= 0.5 * [v_x(i+1,j) - v_x(i-1j) + v_x(i+1,j-1)$$

$$- v_x(i-1,j-1)]/[xv(i+1) - xv(i-1)] .$$

$$\partial(M_V v_y)(i,j)/\partial t = 0.5[p(i-1,j-1) + p(i,j-1)$$

$$- p(i-1,j) - p(i,j)]A_m(j-1)$$

$$- [dvl_{xy}(i,j) + dvl_{yx}(ij)]$$

$$[\mu(i-1,j)A_l(j) + \mu(i-1,j-1)A_u(j-1)]$$

$$+ [dvl_{xy}(i+1,j) + dvl_{yx}(i+1,j)]$$

$$[\mu(i,j)A_l(j) + \mu(i,j-1)A_u(j-1)]$$

$$- [4/3\, dvb_{yy}(i,j) - 2/3\, dvb_{xx}(i,j)]\, 0.5$$

$$[\mu(i-1,j-1) + \mu(i,j-1)]A_m(j)$$

$$+ [4/3\, dvb_{yy}(i,j+1) - 2/3\, dvb_{xx}(i,j+1)]\, 0.5$$

$$[\mu(i-1,j) + \mu(i,j)]A_m(j+1) .$$

The new value of mass times velocity is found by taking the old value plus the time derivative times the time step. The quantities $M_V v_x$ and $M_V v_y$ are kept in vectors. The actual velocities v_x and v_y are also updated at this time.

Next, consider the coordinates $[xv(i), yv(j)]$ of a vector grid point (intersection of solid lines). Let $xvl(i,j)$ and $yvl(i,j)$ be the corresponding coordinates at the end of the Lagrangian part of the time step (this grid is not orthogonal). Then

$$xvl(i,j) = xv(i) + v_x(i,j)\, dt;$$

$$yvl(i,j) = yv(j) + v_y(i,j)\, dt.$$

The Lagrangian volume V' of the scalar control volumes can now be found (see Equation 5). Then the equations in Section B can be applied, and all the scalar quantities can be updated.

It might be more consistent to use the velocities at the end of the last time step, rather than the velocities calculated after the pressure step. However, the integration is more stable using the updated velocities. The flow is kept current with the present pressures.

Next, the grid is updated. In general, the left wall of the combustion chamber is allowed to move at an arbitrary speed, *vleft*. Then the grid velocity at the left $vg(1) = vleft$. The right wall is kept fixed ($vg(nx) = 0.0$). The axial grid is kept evenly spaced, so the grid velocity is assumed to be a linear function of position. The grid velocities at the other values are found by interpolation. Then the new position of the axial vector grid is

$$xv(i) = xv(i) + vg(i)\,dt\,.$$

The radial grid positions are unchanged.

Now the advection terms for the scalar quantities can be found. Conceptually, the boundaries of the Lagrangian control volumes are moved to the boundaries of the new control volumes. The amount of material the boundary passes through is convected from one volume to the next. For instance, consider the left-hand boundary of the scalar control volume (i,j). Assume that both Lagrangian points are to the right of the final boundary points. Compute the volume of the rectangle bounded by the points $[xv(i), yv(j+1)]$, $xvl(i,j+1)$, $yvl(i,j+1)$, $[xvl(i,j), yvl(i,j)]$, and $[xv(i), yv(j)]$, integrating in this order. For the assumed case, this is a positive number, which implies that the flow is from the previous control volume $(i-1,j)$ to the present volume (i,j). Upwind differencing is used, so the value of any quantity on the boundary is set equal to the value in the volume $(i-1,j)$. In this case, the upwind differencing is physically correct, since quantities will be moved from the volume $(i-1,j)$ to the volume (i,j). If, instead, both Lagrangian points are to the left of the final grid boundary, the volume is negative. Material will be convected from the volume (i,j) to the volume $(i-1,j)$. Again, using upwind differencing, the correct values will be used. The ambiguous case is when one Lagrangian point is to the left of the boundary and the other point is to the right. Some material will be

convected to the right and some material to the left. The computation above will give the proper signed volume change for the volume (i,j). However, upwind differencing is no longer exactly correct. The upwind differencing is used because it is stable even in the cases when it is not strictly correct, and for this formulation it is more often correct than other simple differencing schemes.

Consider first the gas mass. Let Vl be the volume between the left boundary of the Lagrangian volume and the left boundary of the final boundary. Then set

$$fluxl = \left[M_G(i-1,j) / V'(i-1,j) \right] Vl(i,j), \quad \text{if } Vl(i,j) > 0$$

$$\left[M_G(i,j) / V'(i,j) \right] Vl(i,j), \quad \text{if } Vl(i,j) < 0 .$$

The flux through the other three boundaries is computed the same way. Then the new gas mass is

$$M_G(i,j) = M_G(i,j) + (fluxl + fluxr + fluxb + fluxt).$$

For the liquid mass, the analogous equations are

$$fluxl = \left[M_L(i-1,j) / V'(i-1,j) \right] Vl(i,j), \quad \text{if } Vl(i,j) > 0$$

$$\left[M_L(i,j) / V'(i,j) \right] Vl(i,j), \quad \text{if } Vl(i,j) < 0$$

and

$$M_L(i,j) = M_L(i,j) + (fluxl + fluxr + fluxb + fluxt).$$

For the energy equation

$$fluxl = \left[M_G(i-1,j)/V'(i-1,j)\right] T(i-1,j)\, Vl(i,j), \qquad \text{if } Vl(i,j) > 0$$

$$\left[M_L(i,j)/V'(i,j)\right] T(i,j)\, Vl(i,j), \qquad \text{if } Vl(i,j) < 0$$

and

$$(M_G T)(i,j) = (M_G T)(i,j) + (fluxl + fluxr + fluxb + fluxt).$$

There is also an equation for the surface area.

$$fluxl = \left[S(i-1,j)/V'(i-1,j)\right] T(i-1,j)\, Vl(i,j), \qquad \text{if } Vl(i,j) > 0$$

$$\left[S(i,j)/V'(i,j)\right] T(i,j)\, Vl(i,j), \qquad \text{if } Vl(i,j) < 0$$

and

$$S(i,j) = S(i,j) + (fluxl + fluxr + fluxb + fluxt).$$

A similar procedure is used for the vector quantities. The vector control volumes are bounded by the scalar points. The boundary locations of the vector control volumes are given by

$$xsl(i,j) = \left[xvl(i,j+1) + xvl(i+1,j+1) + xvl(i+1,j) + xvl(i,j)\right]/4$$

$$ysl(i,j) = \left[yvl(i,j+1) + yvl(i+1,j+1) + yvl(i+1,j) + yvl(i,j)\right]/4 .$$

Let $Vl(i,j)$ now represent the volume change at the left boundary of the vector control volume from the Lagrange to the final position. The density on the left boundary is approximated by an area weighted average

$$\rho l(i,j) = [\rho(i-1,j-1)\, A_u(i-1,j-1) + \rho(i-1,j)\, A_l(i-1,j)]/$$
$$[A_u(i-1,j-1) + A_l(i-1,j)]\,.$$

For the axial velocity,

$$fluxl = \rho l(i,j)\, v_x(i-1,j)\, Vl, \qquad Vl(i,j) > 0$$

$$\rho l(i,j)\, v_x(i,j)\, Vl, \qquad Vl(i,j) < 0$$

and

$$(M_v v_x)(i,j) = (M_v v_x)(i,j) + (fluxl + fluxr + fluxb + fluxt)\,.$$

Similarly, the radial velocity is given by

$$fluxl = \rho l(i,j)\, v_y(i-1,j)\, Vl \qquad Vl(i,j) > 0$$

$$\rho l(i,j)\, v_y(i,j)\, Vl \qquad Vl(i,j) < 0$$

and

$$(M_v v_y)(i,j) = (M_v v_y)(i,j) + (fluxl + fluxr + fluxb + fluxt)\,.$$

The formulas need to be modified for the vector control volumes along the centerline. In this case, the standard form of the vector control volume would extend below the centerline. However, since a volume of rotation is being considered, this does not add anything to the vector control volume. So for a velocity at the centerline, the vector control volume is considered to be only the part above the centerline. So only the part actually in the physical chamber is considered. Special logic is then required for the change in volume. For consistency, the vector control volumes along the top boundary are treated the same way. That is, the vector control volume does not extend past the physical boundary.

Most of the other quantities can now be calculated in a straightforward manner. The exception is the pressure term. By assumption, the pressure in the new control volume (i,j) is

uniform and equal for both the gas and the liquid. The new pressure is somewhere between the pressure in the Lagrangian volume and the pressure(s) of the fluid convected into the final scalar volume. But as the pressure changes, both the liquid and gas volumes change. The constraint is

$$P_L - P_G = 0.0$$

From the gas and liquid equations of state

$$(K_1/K_2)\left[(\rho_L/\rho_o)^{K2} - 1\right] - \rho_G R_s T/(1 - b\rho_G) = 0$$

Rearranging, a function of the liquid volume can be defined

$$f(V_L) = (K_1/K_2)(V - V_L - bM_G)\left[(M_L/\rho_o)^{K2} - V_L^{K2}\right] - R_s M_G T V_L^{K2} = 0 .$$

The equation is transcendental and is solved by the Newton-Raphson iteration. The derivative

$$f'(\vec{V_L}) = -(K_1/K_2)\left[(M_L/\rho_o)^{K2} - V_L^{K2}\right] - K_1(V - V_L - bM_G)\, V_L^{K2-1} - R_s M_G T K_2 V_L^{K2-1}$$

and

$$V_L = V_L - f(V_L)/f'(V_L) .$$

The time step is determined by the Courant-Friedrichs-Lewy condition (McBratney 1980), as modified for compressible flow

$$dt \leq dx/[c + v_x]$$

$$dt \leq dy/[c + v_y] .$$

That is, a signal cannot propagate farther than a cell length during one time step. The code loops over all the scalar control volumes and finds the minimum *dt* by the above criteria. The velocity in the cell is taken to be the average of the four corner velocities. The time step is then multiplied by a user-supplied safety factor (usually 0.5). This is further modified so that the output times are hit exactly.

3.5 Boundary Conditions. An extra set of scalar control volumes are placed around the physical chamber. These volumes are the same size as the scalar control volumes just inside the physical boundary, except at the top boundary.

Consider the case where the chamber is completely closed (no inflow or outflow). The physically correct boundary condition on the walls is a no slip condition. That is, the velocities on the boundary are zero. This is included as an option in the code.

For this case, consider a scalar control volume next to the physical boundary. To integrate the scalar quantities, the four sets of velocities at the corners of the control volume are required. These are known. Values for the four scalar control volumes adjacent to the volume of interest are also required. This includes one scalar control volume outside the physical chamber. However, there is no convection across the boundary. So while these control volumes are put in to avoid having a special code for the boundaries, it is irrelevant what values are assigned to the extra volumes. Consider the vector control volume nearest the boundary. The values in the four control volumes that make up the vector control volume as well as the eight velocities in a box around the point of interest are required. These are all available.

At the centerline, the radial velocities must be zero, so there is no mass flow across the centerline. The axial velocity under the boundary ($j = 0$) is given the same value as the axial velocity over the boundary ($j = 1$). The radial velocity is reversed (flow up becomes flow down).

For the high pressures and velocities in a gun simulation, the boundary layers will be very small, and it is impractical to resolve these in detail. Instead, a slip condition is normally used. It is assumed that the boundary layer is negligibly small compared to the grid spacing, and the boundary layer is ignored. Instead, the tangential velocity is calculated using the standard set of equations. The normal velocity is, of course, still zero. This has no effect on the scalar quantities, since the flux through the boundary is still zero. However, the tangential velocities at the boundaries must be calculated.

Consider a point on the top boundary. The scalar quantities just outside the boundary are given the same values as the scalars just inside the boundary. However, the axial areas are set to zero. Then the pressure equation can be used unchanged. To obtain the proper velocity derivative terms, extrapolation conditions are used for the velocities —that is,

$$v_x(i,nr+1) = v_x(i,nr) + \left[v_x(i,nr) - v_x(i,nr-1)\right]$$
$$v_y(i,nr+1) = v_y(i,nr) + \left[v_y(i,nr) - v_y(i,nr-1)\right].$$

On the right and left boundaries analogous conditions are used.

The code allows for injection of liquid through an annulus in the left boundary. The upper and lower boundaries y_u and y_l are input, as well as the injection rate $\dot{m}_{in}$ in *g/s*, and the injected droplet diameter d_{in}. The injection area is denoted by A_{in}. Consider the scalar control volumes which are totally or partially inside the injection annulus. The corresponding scalar control volumes just to the left of the boundary are assumed to be pure liquid with the density of the liquid just inside the boundary but made of droplets with the diameter d_{in}. Pure liquid cannot really be made up of droplets, but this is a way of simulating the assumption that the liquid breaks up into droplets of the specified size as soon as it enters the chamber. Now consider the vector points between y_u and y_l. Let $r_{in}(j)$ be the ratio of the area of the left boundary of the vector control volume that is in the injection annulus to the entire control volume area. That is, the vector control volume might only be partially in the annulus. Then

$$v_x(1,j) = vleft + r_{in}(j)\left(\dot{m}_{in}/A_{in}(j)\right) / 0.5\left[\rho_L(1,j) + \rho_L(1,j-1)\right].$$

The other boundary quantities are found as before.

There is a problem if the injection area is small compared to the grid. The amount of liquid injected depends on the Lagrange volume computed. The Lagrange volume calculation assumes that the gas velocity varies linearly from one vector grid point to the next. For the injection process, however, there is a physical boundary where the velocity should suddenly change to zero. To obtain the proper injection rate even for a coarse grid, special logic is used to compute the volume change over the injection area. The volume change at the left boundary of a scalar control volume is the sum of the axial velocities at the boundary times the appropriate vector areas times the time step. The injection area is allowed to vary with time.

There is also a primer injection model. In the gun, the primer pressurizes the combustion chamber to start the firing cycle. The actual primer is injected through a circular opening and can only be modeled by a three-dimensional code. However, the details of the primer injection are not of interest, and the requirement is just to bring the chamber up to about the correct pressure. The model used in the lumped parameter code is extended to the present case. The primer is assumed to inject a specified mass of hot gas M_p uniformly over a time period t_p. The injection rate is then $\dot{m}_p = M_p/t_p$. A top and bottom boundary in the right wall is specified, and the injection area A_p is calculated. Normally about 50% of the primer energy is lost during the injection process. So an energy loss term f_p is also input.

During the primer injection, the scalar control volumes outside of the injection area are assumed to be pure gas. The density is more or less arbitrarily set to 0.2. The primer is assumed to be the same material as the liquid propellant. The temperature of the gas is the energy term f_p times the chemical energy of the propellant divided by the specified heat at constant volume. Consider all the vector points in the annulus. Let r_p be the ratio of the area of the right boundary of the vector control volume that is in the injection annulus to the entire control volume area. Then

$$v_x(nx,j) = - r_p(j) \left[\dot{m}_p / A_p(j) \right] / 0.5 \left[\rho_G(nx,j) + \rho_G(nx,j-1) \right] .$$

After the primer has been injected, this boundary is treated like a standard wall.

Finally, there is the flow into the gun tube. This is a circular opening at the centerline of the chamber. The gun tube must not overlap the primer injection annulus. The radial grid is adjusted so that the top of the gun tube always coincides with a vector grid point. Since the formulation of the equations does not depend on the radial grid being evenly spaced, this does not cause any problems. The gun tube can be modeled in detail (see below), or this can be viewed just as an outflow boundary.

If the detailed gun tube model is not used, the pressure p_t just outside the chamber must be specified. This is the pressure in the scalar control volumes just outside the chamber in the tube region. The flow through the boundary is assumed to be isentropic. For a Noble-Abel equation of state, the process equation is

$$p(1/\rho - b)^{\gamma} = \text{constant} .$$

Then the gas density can be found from the process equation and the gas temperature from the equation of state. The mass of liquid just outside the chamber is assumed to be the same as the mass of liquid just inside the chamber. The liquid density is found from the liquid equation of state. The velocity just outside the chamber is found by extrapolation.

There is a sharp corner at the top of the gun tube region. The top right corner of the vector control volume for this point is not actually in the fluid. There is flow out of the chamber through the bottom part of the vector volume, but the top part of the vector volume still includes the chamber wall. So the axial velocity at this corner is considered only to apply to the bottom part of the vector volume. Similarly, the radial velocity only applies to the left-hand part of the vector volume. Special logic is put into the integrator to handle this one special case.

For some problems, there may be flow into the chamber. The above boundary conditions are not consistent for inflow, since extrapolation should be done in the upwind direction. Generally, the conditions outside the chamber are not known in detail. So to preserve stability, back flow into the chamber is not allowed. If the flow reverses, the exit velocity is arbitrarily set to zero.

For guns, the flow out of the chamber will, in general, be subsonic. There is a test fixture at Sandia Laboratories (see below) where the chamber empties into atmospheric pressure and the flow is choked. A burst disc prevents flow until the chamber is properly pressurized.

To model this case, the outflow is set to zero until the pressure at the right centerline goes over the burst disc pressure. Then the assumption is made that choked flow is instantaneously established.

For an ideal gas, there are algebraic formulas for choked flow (Fox and McDonald 1985). Let M be the mach number of the gas on the centerline.

$$M = v_x(nx-1,1)/c(nx-1,1) .$$

The stagnation pressure, p_o, is the pressure of the gas if the velocity is isentropically reduced to zero.

$$p_o = p(nx-1,1)\left[1 + (\gamma-1)M^2/2\right]^{[\gamma/(\gamma-1)]} .$$

The critical pressure is the pressure at which the Mach number is unity.

$$p_c = p_o\left[(\gamma+1)/2\right]^{[-\gamma/(\gamma-1)]} .$$

For choked flow, the pressure at the throat is the critical pressure, and the velocity is the local speed of sound. The stagnation enthalpy of the fluid is defined as

$$h_o = h + v^2/2 ,$$

and this is constant throughout an adiabatic flow field.

For the present two-phase mixture, where the gas follows the Noble-Able equation of state, an analytic solution is not possible. Instead, an iterative procedure is used. The initial guess for the value of p_c is found using the above ideal gas equations. The corresponding

gas density is found from the process equation, and the gas temperature from the equation of state. The mass fraction $\varepsilon_{MG} = M_G/(M_G + M_L)$ is assumed to be the same as just inside the chamber. The liquid density is found from the liquid equation of state. The enthalpy of the fluid in the throat is given by

$$h_c = (c_p T_c + b p_c)\,\varepsilon_{MG} + (e_L + p_c/\rho_{Lc})(1 - \varepsilon_{MG}).$$

The throat velocity is found from the stagnation enthalpy equation. The throat speed of sound is found from the usual equations. The difference between the speed of sound and the fluid velocity is computed. If this is less than 10^{-7}, the iteration is concluded. Otherwise, the critical pressure is modified by

$$p_c = p_c\left[1 + (v_c - c_c)/c_c\right],$$

and the calculation is redone. Once the iteration concludes, the conditions outside the chamber are set equal to the critical conditions, and the velocity at the exit is the speed of sound at the critical conditions. However, in the code, the velocity acts on the fluid just inside the chamber. So the critical sound speed is multiplied by the ratio of the critical density and the density just inside the chamber. This gives the appropriate mass flow out (density times velocity times area). For simplicity, the calculation is only done for the centerline values, and the exit velocity is assumed to be uniform. The radial velocities at the exit are set to zero.

3.6 Combustion Rate. All the problems considered in this report involve LGP1846. The surface regression rate has been measured as

$$1.64\,p^{0.103} \qquad 0 < p < 60$$

by McBratney (1980, 1981). McBratney observed some indication of a slope break in the burning rate above 60 MPa. More recent work by Oberle and Wren (1990) indicates a regression rate of

$$0.000577\,p^{2.009} \qquad 100 < p < 200\,.$$

In the code, a two-part burning rate is used, with the McBratney rate used under 67 MPa and the Oberle and Wren rate above 67 MPa.

Due to the rapid burning rate, very high pressures can be generated near the injector. To simplify the numerics, the burning rate is assumed to reach a maximum at 1,000 MPa. That is, for pressures above 1,000 MPa, the burning rate is set equal to the value at 1,000 MPa. In actuality, the burning rate is expected to level off at some value, but the point where this will happen is not known.

To set up acoustic pressure oscillations, there must be some liquid accumulation in the chamber. Initial combustion generates a pressure wave. The pressure wave bounces off the chamber wall and returns to the combustion region. The higher pressure increases the combustion rate, which further increases the pressure. The pressure wave then becomes steadily larger until nonlinear effects come into play. From studies of liquid propellant rockets, it is known that acoustic oscillations can only be set up if the pressure exponent of the regression rate is large enough (generally greater than one) (Harrje 1972). In fact, if the McBratney rate alone is used, the code will not generate pressure waves under any circumstances. For infinitesimal pressure waves, the natural frequencies of a chamber can be solved for analytically (acoustic modes) (Harrje 1972). Even for large pressure waves, the observed frequencies are usually close to the acoustic modes.

4. VALIDATION

Some simple test problems were set up. The various options were tested with a closed chamber (no outflow) and then with an open chamber.

4.1 Closed Chamber. First, consider a closed chamber 5.0 cm long and 5.0 cm in diameter. The chamber was filled with a uniform gas mixture at 100 MPa and 2,000 K. The code was run for several milliseconds. The velocities become nonzero because of round-off error. However, the velocities stay negligibly small, and the pressures and temperatures do not change noticeably. This indicates that the code is stable.

Next, a 10-cm-long chamber is considered. The left side of the chamber is filled with gas at 50 MPa and the right side at 100 MPa. At time zero, a rarefaction wave propagates to the right and a shock wave to the left. This case can be solved analytically (Hughes and Brighton 1967; Band 1960). The rarefaction wave spreads out as it propagates. The front of the wave moves at the speed of sound, and the back of the wave moves at the sound speed minus the gas velocity. The shock wave, on the other hand, will become steeper.

With the no slip boundary conditions, this reduces to a one-dimensional problem. In the code, all the quantities are, in fact, uniform in the radial direction. Figure 5 compares the theoretical solution with four different axial grids after a short time period. Even with the coarse grid, the solution is reasonable. The fine grid is very close to the theoretical solution.

There is one problem here. The pressure between the shock wave and the rarefaction wave should be flat. Instead, there is a rise in pressure just to the right of the shock (Gibbs phenomenon). This is an artifact of the numerical procedure and cannot be eliminated by grid refinement. There are techniques for eliminating this phenomenon. Artificial viscosity can be added to the equations. However, this will smear out all the peaks in the solution, including the pressure waves of interest. A more sophisticated procedure is flux-corrected transport (Peyret and Taylor 1983; Boris and Book 1976). This is a procedure for diffusing out numerically introduced peaks while having minimal effect on the rest of the solution. Unfortunately, for the problems of interest, some high frequency oscillations will only be a few grid points in size, and the flux-corrected transport will also tend to damp these physical peaks. Flux-corrected transport has been implemented as an option in the code but will usually not be used. For a fine enough grid, essentially the same solution is obtained with and without flux-corrected transport.

Next, a uniform mixture of gas and liquid is put in the chamber. The liquid is assumed to be LGP1846, which has a flame temperature of (e_L/c_v) = 2,468.5 K. A total of 5 g of liquid is distributed in the chamber, with a droplet diameter of 100 μm. The initial gas temperature is set to the flame temperature. At the end of the combustion, there is a uniform gas mixture at the flame temperature. So the combustion procedure works properly. Both mass and energy are conserved.

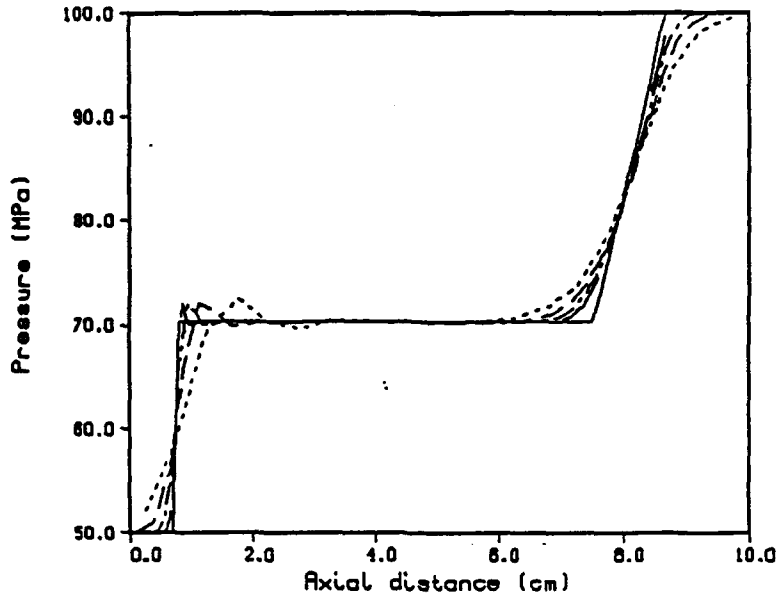

Figure 5. Shock Tube Simulation. Time = 0.1 ms. Theoretical Pressure Curve (line). Axial Grid = 20 (dot). 40 (dash). 80 (dot-dash). 160 (long dash).

The liquid was then axially put into the first centimeter of distance. Again, a purely one-dimensional solution was generated. Oscillations matched a first longitudinal mode with overtones. Next, the liquid was radially put into the first centimeter of distance. This is also a one-dimensional problem, with the profiles uniform in the axial direction. A first radial mode was generated. In both cases, accurate solutions were obtained with a fairly coarse grid. Mass was conserved almost exactly. There were energy errors due to the work term. The implicit formulation reduces these errors but does not eliminate them. For a coarse grid, the energy error was a small fraction of 1%. For the fine grids, the energy error was near 1%. The reason the energy error gets worse for a fine grid is due to the procedure for choosing a time step. Values are generated every 0.002 ms. For a coarse grid, the time step from the Courant condition would be larger than this. Since the code hits the output times exactly, it takes a smaller step than required for stability and so has improved accuracy. For the finer grids, with much smaller control volumes, the time step would have to be made smaller to get equivalent accuracy. A 1% error in the energy conservation is judged acceptable.

To obtain an actual two-dimensional problem, 2.5 g of liquid was axially and radially put into the first centimeter. Figure 6 shows the resulting pressure, measured at the wall in the

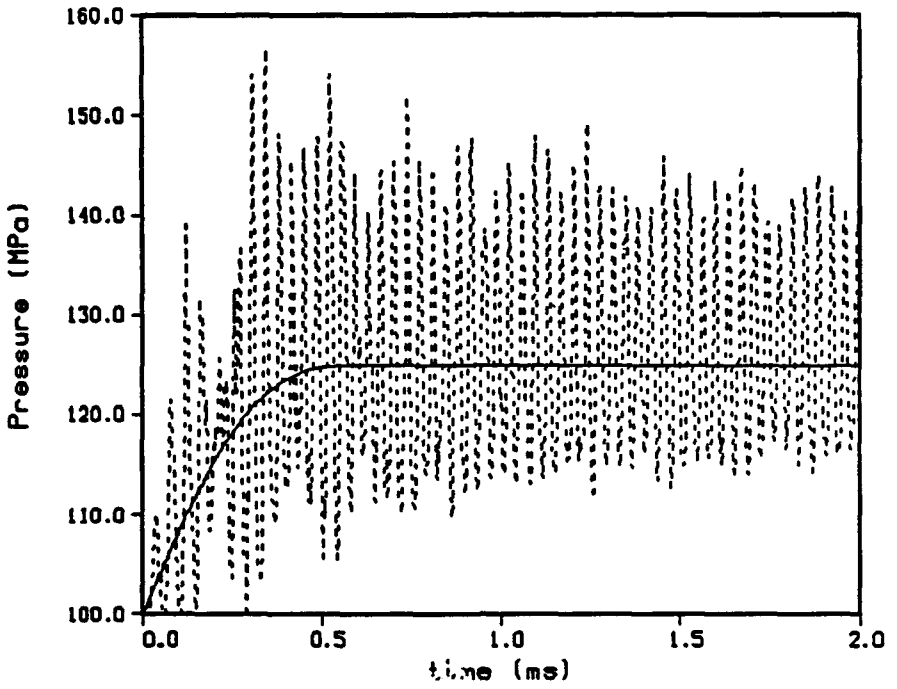

Figure 6. Closed Chamber. Uniform Liquid Distribution (line). Liquid in Left Center of Chamber (dot).

middle of the chamber. The pressure from the corresponding uniform distribution is shown for comparison. Figure 7 shows a blowup of part of the curve for three different grids. Grids with higher resolution in the radial direction were used since the radial modes are more important than the longitudinal modes. Figure 8 shows the Fourier transform of the pressure curve between 1 and 2 ms for the different grids. The major peak is the first radial (28 kHz), and the second highest peak is the first longitudinal (23 kHz). Since the curves are not pure sinusoidals, higher overtones are also generated. The first radial becomes more clearly defined as the grid is refined. However, even the coarse grid shows the main features of the solution.

To check the injection algorithm, the chamber is filled with gas at 100 MPa and 2,468.5 K. Then 5 g of liquid is injected over the first millisecond through a circular opening 1.0 cm in radius. Mass conservation is exact for all the grids tried. To check energy conservation, the chemical energy of the injected liquid must be added to the internal energy of the gas in the chamber. In addition, the injected liquid does work on the gas in the chamber, compressing it

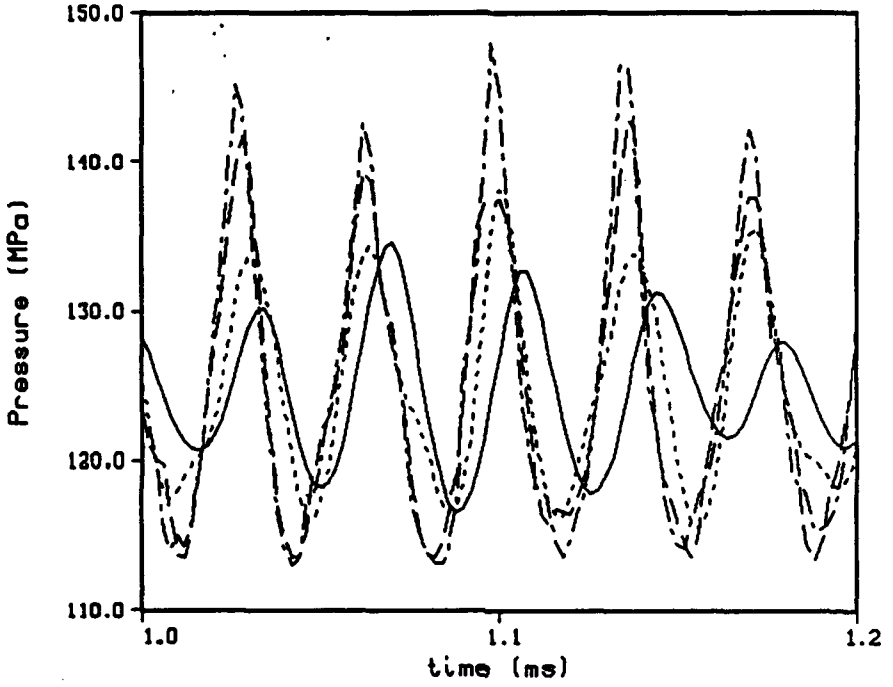

Figure 7. Closed Chamber. Liquid in Left Center of Chamber. Wall Pressure. 10 x 10 Grid (line). 20 x 20 Grid (dot). 40 x 40 Grid (dash).

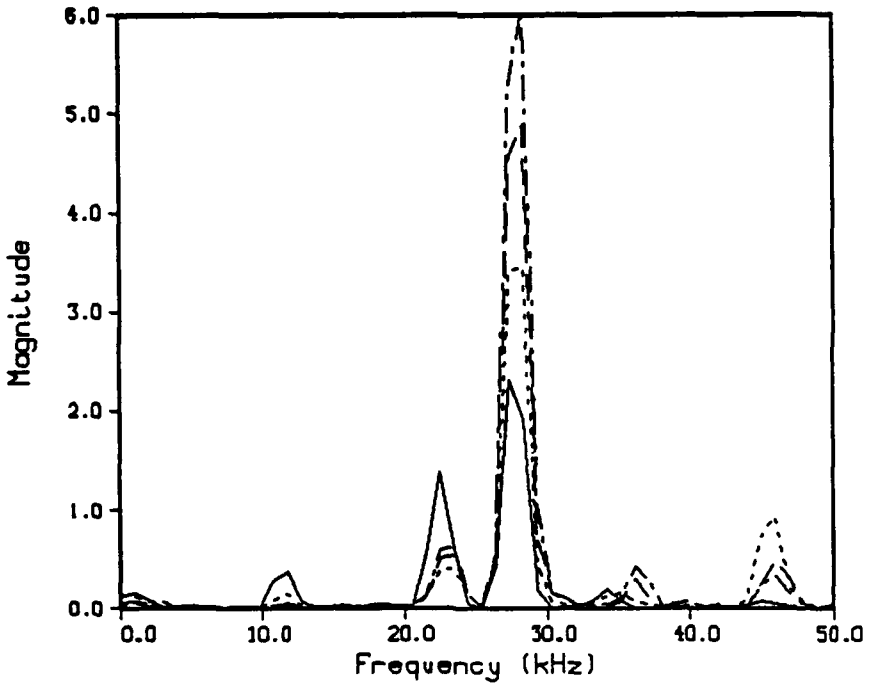

Figure 8. Closed Chamber. Liquid in Left Center of Chamber. Fourier Transform From 1 to 2 ms. 10 x 10 Grid (line). 20 x 20 Grid (dot). 40 x 40 Grid (dash).

into a smaller volume. When this is taken into effect, the energy error is much less than 1%. The first radial and first longitudinal modes are set up as before. However, the amplitudes are smaller, since there is much less liquid accumulation.

The primer model was also checked by injecting 5 g of hot gas over the first millisecond. A very small first longitudinal mode is set up. This is caused by the injected gas displacing gas already in the chamber.

Some unexpected results also were observed. When liquid was radially put into the first centimeter, a clean first radial mode was observed. Next, a smaller amount of liquid was radially put into the first 0.25 cm. The liquid was again assumed to be in 100-μm-diameter droplets. Figure 9 shows the observed frequencies. The first four radial modes were excited. For a fine grid, the main frequency is the third radial mode.

At time zero, the liquid combusts rapidly and generates a high pressure region. This begins to move the fluid away from the centerline. Eventually, enough fluid has been accelerated toward the wall that the pressure drops, and combustion slows drastically. However, because of momentum, the fluid continues to move, and the pressure drops below the initial pressure. The flow reverses, and combustion picks up again. Because of the high burning rate of the propellant, this process can generate fairly large pressure oscillations before there are any reflections from the chamber wall. The smaller the liquid region, the higher the frequency of the generated waves. For the present problem, the natural frequency of the liquid region is close to the third radial mode of the chamber, and this mode is preferentially pumped. The coarse grid cannot resolve the steep pressure gradient in the liquid region. So as the grid is refined, the main effect is to increase the resolution of the third radial mode.

I also tried the same initial setup but with 50-μm-diameter droplets (Figure 10). The oscillations are larger. But the natural frequency of the liquid region has been changed, and now the first radial mode is preferred.

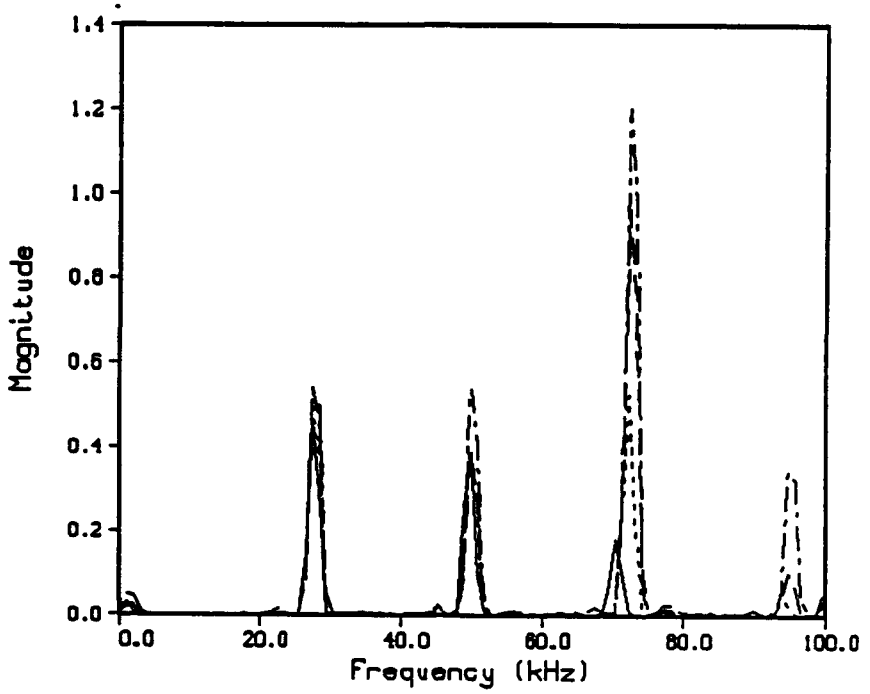

Figure 9. Closed Chamber. Liquid in First 0.25 cm Radially. 100-μm droplets. Fourier Transform. Radial Grid 10 (line), 20 (dot), 40 (dash), 80 (dot-dash).

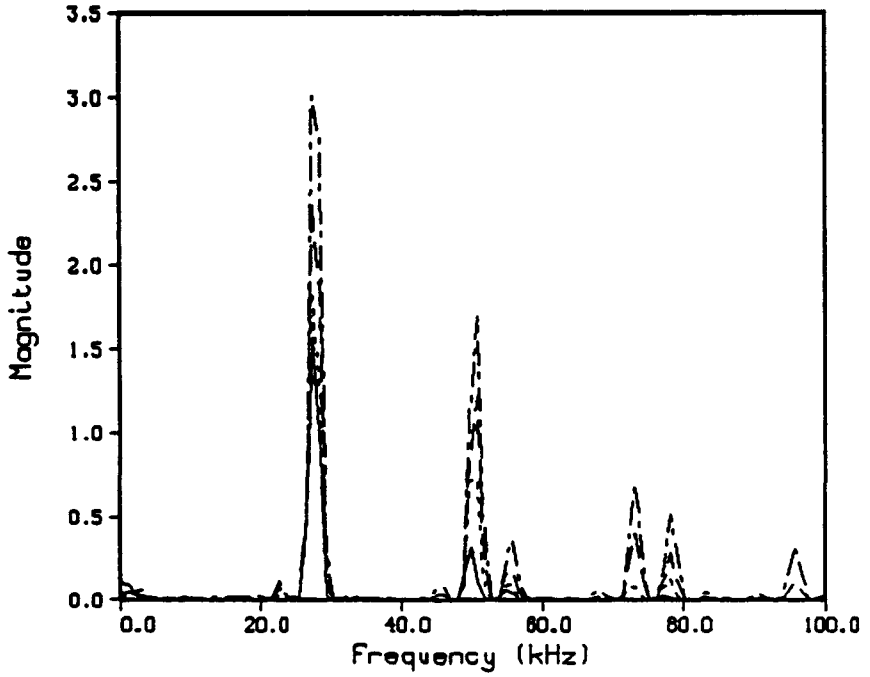

Figure 10. Closed Chamber. Liquid in First 0.25 cm Radially. 50-μm Droplets. Fourier Transform. Radial Grid 10 (line), 20 (dot), 40 (dash), 80 (dot-dash).

In liquid rockets, the propellant is usually injected as uniformly as is practical. In liquid guns, on the other hand, the propellant is usually injected through an annulus that is small compared to the chamber area. Hence, higher frequencies can be generated.

4.2 Open Chamber. An opening 0.5 cm in radius is put into the right-hand wall. For a first test, gas is put into the chamber at 100 MPa and 2,000 K, and the exit pressure just outside the chamber is put at 90 MPa. Figure 11 shows the outflow rate. For comparison, a solution is also given for a lumped parameter model (Coffee 1988). That is, the conditions in the chamber are assumed to be uniform, and the flow velocity out is given by assuming steady-state isentropic flow. For the detailed equations, there is a time delay as the flow gets going. The flow does not get as large as for the lumped parameter model since there is a delay in getting fluid from inside the chamber to the exit plane. This means the chamber takes longer to empty. However, the time scale is similar. The exit flow is almost grid independent. There are no noticeable pressure oscillations in this case.

Next, uniform injection at the left wall was implemented at a rate of 5 g/ms. Figure 12 shows the resulting outflow rates. The rate is almost grid independent. The model does reach a steady state, where the outflow matches the inflow. There are some very small oscillations. Pressure waves that hit the right wall reflect, but pressure waves that hit the opening exit, and a rarefaction wave propagates back into the chamber. The two effects tend to cancel, and it is difficult to start up oscillations.

The same basic setup was created with choked outflow. The injection rate was increased to 7.25 g/ms to compensate for the higher outflow. For this case, large oscillations were set up. The choked flow boundary acts more like a reflecting wall. Figure 13 shows the pressure at the chamber wall, and Figure 14 shows the Fourier transforms of the wall pressure for different grids. There is a longitudinal mode. Since the outflow is only near the centerline, conditions are not uniform in the radial direction. Once the flow becomes disturbed, the first radial mode is preferred. However, a fine grid is necessary to pick up the radial mode. There is also a very low frequency around 1 kHz. This is probably due to bulk oscillations of the material in the chamber as a whole.

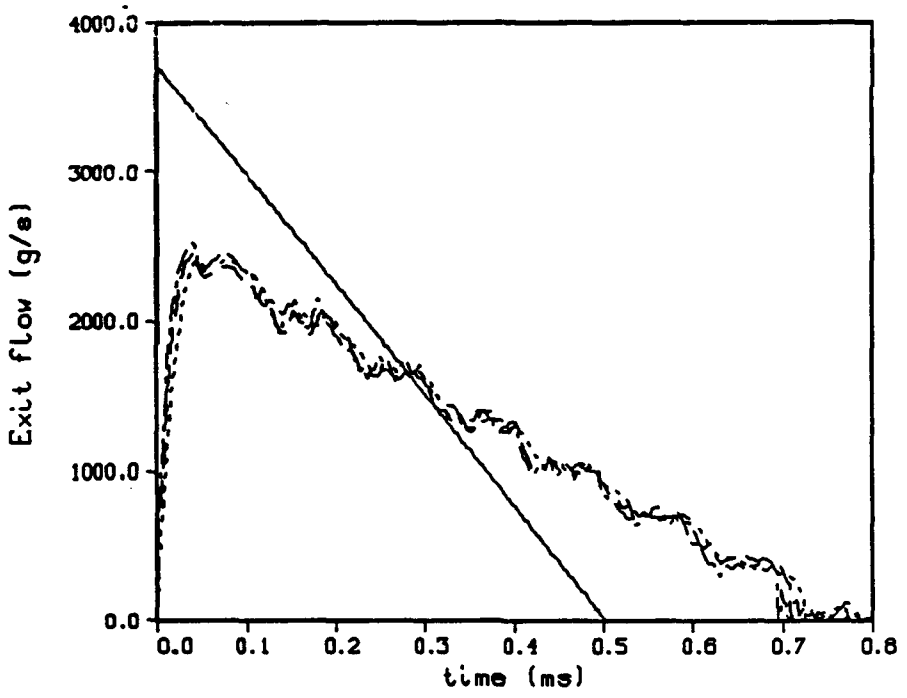

Figure 11. Chamber With Outflow. Initial Uniform Gas Distribution. Exit Flow. Lumped Parameter Model (line). 10 x 10 Grid (dot). 20 x 20 Grid (dash). 40 x 40 Grid (dot-dash).

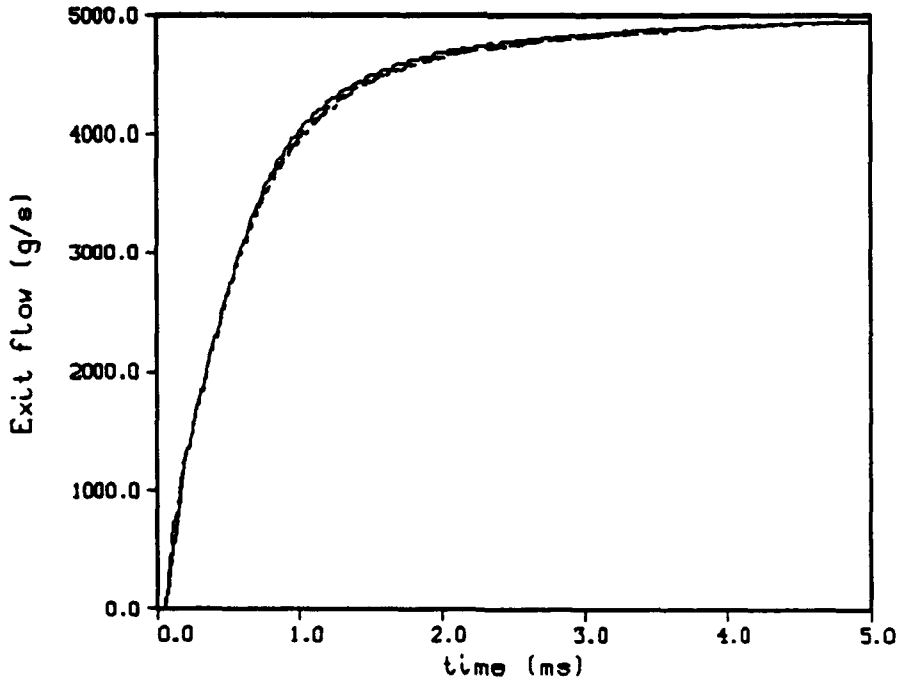

Figure 12. Chamber With Outflow. Uniform Injection at 5 g/ms. Exit Flow. 10 x 10 Grid (line). 20 x 20 Grid (dot). 40 x 40 Grid (dash).

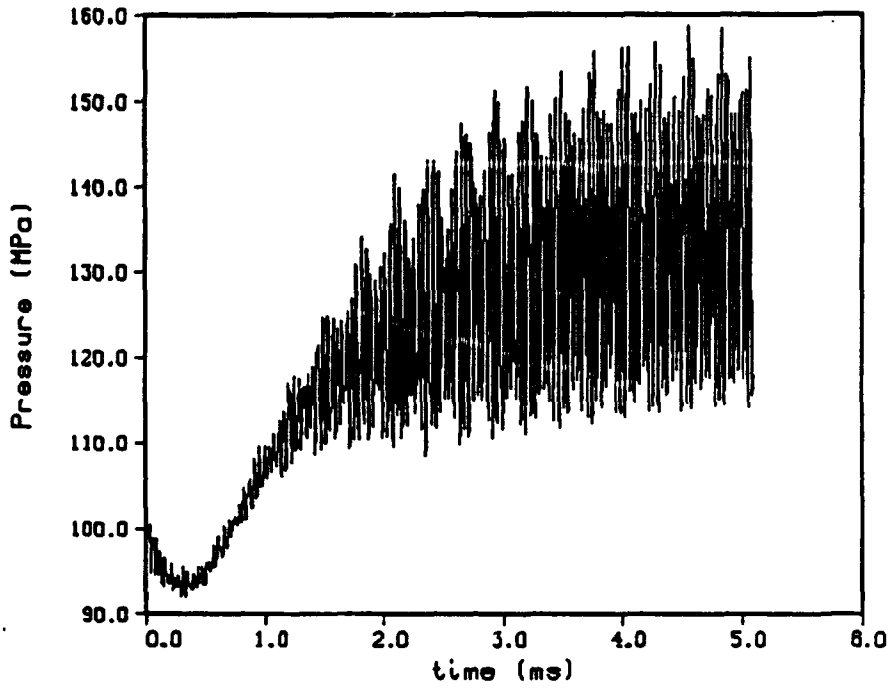

Figure 13. Chamber With Choked Outflow. Uniform Injection at 7.25 g/ms. Wall Pressure. 40 x 40 Grid.

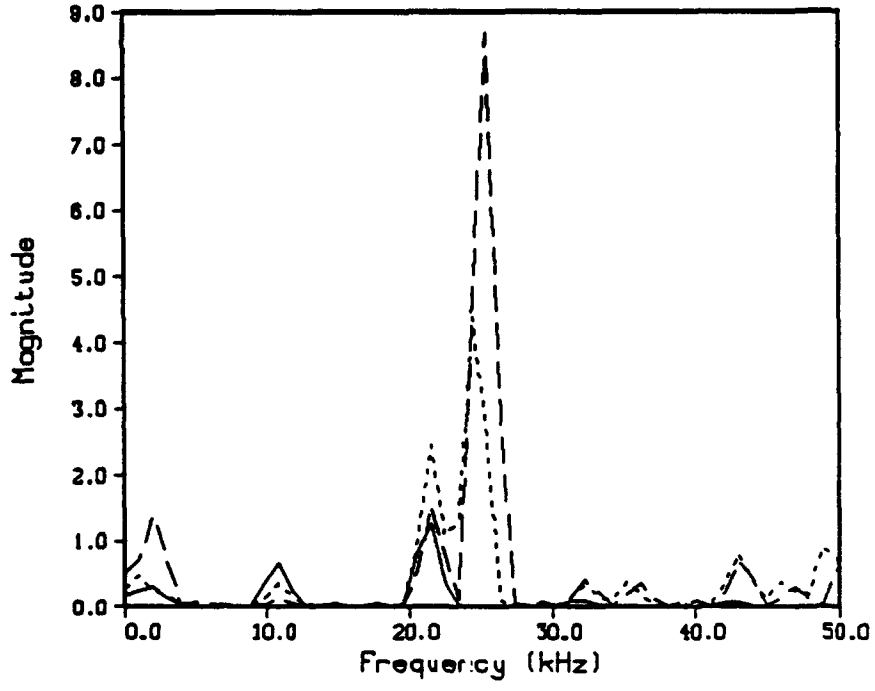

Figure 14. Chamber With Choked Outflow. Uniform Injection at 7.25 g/ms. Fourier Transform of Wall Pressure. 10 x 10 Grid (line). 20 x 20 Grid (dot). 40 x 40 Grid (dash).

Next, injection through an opening 1 cm in radius in the left wall was considered. Figure 15 shows the Fourier transform for the pressure at the middle wall. With the coarse 10 × 10 grid, there are no oscillations. However, the 20 × 20 grid shows the proper behavior. The pressure shows a clean first radial mode with overtones. That is, the pressure is not a pure sinusoidal wave, so higher frequencies appear at multiples of the first radial frequency. This can be distinguished from the higher radial modes, which have slightly different frequencies.

Figure 16 shows the corresponding result for choked flow. The oscillations are almost the same magnitude. The coarse grid shows only the longitudinal modes. The finer grids show primarily the first radial mode with overtones.

Next, the same amount of liquid was injected through a hole 0.25 cm in radius. Figure 17 shows the Fourier transforms. For the 20 × 20 grid, the highest frequency is the first radial. There is a frequency corresponding to twice the first radial, and a slightly lower frequency corresponding to the second radial. For the 40 × 40 grid, it is primarily the second radial mode that appears. The 60 × 60 grid shows results very close to the 40 × 40 grid. Since the liquid appears in a small volume, it will generate pressure pulses that may excite higher modes. It takes a fine grid to resolve this. The 20 × 20 case takes about 5 min to run on the U.S. Army Ballistic Research Laboratory (BRL) Cray X-MP, while the 60 × 60 grid takes over 7 hr.

Figure 18 shows the early pressure at the control volume on the centerline next to the injector. The time is too early for any reflected waves to return from the walls. The large oscillations are generated from the inertial confinement of the liquid. A fine grid can better resolve the very steep pressure gradient in the small volume of liquid. However, this behavior may owe something to the simplifications in the model. The model assumes that liquid is injected at a steady rate, independent of the pressure by the inlet. The liquid breaks up instantaneously into droplets and also ignites instantaneously. In reality, there must be some delay while the liquid breaks up and ignites. The combustion front will start on the outside of the jet and move in. The model merely shows that inertial confinement is capable of generating large pressure waves. Whether this happens in reality is still to be determined. In the future more sophisticated jet breakup models may be implemented in the code.

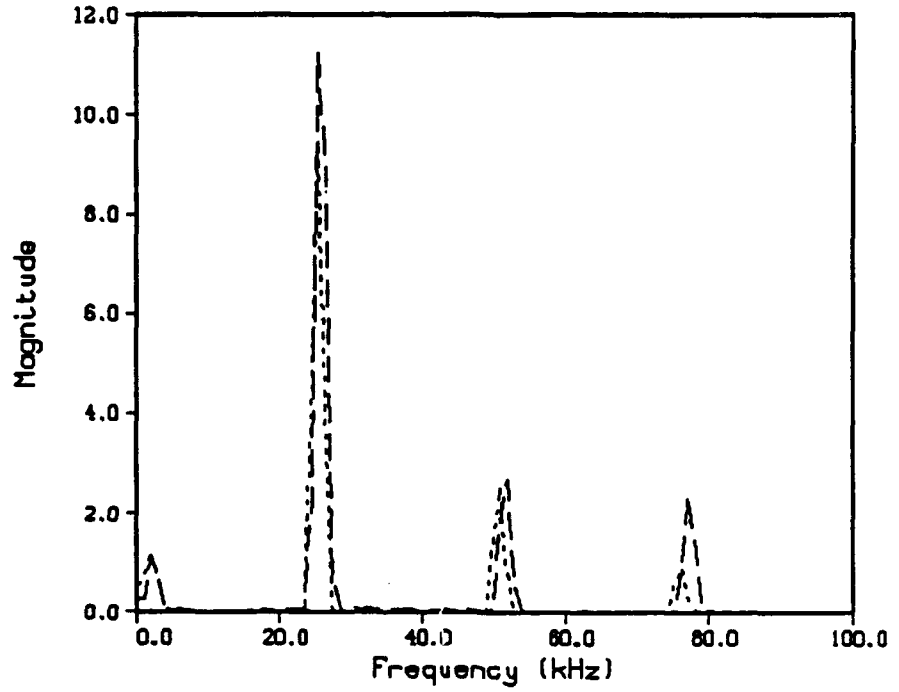

Figure 15. Chamber With Outflow. Injection Through a 1-cm-Radius Hole. Fourier Transform of Wall Pressure. 10 x 10 Grid (line). 20 x 20 Grid (dot). 40 x 40 Grid (dash).

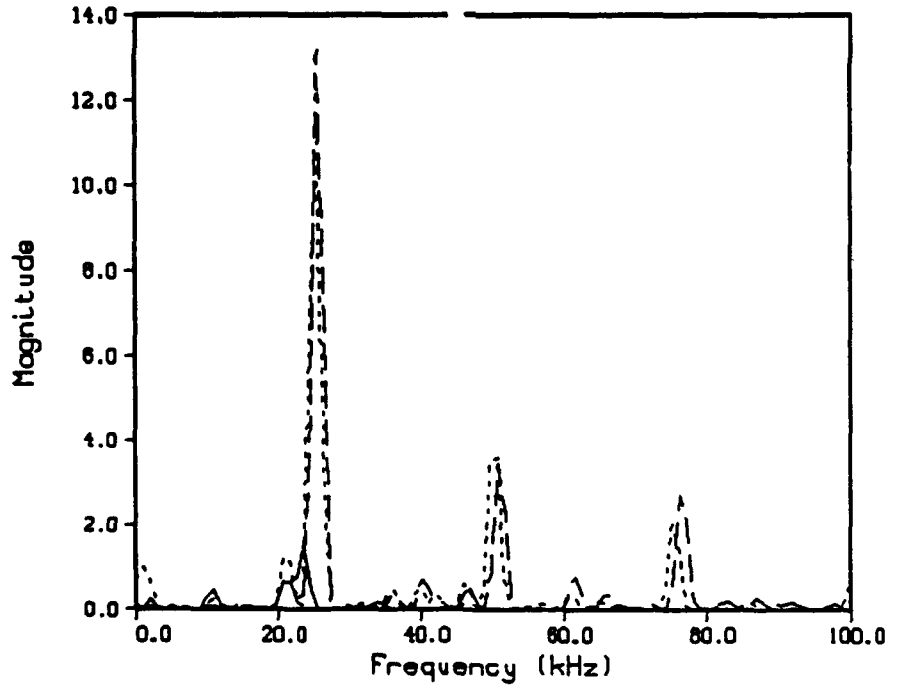

Figure 16. Chamber With Choked Outflow. Injection Through a 1-cm-Radius Hole. Fourier Transform of Wall Pressure. 10 x 10 Grid (line). 20 x 20 Grid (dot). 40 x 40 Grid (dash).

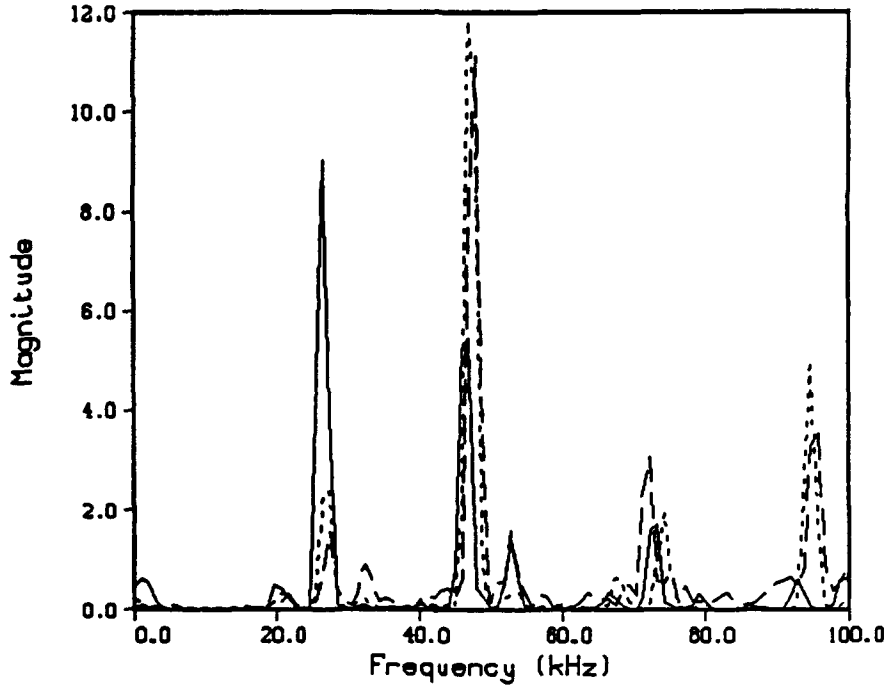

Figure 17. Chamber With Outflow. Injection Through a 0.25-cm-Radius Hole. Fourier Transform of Wall Pressure. 20 x 20 Grid (line). 40 x 40 Grid (dot). 60 x 60 Grid (dash).

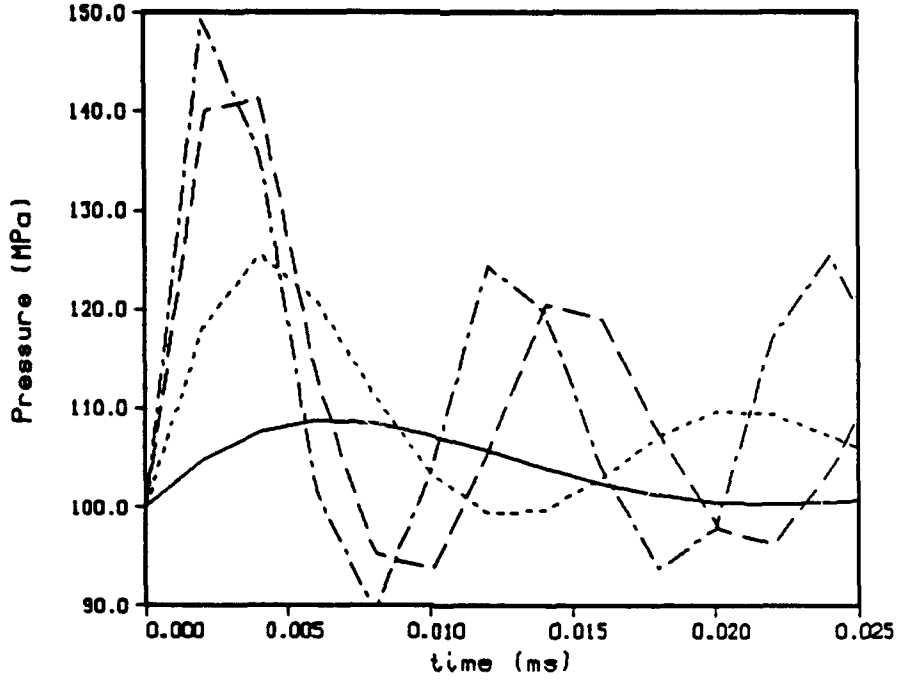

Figure 18. Chamber With Outflow. Injection Through a 0.25-cm-Radius Hole. Pressure in Front of Injector. 10 x 10 Grid (line). 20 x 20 Grid (dot). 40 x 40 Grid (dash). 60 x 60 Grid (dot-dash).

Figure 19 shows the corresponding Fourier transforms for the choked outflow. The major frequency is the first radial. It is not clear why the behavior is so different for choked and unchoked flow. It is clear that rapid injection of liquid into a small volume can cause complicated behavior.

5. TURBULENCE

With the large velocities in the gun, flow is unlikely to be laminar. So a turbulence model is included as an option in the code.

Turbulence is a three-dimensional phenomenon. Relatively large eddies are developed in the flow. These eddies decay into smaller eddies. At a very small length scale, the physical viscosity turns the eddies into heat. Normally, the physical viscosity is not the rate-limiting step, so the value of the physical viscosity is immaterial.

The k-ε model of turbulence is used in the code (Jones and Launder 1972; Ng and Spalding 1972; Hinze 1975; Bradshaw 1978; Kollmann 1980; Jones and Whitelaw 1982). The simpler mixing length models do not take into account the history of the flow, which is important for the transient problems of interest. The more complicated Reynold's stress models are not really developed enough for practical use. All the turbulence models are only approximations. The k-ε model is normally adequate for internal flows. It does, however, ignore some effects, such as curved streamlines. It is also very poor at predicting flow separation.

The effect of turbulence is considered in the momentum equations. There is also a turbulent transfer of energy. However, for the problems of interest, the temperature does not vary much, and this effect should be unimportant.

Because the full three-dimensional equations are required, tensor notation is used. That is, repeated subscripts indicate summation. The subscript 1 indicates the x direction, which is assumed to be the main direction of flow (if there is one). The subscript 2 indicates the y direction, which is assumed to be the main direction of shear (if there is one). The subscript 3 indicates the z direction.

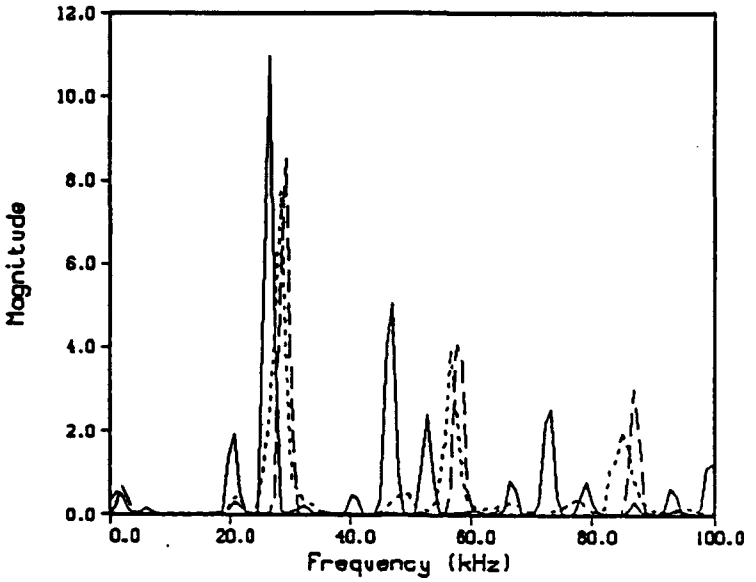

Figure 19. Chamber with Exit Hole - Choked. Injection Through Small Hole. 20 × 20 Grid (Line). 40 × 40 Grid (Dot). 60 × 60 Grid (Dash).

The vast majority of work has been for incompressible flow. First, the equations for this case are derived. Then the equations are generalized to compressible flow.

5.1 Incompressible Flow. The flow is assumed to be incompressible and the viscosity constant. The continuity equation reduces to

$$\partial v_j / \partial x_j = 0 . \tag{6}$$

The momentum equations are given by

$$\partial v_i / \partial t + \partial v_i v_j / \partial x_j = -(1/\rho)\{\partial p / \partial x_i + \partial \tau_{ji} / \partial x_j\},$$

with

$$\begin{aligned} \tau_{ji} &= -\mu(\partial v_i / \partial x_j + \partial v_j / \partial x_i) + 2/3\,\mu\,\delta_{ij}\partial v_k / \partial x_k \\ &= -\mu(\partial v_i / \partial x_j + \partial v_j / \partial x_i) . \end{aligned}$$

Using the kinematic viscosity (cm^2/s),

$$\nu = \mu/\rho,$$

the momentum equations can be rewritten as

$$\partial v_i/\partial t + \partial v_i v_j/\partial x_j = -(1/\rho)\partial p/\partial x_i + \partial/\partial x_j\{\nu[\partial v_i/\partial x_j + \partial v_j/\partial x_i]\}. \quad (7)$$

The basic idea is to split the flow into a mean part and a fluctuating part. Since transient problems are of interest, an ensemble average is used. That is, the problem is repeated N times, where N is a large number, and the mean is defined by

$$\bar{f}(t) = \Sigma f(t)/N.$$

For any given run of the problem, $f = \bar{f} + f'$, where f' is the fluctuating component. By definition, the mean of the fluctuating part is zero.

Now the mean of the momentum equations is taken. The only term that is nontrivial is

$$\begin{aligned}\overline{v_i v_j} &= (\bar{v}_i + v_i')(\bar{v}_j + v_j') \\ &= \bar{v}_i\bar{v}_j + v_i'\bar{v}_j + \bar{v}_i v_j' + \overline{v_i' v_j'} \\ &= \bar{v}_i\bar{v}_j + \overline{v_i' v_j'}.\end{aligned}$$

Note that a mean quantity can be moved out from under an overbar and that the mean of a fluctuating component is zero.

The momentum equations become

$$\partial \bar{v}_i/\partial t + \partial \bar{v}_i\bar{v}_j/\partial x_j = -(1/\rho)\partial \bar{p}/\partial x_i + \partial/\partial x_j\left\{\nu\left[\partial \bar{v}_i/\partial x_j + \partial \bar{v}_j/\partial x_i\right] - \overline{v_i' v_j'}\right\}. \quad (8)$$

The new term, the product of the mean of the fluctuating velocities, is called the Reynold's stress tensor. This is the only term by which the turbulent fluctuating velocities affect the mean flow.

The continuity equation is simply

$$\partial v_j/\partial x_j = \partial \bar{v}_j/\partial x_j = \partial v_j'/\partial x_j = 0.$$

For the k-ε model, the quantity of interest is the kinetic energy of the turbulent fluctuations, defined by

$$k = 0.5\ \overline{v_i' v_i'}.$$

Note that all information about the directional intensity of the turbulence is lost. Basically the turbulence is assumed to be isotropic (the same in all directions). This is expected to be true at small distance scales, where the turbulence is dissipated. However, the turbulence is created at large distance scales and often in a preferred direction. So information that is important for some problems is lost.

To obtain a turbulent kinetic energy equation, multiply the instantaneous momentum Equation 7 by v_i' and take the mean. The time-dependent term becomes

$$\overline{v_i' \partial v_i/\partial t} = \overline{v_i' \partial \bar{v}_i/\partial t} + \overline{v_i' \partial v_i'/\partial t}$$

$$= 0 + 0.5\ \overline{\partial v_i' v_i'}/\partial t = \partial k/\partial t.$$

The advection term becomes

$$\overline{v_i' \partial v_i v_j / \partial x_j} = \overline{v_i' \partial \bar{v}_i v_j' / \partial x_j} + \overline{v_i' \partial v_i' \bar{v}_j / \partial x_j} + \overline{v_i' \partial v_i' v_j' / \partial x_j},$$

where

$$\text{1st part} = \overline{v_i' v_j' \partial \bar{v}_i / \partial x_j} + \overline{v_i' \bar{v}_i \partial v_j' / \partial x_j} = \overline{v_i' v_j'} \partial \bar{v}_i / \partial x_j,$$

$$\text{2nd part} = \overline{v_i' v_i' \partial \bar{v}_j / \partial x_j} + \overline{v_i' \bar{v}_j \partial v_i' / \partial x_j} = \overline{v_i' \bar{v}_j \partial v_i' / \partial x_j}$$
$$= \bar{v}_j \partial k / \partial x_j = \partial \bar{v}_j k / \partial x_j - k \partial \bar{v}_j / \partial x_j = \partial \bar{v}_j k / \partial x_j,$$

and

$$\text{3rd part} = \overline{v_i' v_i' \partial v_j' / \partial x_j} + \overline{v_i' v_j' \partial v_i' / \partial x_j}$$
$$= 0 + \overline{0.5 v_j' \partial v_i' v_i' / \partial x_j}$$
$$= 0.5 \overline{\partial v_j' v_i' v_i'} / \partial x_j - 0.5 \overline{v_i' v_i' \partial v_j' / \partial x_j}$$
$$= 0.5 \overline{\partial v_j' v_i' v_i'} / \partial x_j.$$

The pressure term becomes

$$- \overline{(v_i' / \rho) \partial p / \partial x_i} = -(1/\rho) \left\{ \overline{\partial v_i' p} / \partial x_i - \overline{p \partial v_i' / \partial x_i} \right\}$$
$$= -(1/\rho) \overline{\partial v_i' p} / \partial x_i.$$

The viscosity term becomes

$$v_i' \partial / \partial x_j \left\{ \nu \left[\bar{\partial} v_i / \partial x_j + \partial v_i' / \partial x_j + \bar{\partial} v_j / \partial x_i + \partial v_j' / \partial x_i \right] \right\} = \nu v_i' \partial^2 v_i' / \partial x_j^2$$

$$+ \nu v_i' \partial^2 v_j' / \partial x_j \partial x_i = \nu v_i' \partial^2 v_i' / \partial x_j^2 + 0 = \nu \partial^2 k / \partial x_j^2 - \nu \overline{(\partial v_i' / \partial x_j)^2}.$$

Putting it all together,

$$\partial k/\partial t + \partial \bar{v}_j k/\partial x_j = -\overline{v_i' v_j'}\,\partial \bar{v}_i/\partial x_j - \partial/\partial x_j\{\overline{v_j' v_i' v_i'}/2 + \overline{\delta_{ij} p v_i'}/\rho - \nu \partial k/\partial x_j\} - \nu\overline{(\partial v_i'/\partial x_j)^2}. \qquad (9)$$

The left side of the equation is now standard. There is a time-dependent term and an advection term. The right side consists of a production term (turbulence is created from the mean flow), three diffusion terms, and a dissipation term. The last term is given the notation

$$\varepsilon = \nu\overline{(\partial v_i'/\partial x_j)^2}.$$

Normally, the physical viscosity terms are negligibly small. However, for this last term, gradients in the fluctuating velocities are considered, and this has a small length scale. This term is the only term that destroys turbulent kinetic energy.

Older theories are based on the idea of a mixing length, which is a length scale for the turbulent eddies. The relation is

$$l = k^{1.5}/\varepsilon .$$

Under the k-ε theory, the mixing length can change with time and/or space, rather than being held constant.

The problem now is to find expressions for the various correlations in Equation 9. So consider a very simple test case. Assume a steady-state shear flow. That is, the only nonzero mean velocity is in the *x* direction, and the only nonzero space derivative of the mean velocities is in the *y* direction. Also assume that the diffusion term is negligible. Then Equation 9 reduces to

$$-\overline{v_1' v_2'}\,\partial \bar{v}_1/\partial x_2 = \varepsilon .$$

Define

$$c_u = (\overline{v_1' v_2'}/k)^2 .$$

Then

$$\varepsilon^2 = c_u k^2 (\partial \bar{v}_1 / \partial x_2)^2,$$

or

$$\varepsilon = c_u (k^2/\varepsilon)(\partial \bar{v}_1 / \partial x_2)^2,$$

and

$$-\overline{v_1' v_2'} = c_u (k^2/\varepsilon) \ \partial \bar{v}_1 / \partial x_2.$$

Define the turbulent viscosity

$$\nu_t = c_u (k^2/\varepsilon).$$

Then

$$-\overline{v_1' v_2'} = \nu_t \partial \bar{v}_1 / \partial x_2,$$

or after much effort, the Reynold's stress now looks just like the molecular stress term, only with a turbulent viscosity rather than a physical viscosity.

So now the major assumption is made that in general flows, the Reynold's stress looks like a viscosity term. That is,

$$-\overline{v_i' v_j'} = \nu_t [\partial \bar{v}_i / \partial x_j + \partial \bar{v}_j / \partial x_i] - (2/3) \delta_{ij} k.$$

The last term is required to balance the equation. That is, if $i = j$, then

$$-\overline{v_i' v_i'} = -2k.$$

The molecular stress also breaks into the following two parts: the inhomogeneous term (dependent on direction) which becomes the viscosity term, and the homogeneous term (independent of direction) which is called the pressure.

Now the Reynold's stress formula is substituted into the mean momentum Equation 8, and the result is

$$\partial \bar{v}_i/\partial t + \partial \bar{v}_i \bar{v}_j/\partial x_j = -(1/\rho)\partial \bar{p}/\partial x_i - (2/3)\partial k/\partial x_i$$
$$+ \partial/\partial x_j\{ (\nu + \nu_t)[\partial \bar{v}_i/\partial x_j + \partial \bar{v}_j/\partial x_i] \}. \qquad (10)$$

So there is a turbulent pressure term and a turbulent viscosity term. The turbulent pressure is normally small compared to the actual pressure. In most cases, the turbulent viscosity is much larger than the physical viscosity. One exception is in a boundary layer, such as near a wall. The flow will have a laminar sublayer, as well as a region where laminar and turbulent effects are about the same size (see below).

For the turbulent kinetic energy Equation 9, first consider the production term. This now becomes

$$P_k = -\overline{v_i' v_j'}\,\partial \bar{v}_i/\partial x_j$$
$$= \nu_t \partial \bar{v}_i/\partial x_j [\partial \bar{v}_i/\partial x_j + \partial \bar{v}_j/\partial x_i] - (2/3) k \partial \bar{v}_i/\partial x_i$$

or

$$P_k = \nu_t \partial \bar{v}_i/\partial x_j [\partial \bar{v}_i/\partial x_j + \partial \bar{v}_j/\partial x_i].$$

The diffusion term is very messy and is expected to be of secondary importance. So the assumption is made that diffusion works like molecular diffusion. The result is the equation

$$\partial k/\partial t + \partial \bar{v}_j k/\partial x_j = \partial/\partial x_j[(\nu_t/\sigma_k)\partial k/\partial x_j] + P_k - \varepsilon, \qquad (11)$$

where σ_k is a constant to be determined from experimental data.

An equation for the dissipation is still required. This can be derived using the same general procedure as for the turbulent energy equation. However, the resulting equation has messy correlations that cannot easily be simplified. Instead, the standard procedure is to just apply dimensional analysis and get an equation following the kinetic energy Equation 11. That is,

$$\partial\varepsilon/\partial t + \partial \bar{v}_j\varepsilon/\partial x_j = \partial/\partial x_j[(\nu_t/\sigma_\varepsilon)\partial\varepsilon/\partial x_j] + c_{\varepsilon 1}(\varepsilon/k)P_k - c_{\varepsilon 2}(\varepsilon^2/k). \quad (12)$$

The constants are determined by looking at expe.imental data for some simple cases. These cases are normally homogeneous, decaying turbulence behind a grid, near wall turbulence in local equilibrium, and free shear flows. The standard set of values is

c_μ	$c_{\varepsilon 1}$	$c_{\varepsilon 2}$	σ_k	σ_ε
0.09	1.44	1.92	1.0	1.3 .

The above standard model generally does well for internal flows, as long as body forces are negligible and the streamlines are not curved. However, some people believe that it is fundamentally wrong and only works because the constants have been adjusted to match experimental data. Unfortunately, this makes it a little risky to extrapolate to gun conditions, since almost all measurements have been made at low pressures.

5.2 Compressible Flow. The case of actual interest is compressible flow. The kinematic viscosity is assumed to be the same as the mean kinematic viscosity. The continuity equation is now

$$\partial\rho/\partial t + \partial\rho v_j/\partial x_j = 0. \quad (12)$$

The momentum equations are given by

$$\partial\rho v_i/\partial t + \partial\rho v_i v_j/\partial x_j = -\partial p/\partial x_i - \partial\tau_{ji}/\partial x_j, \quad (13)$$

with

$$\tau_{ji} = -\mu(\partial v_i/\partial x_j + \partial v_j/\partial x_i) + 2/3\,\mu\delta_{ij}\partial v_k/\partial x_k$$
$$= -\rho\nu(\partial v_i/\partial x_j + \partial v_j/\partial x_i) + 2/3\,\rho\nu\delta_{ij}\partial v_k/\partial x_k.$$

Note that the last term of the stress tensor is no longer zero. The standard ensemble average introduced above is used for the density,

$$\rho = \bar{\rho} + \rho' .$$

However, for the velocity, a mass-averaged quantity is introduced—that is,

$$v_i = \bar{v}_i + v_i' = \underline{v}_i + v_i'' ,$$

where

$$\underline{v}_i = \overline{\rho v_i}/\bar{\rho}$$

or

$$\overline{\rho v_i} = \bar{\rho}\,\underline{v}_i .$$

This implies that

$$\overline{\rho v_i''} = \overline{\rho v_i} - \overline{\rho \underline{v}_i} = 0 .$$

Then

$$\begin{aligned}\overline{\rho v_i v_j} &= \overline{\rho \underline{v}_i \underline{v}_j} + \overline{\rho \underline{v}_i v_j''} + \overline{\rho v_i'' \underline{v}_j} + \overline{\rho v_i'' v_j''} \\ &= \bar{\rho}\,\underline{v}_i \underline{v}_j + \underline{v}_i \overline{\rho v_j''} + \underline{v}_j \overline{\rho v_i''} + \bar{\rho}\,\underline{v_i'' v_j''} \\ &= \bar{\rho}\,\underline{v}_i \underline{v}_j + \bar{\rho}\,\underline{v_i'' v_j''} .\end{aligned}$$

Take the mean of the continuity equation,

$$\partial \bar{\rho}/\partial t + \partial \bar{\rho}\,\underline{v}_j/\partial x_j = 0 .$$

Take the mean of the momentum equations,

$$\partial \bar{\rho}\,\underline{v}_i/\partial t + \partial \bar{\rho}\,\underline{v}_i \underline{v}_j/\partial x_j = -\partial \bar{p}/\partial x_i + \partial/\partial x_j \Big(\bar{\rho} \nu \big[\partial \underline{v}_i/\partial x_j + \partial \underline{v}_j/\partial x_i \big] - 2/3\, \bar{\rho} \nu \delta_{ij} \partial \underline{v}_k/\partial x_k - \bar{\rho}\,\underline{v_i'' v_j''} \Big) .$$

Now define the turbulent kinetic energy as

$$k = 0.5 \underline{v_i'' v_i''}.$$

As before, assume that the Reynold's stress can be written as

$$-\bar{\rho} \underline{v_i'' v_j''} = \bar{\rho} \nu_t [\partial \underline{v_i}/\partial x_j + \partial \underline{v_j}/\partial x_i] - (2/3)\delta_{ij}\bar{\rho} \nu_t \partial \underline{v_k}/\partial x_k - (2/3)\delta_{ij}\bar{\rho} k.$$

Then the mean momentum equations become

$$\partial \bar{\rho} v_i/\partial t + \partial \bar{\rho} \underline{v_i v_j}/\partial x_j = -\partial \bar{p}/\partial x_i - (2/3)\partial \bar{\rho} k/\partial_i + \partial/\partial x_j\{\bar{\rho}(\nu + \nu_t)[\partial \underline{v_i}/\partial x_j + \partial \underline{v_j}/\partial x_i] - 2/3\,\bar{\rho}(\nu + \nu_t)\delta_{ij}\partial \underline{v_k}/\partial x_k\}. \quad (14)$$

Next, take the instantaneous momentum Equations 13, rearrange using the continuity Equation 12, and plug in the stress term to obtain

$$\rho \partial v_i/\partial t + \bar{\rho} v_j \partial v_i/\partial x_j = -\partial p/\partial x_i + \partial/\partial x_j(\rho \nu[\partial v_i/\partial x_j + \partial v_j/\partial x_i] - 2/3\,\rho \nu_{ij}\partial v_k/\partial x_k).$$

Multiply by v_i'' and take the average. The time-dependent term becomes

$$\underline{\rho v_i'' \partial v_i/\partial t} = \bar{\rho} \underline{v_i'' \partial v_i''/\partial t} = \bar{\rho} \partial k/\partial t.$$

The advection term becomes

$$\overline{\rho v_i'' v_j \partial v_i/\partial x_j} = \bar{\rho}\, \underline{v_i'' v_j''}\, \partial \underline{v_i}/\partial x_j + \bar{\rho}\, \underline{v_i'' \underline{v_j} \partial v_i''/\partial x_j}$$

$$+ \bar{\rho}\, \underline{v_i'' v_j'' \partial v_i''/\partial x_j}$$

$$= \bar{\rho}\, \underline{v_i'' v_j''}\, \partial \underline{v_i}/\partial x_j + \bar{\rho}\, \underline{v_j} \partial k/\partial x_j + \bar{\rho}\, 0.5\, \underline{v_j'' \partial v_i'' v_i''/\partial x_j}.$$

The pressure term becomes

$$-\overline{v_i'' \partial p/\partial x_i}.$$

The first part of the viscosity term becomes

$$\overline{v_i'' \partial/\partial x_j\{\rho\nu\,(\partial v_i/\partial x_j + \partial v_j/\partial x_i)\}} = \partial/\partial x_j\{\bar{\rho}\nu\, \underline{v_i''\,(\partial v_i''/\partial x_j + \partial v_j''/\partial x_i)}\}$$

$$- \bar{\rho}\nu\, \underline{(\partial v_i''/\partial x_j + \partial v_j''/\partial x_i)\partial v_i''/\partial x_j}.$$

The second part of the viscosity term becomes

$$\overline{-v_i'' \partial/\partial x_j(2/3\,\rho\nu\,\delta_{ij}\partial v_k/\partial x_k\}} = \overline{-v_i'' \partial/\partial x_i(2/3\,\rho\nu\,\partial v_k/\partial x_k)}$$

$$= -\partial/\partial x_i(2/3\,\bar{\rho}\nu\, \underline{v_i''\,\partial v_k''/\partial x_k}) - 2/3\,\bar{\rho}\nu\, \underline{\partial v_k''/\partial x_k \partial v_i''/\partial x_i}.$$

Combining

$$\bar{\rho}\,\partial k/\partial t + \bar{\rho}\,\underline{v_j}\,\partial k/\partial x_j = -\bar{\rho}\,\underline{v_i''\,v_j''}\,\partial \underline{v_i}/\partial x_j$$

$$- \bar{\rho}\,0.5\,\underline{v_j''\,\partial v_i''\,v_i''}/\partial x_j - \overline{v_i''\,\partial p/\partial x_i}$$

$$+ \partial/\partial x_j\{\bar{\rho}\,\nu\,\underline{v_i''\,(\partial v_i''/\partial x_j + \partial v_j''/\partial x_i)}\}$$

$$- \partial/\partial x_i(2/3\,\bar{\rho}\,\nu\,\underline{v_i''\,\partial v_k''/\partial x_k)}$$

$$- \bar{\rho}\,\nu\,\underline{(\partial v_i''/\partial x_j + \partial v_j''/\partial x_i)\,\partial v_i'''/x_j}$$

$$- 2/3\,\bar{\rho}\,\nu\,\underline{\partial v_k''/\partial x_k \partial v_i''/\partial x_i}. \qquad (15)$$

This is somewhat messier than Equation 9 for incompressible flow, but the basic structure is the same. The first line gives the time-dependent term, the advection term, and the production term. The next three lines are diffusion terms. Again, for lack of a better idea, it is assumed that diffusion works like molecular diffusion. The last two lines are dissipation terms, and all of them are set equal to $\rho\varepsilon$. So the result is

$$P_k = \nu_t[\partial \underline{v_i}/\partial x_j + \partial \underline{v_j}/\partial x_i]\,\partial \underline{v_i}/\partial x_j$$

$$- (2/3)\,\nu_t\,\partial \underline{v_k}/\partial x_k\,\partial \underline{v_k}/\partial x_k - (2/3)\,k\,\partial \underline{v_k}/\partial x_k$$

and

$$\varepsilon = -\nu\,\underline{(\partial v_i''/\partial x_j + \partial v_j''/\partial x_i)\,\partial v_i''/\partial x_j}$$

$$- 2/3\,\nu\,\underline{\partial v_k''/\partial x_k \partial v_k''/\partial x_k}.$$

Rearranging the left side of Equation 15 using the continuity equations and plugging in the indicated expressions on the right-hand side results in

$$\partial \bar{\rho}\,k/\partial t + \partial \bar{\rho}\,\underline{v_j}\,k/\partial x_j = \partial/\partial x_j[(\mu_t/\sigma_k)\,\partial k/\partial x_j] + \bar{\rho}\,P_k - \bar{\rho}\,\varepsilon. \qquad (16)$$

Similarly, the dissipation equation becomes

$$\partial \bar{\rho}\varepsilon/\partial t + \partial \bar{\rho}\underline{v_j}\varepsilon/\partial x_j = \partial/\partial x_j[(\mu_t/\sigma_\varepsilon)\partial\varepsilon/\partial x_j] + c_{\varepsilon 1}(\varepsilon/k)\bar{\rho}P_k - c_{\varepsilon 2}\bar{\rho}(\varepsilon^2/k). \quad (17)$$

Since there is almost no data for compressible flows, the constants are given the same values as for incompressible flow.

5.3 Implementation. This new set of equations must be solved. From now on all quantities are assumed to be the appropriate means, so overbars and underlines will be omitted. Taking Equation 14 and writing it for the x momentum gives

$$\begin{aligned}\partial(\rho v_x)/\partial t = &- \partial(\rho v_x^2)/\partial x - \partial(\rho v_x v_y)/\partial y - \partial p/\partial x - (2/3)\partial\rho k/\partial x \\ &+ \partial/\partial x[4/3(\mu+\mu_t)\partial v_x/\partial x - 2/3(\mu+\mu_t)\partial v_y/\partial y] \\ &+ \partial/\partial y[(\mu+\mu_t)\partial v_x/\partial y + (\mu+\mu_t)\partial v_y/\partial x]. \end{aligned} \quad (18)$$

Applying the divergence theorem,

$$\begin{aligned}\partial/\partial t\int_V(\rho v_x)\,dV = &- \int_S(\rho v_x v_x I + \rho v_x v_y J + [p+(2/3)\rho k]I)\,n\,dS \\ &+ \int_S\Big(\big[4/3(\mu+\mu_t)\partial v_x/\partial x - 2/3(\mu+\mu_t)\partial v_y/\partial y\big]I \\ &+ \big[(\mu+\mu_t)\partial v_x/\partial y + (\mu+\mu_t)\partial v_y/\partial x\big]J\Big)\,n\,dS.\end{aligned}$$

Similarly, the momentum equation in the radial direction is

$$\begin{aligned}\partial(\rho v_y)/\partial t = &- \partial(\rho v_x v_y)/\partial x - \partial(\rho v_y v_y)/\partial y - \partial p/\partial y - (2/3)\partial\rho k/\partial y \\ &+ \partial/\partial x[(\mu+\mu_t)\partial v_x/\partial y + (\mu+\mu_t)\partial v_y/\partial x] \\ &+ \partial/\partial y[4/3(\mu+\mu_t)\partial v_y/\partial y - 2/3(\mu+\mu_t)\partial v_x/\partial x]. \end{aligned} \quad (19)$$

Applying the divergence theorem,

$$\partial/\partial t \int_V (\rho v_y)\, dV = -\int_S (\rho v_x v_y I + \rho v_y v_y J + [p + (2/3)\rho k] J)\, n\, dS$$
$$+ \int_S \Big([(\mu + \mu_t)\partial v_x/\partial y + (\mu + \mu_t)\partial v_y/\partial x] I$$
$$+ \big[4/3(\mu + \mu_t)\partial v_y/\partial y - 2/3(\mu + \mu_t)\partial v_x/\partial x \big] J \Big) n\, dS.$$

Next consider the turbulent production term. For a two-dimensional problem, this becomes

$$\rho P_k = \mu_t \big[(4/3)(\partial v_x/\partial x)^2 + (\partial v_x/\partial y)^2 + (\partial v_y/\partial x)^2$$
$$+ (4/3)(\partial v_y/\partial y)^2 + 2(\partial v_x/\partial y)(\partial v_y/\partial x)$$
$$- (4/3)\ (\partial v_x/\partial x)(\partial v_y/\partial y) \big]$$
$$- (2/3)\rho k(\partial v_x/\partial x + \partial v_y/\partial y).$$

The turbulent energy Equation 16 becomes

$$\partial \rho k/\partial t = -\partial \rho v_x k/\partial x - \partial \rho v_y k/\partial y + \partial/\partial x(\mu_t \partial k/\partial x)$$
$$+ \partial/\partial y(\mu_t \partial k/\partial y) + \rho P_k - \rho \varepsilon$$

or

$$\partial/\partial t \int_V (\rho k)\, dV = \int_V (\rho P_k - \rho \varepsilon)\, dV - \int_S (\rho v_x k I + \rho v_y k J)\, n\, dS$$
$$+ \int_S (\mu_t \partial k/\partial x I + \mu_t \partial k/\partial y J)\, n\, dS.$$

The dissipation Equation 17 becomes

$$\partial \rho \varepsilon/\partial t = -\partial \rho v_x \varepsilon/\partial x - \partial \rho v_y \varepsilon/\partial y + \partial/\partial x[(\mu_t/1.3)\partial \varepsilon/\partial x]$$
$$+ \partial/\partial y[(\mu_t/1.3)\partial \varepsilon/\partial y] + 1.44(\varepsilon/k)\rho P_k - 1.92\rho(e^2/k)$$

or

$$\partial/\partial t \int_v (\rho\varepsilon)\, dV = \int_v [1.44(\varepsilon/k)\rho P_k - 1.92\rho(\varepsilon^2/k)]\, dV$$
$$- \int_s (\rho v_x \varepsilon I + \rho v_y \varepsilon J)\, n\, dS$$
$$+ \int_s [(\mu_t/1.3)\partial\varepsilon/\partial x I + (\mu_t/1.3)\partial\varepsilon/\partial y J]\, n\, dS.$$

The new quantities are put on the scalar grid. There is still the problem of initial conditions. A gun firing cycle starts with stagnant gas, so there should be no turbulence. However, the turbulent terms cannot be zero because then the turbulent viscosity is undefined. If the turbulent kinetic energy is set to zero, but the dissipation is nonzero, the kinetic energy term will become negative. So for initial conditions, ρk is set equal to 10^{-2} and $\rho\varepsilon$ is set equal to 10^{-5}. The density times the turbulent quantities is used since the equations are being solved in conservation form. This makes the turbulent kinetic energy, dissipation, and turbulent viscosity all small.

5.4 Boundary Conditions. For flow close enough to a wall, the flow must be laminar, and the turbulent kinetic energy will be zero. However, while kinetic energy cannot be generated at a wall, it can diffuse in and be dissipated at the wall. Hence, a common boundary condition for the dissipation is to assume a zero gradient. That is, the dissipation in a scalar control volume next to the boundary equals the dissipation in the next scalar control volume away from the wall. The turbulent kinetic energy is then still defined (equals zero). At the centerline, reflection boundary conditions are used, and at the exit from the chamber, extrapolation conditions are used.

In practice, the boundary layers are too small to be resolved with a reasonable grid, and more complicated procedures are required. So consider flow near a wall. Assume that the radial flow (perpendicular to the wall) is negligibly small. Assume that the axial gradients are negligibly small. These assumptions will be good if we go close enough to the wall, where close enough depends on the conditions of the flow. Under these assumptions, the only nonzero stress is

$$\tau_{xy} = -(\mu + \mu_t)\partial v_x/\partial y.$$

Very near the wall, the flow becomes laminar. So the stress at the wall is given by

$$\tau_w = -\mu \partial v_x / \partial y .$$

Assume that the stress is constant through the boundary layer. Define the wall friction velocity as

$$u^* = \sqrt{-\tau_w / \rho} .$$

In this derivation, to be consistent with the usual notation, y is the distance from the wall rather than the distance from the centerline. In the laminar sublayer,

$$\partial v_x / \partial y = -\tau_w / \mu$$

$$v_x = -(\tau_w / \mu) y$$

$$v_x = \rho u^{*2} y / \mu$$

$$v_x / u^* = u^* y / \nu .$$

Defining

$$v_x^+ = v_x / u^* \qquad y^+ = u^* y / \nu$$

then in the laminar sublayer,

$$v_x^+ = y^+ . \tag{20}$$

Next, consider flow in the turbulent layer, where the laminar viscosity is negligible compared to the turbulent viscosity. Then

$$\partial v_x / \partial y = -\tau_w / \mu_t .$$

Assume that the kinematic turbulent viscosity is given by

$$\nu_t = \kappa u^* y,$$

where κ is a constant to be determined. The basic idea is that the turbulent eddy size is constrained by the distance to the wall. The formula is in good agreement with the experiment. Then

$$\kappa u^* y \partial v_x / \partial y = -\tau_w / \rho = u^{*2}$$

$$\partial v_x / \partial y = u^* / \kappa y$$

or

$$\kappa y^* \partial v_x^* / \partial y^* = 1$$

$$v_x^* = (1/\kappa) \ln y^* + C.$$

From experimental data, the usual constants chosen are

$$v_x^* = 2.5 \ln y^* + 5 . \qquad (21)$$

There will be a regime in between the above regions where both laminar and turbulent viscosity is important. Various models have been proposed for this region. However, for simplicity, this will be ignored. Instead, the boundary layer profile will be assumed to change instantaneously from the laminar sublayer to the turbulent layer. This will occur when the two velocities match, that is,

$$y^* = 2.5 \ln y^* + 5$$

or

$$y^* = 10.993 .$$

To implement this formulation, consider the first vector grid point next to the top wall, at a distance y_b from the wall. This point is assumed to be in the turbulent layer, and Equation 21 is solved iteratively for u^*.

Given the wall friction velocity, the distance from the wall to the point where the transition from laminar to turbulent flow takes place, denoted by y_c, can be computed. Suppose that y_c is greater than y_b. This implies that the original assumption was wrong and that, in fact, the vector grid point is in the laminar sublayer. In this case, the previous boundary conditions are used.

Next, suppose that y_c is much less than y_b. So the laminar sublayer is negligibly small. Either Equation 20 or Equation 21 can be solved to obtain the velocity at y_c, denoted as v_c. This can be taken as the velocity at the wall, neglecting the very thin laminar sublayer.

Since a simulation normally starts with stagnant gas, there will be a transition from the laminar to the turbulent regime. To make the transition smooth, the wall velocity is actually defined as

$$v_w = v_c(y_b - y_c)/y_b \qquad 0 < y_c < y_b.$$

Boundary conditions on the turbulent quantities are also required. Various assumptions are possible. The simplest of the standard assumptions is that local equilibrium exists in the turbulent boundary layer, that is

$$\varepsilon = P_k = \nu_t(\partial v_x/\partial y)^2.$$

This means that the production of turbulent kinetic energy exactly matches the dissipation. The production term simplifies to the right-hand expression in a boundary layer. Using the expressions derived above for the turbulent part of the boundary layer, the above equation becomes

$$\varepsilon = \kappa u^* y(u^*/\kappa y)^2 = 2.5\,u^{*3}/y.$$

By the definition of the turbulent viscosity,

$$\nu_t = 0.09\,(k^2/\varepsilon)$$

or

$$k = u^{*2}/0.3\,.$$

Now consider the laminar sublayer. By definition, $k = 0$. The simplest standard assumption is that the dissipation is constant in the laminar sublayer, or

$$\varepsilon = 2.5\,u^{*3}/y_c\,.$$

Now what is required is the integral over the volume of the density times the turbulence quantities. Consider first the top boundary. Let R_t be the radius of the cylinder. Let R_b be the radius up to the bottom of the scalar control volume at the boundary, and let R_c be the radius up to the crossover point between the turbulent and laminar regions. Then the control volume can be split into a turbulent and laminar section

$$V_t = dx\pi\,(R_c^2 - R_b^2)$$

$$V_1 = dx\pi\,(R_t^2 - R_c^2)\,.$$

The turbulent kinetic energy is zero in the laminar part and constant in the turbulent part. So

$$\int_V \rho\,k\,dV = (\rho\,u^{*2}/0.3)\,V_t.$$

The dissipation is constant over the laminar sublayer, so

$$\int_V \rho\,\varepsilon\,dV_1 = (2.5\,\rho\,u^{*3}/y_c)\,V_1\,.$$

Over the turbulent layer

$$\int_V \rho \varepsilon \, dV_t = \int_V (2.5 \rho u^{*3}/y) \, dV_t$$

$$= \int_{y_c}^{y_b} (2.5 \rho u^{*3}/y) \, 2\pi (R_t - y) \, dx \, dy$$

$$= 5\pi \rho u^{*3} dx [R_t \ln y - y]_{y_c}^{y_b}$$

$$= 5\pi \rho u^{*3} dx [R_t (\ln y_b - \ln y_c) - (y_b - y_c)].$$

The two terms are added.

It is slightly simpler to work directly with the turbulent viscosity. The turbulent viscosity in the laminar sublayer is zero. The turbulent viscosity in the turbulent layer is given by the formula

$$\mu_t = \kappa \rho u^* y.$$

So

$$\int_V \mu_t dV = \int_V 0.4 \rho u^* y \, dV$$

$$= 0.4 \rho u^* \int_{y_c}^{y_b} y \, 2\pi (R_t - y) \, dx \, dy$$

$$= 0.8 \pi \, dx \, u^* [R_t y^2/2 - y^3/3]_{y_c}^{y_b}$$

$$= 0.8 \pi \rho \, dx \, u^* [R_t (y_b^2 - y_c^2)/2 - (y_b^3 - y_c^3)/3].$$

This is divided by the control volume to obtain the average turbulent viscosity, and the average dissipation is then found from the standard relation

$$\nu_t = 0.09 (k^2/\varepsilon).$$

The dissipation integrals then do not have to be evaluated.

Similar but slightly simpler expressions can be derived for the left-hand and right-hand boundaries.

5.5 Solution Procedure. The two new turbulence equations are solved along with the previous equations. The first step is still the Lagrangian step. The pressure and viscosity terms for the momentum equations are evaluated, and the velocities are updated. Then the turbulent energy production term is evaluated. The diffusion of the kinetic energy and the dissipation can then be computed, and the turbulence terms are all updated. The boundary conditions are also updated.

Then the Lagrangian step is taken. The combustion term is computed. It is assumed that the turbulence quantities do not change during this stage.

Finally, the convection terms are computed. Convection for the turbulence quantities is done exactly the same as for the other scalar quantities. The boundary conditions are applied, and all the quantities are updated.

5.6 Test Problems. The laminar flow test problems were now done assuming turbulent flow. Since there is now a boundary layer, none of the test problems reduces to a one-dimensional problem. So the two-dimensional problems are the ones of most interest. For the closed chamber problems, the additional turbulence had only a minor effect. Qualitatively, the results were the same.

For the open chamber, the results were more interesting. Consider the chamber with uniform injection. Figure 20 shows the new exit flow (comparable to Figure 12). The outflow rate is no longer grid independent because of the boundary layer at the exit corner. However, convergence is good with the 20×20 grid. Small oscillations do eventually start in this case.

Next, the problem was run with choked outflow. Figure 21 shows the Fourier transforms from 4 to 5 ms (comparable to Figure 14). The first radial mode now shows up even with the coarse grid. This is probably due to the boundary layers disturbing the flow. Because of the turbulent viscosity, the oscillations are not quite as large. However, this also means that the coarser grids are a better approximation. The turbulent viscosity will smooth out some of the very fine structure.

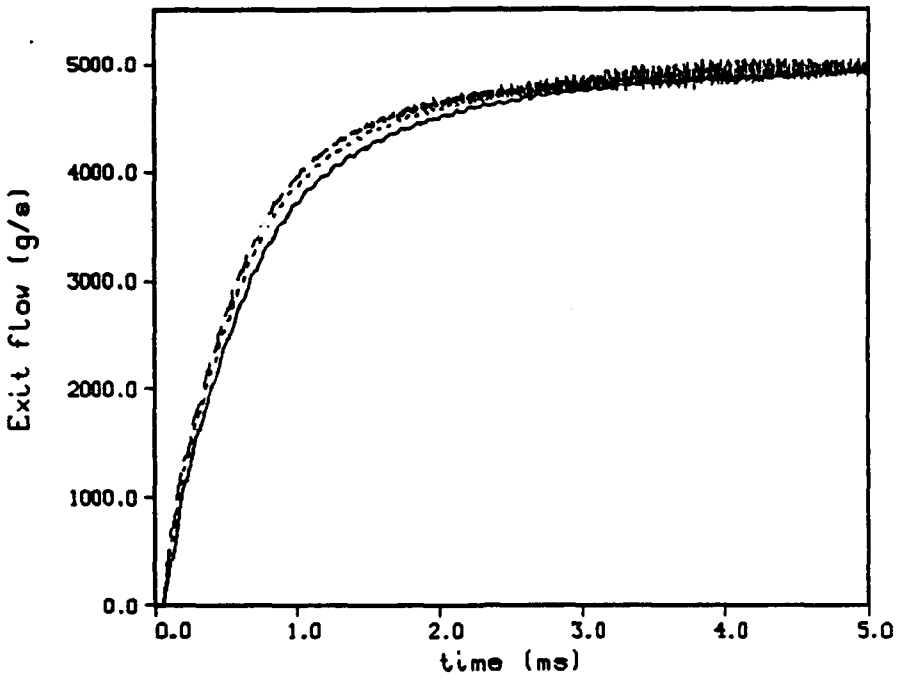

Figure 20. Chamber With Outflow. Uniform Injection at 5 g/ms. Turbulence. Exit Flow. 10 x 10 Grid (line). 20 x 20 Grid (dot). 40 x 40 Grid (dash).

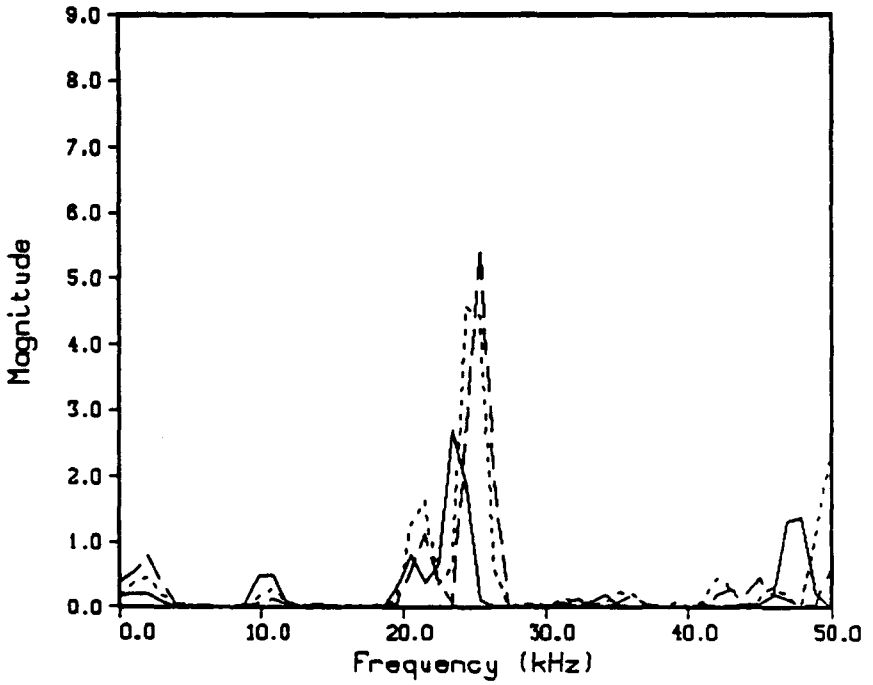

Figure 21. Chamber With Choked Outflow. Uniform Injection at 7.25 g/ms. Turbulence. Fourier Transform of Wall Pressure. 10 x 10 Grid (line). 20 x 20 Grid (dot). 40 x 40 Grid (dash).

The chamber was run with injection through a large hole (Figures 22 and 15). The results are similar to the laminar case except that the first radial does appear even with the coarse grid and the magnitudes are slightly smaller. The same behavior occurs if the outflow is choked (Figures 23 and 16).

Next, injection through the small hole was considered (Figures 24 and 17). The second radial mode is the primary frequency. For the 40 x 40 grid, the oscillations are very small. For choked flow (Figures 25 and 19), convergence is very bad. The agreement is actually better at earlier times. For the finer grids, the oscillations start to die out at the later times. As for laminar flow, rapid injection into a small volume can cause complicated behavior.

6. GUN TUBE

The model for the gun tube is set up almost exactly like the chamber model. The gun tube is a cylinder with a projectile for the right-hand wall. The projectile acceleration depends on the average pressure on its base. The velocity and displacement are found by using the usual equations of motion. The grid in the tube is attached to the base and stretches uniformly as the projectile moves.

Because the gun tube volume will increase dramatically over the firing cycle, additional grid points can be added as the projectile moves. When the grid spacing becomes larger than a specified value, a grid point is added at the end of the time step. A new scalar control volume will normally contain parts of two old scalar control volumes. The appropriate fractions of the old scalar quantities are combined to obtain the new scalar quantity, so the regridding is conservative. The new velocities are found by interpolation.

The only new boundary condition is at the interface with the chamber. The values on the gun tube grid just to the left of the tube are given the corresponding chamber values. Some adjustment may be necessary, since the grids in the chamber and tube normally have different spacing. Similarly, the values on the chamber grid just to the right of the chamber are given the corresponding tube values.

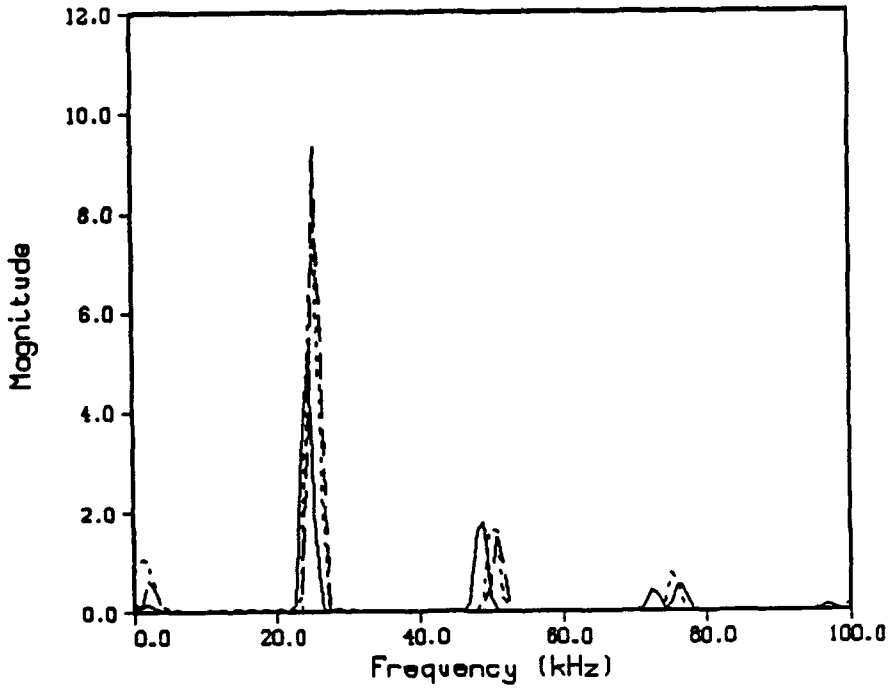

Figure 22. Chamber With Outflow. Injection Through a 1-cm-Radius Hole. Turbulence. Fourier Transform of Wall Pressure. 10 x 10 Grid (line). 20 x 20 Grid (dot). 40 x 40 Grid (dash).

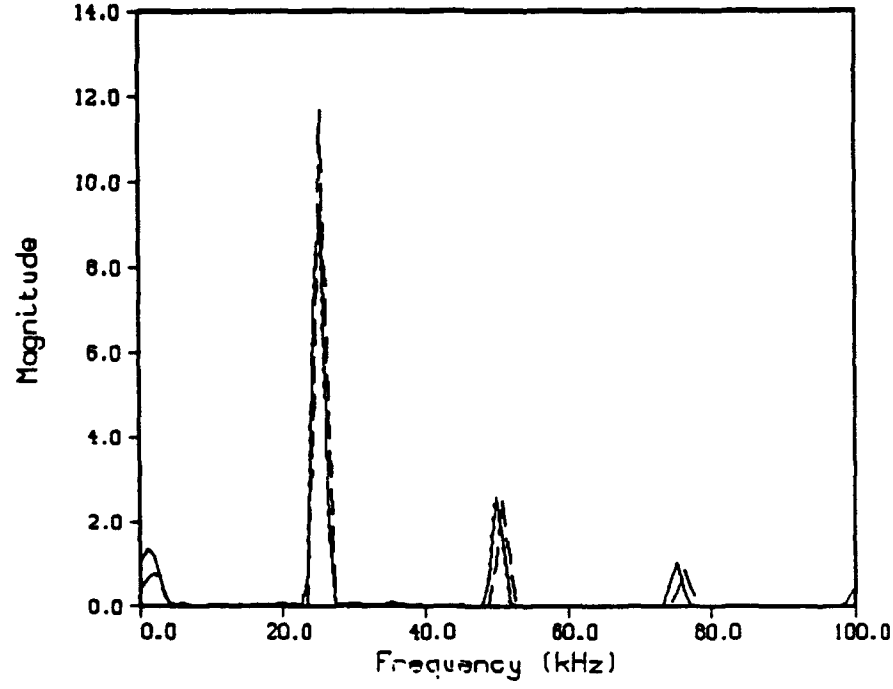

Figure 23. Chamber With Choked Outflow. Injection Through a 1-cm-Radius Hole. Turbulence. Fourier Transform of Wall Pressure. 10 x 10 Grid (line). 20 x 20 Grid (dot). 40 x 40 Grid (dash).

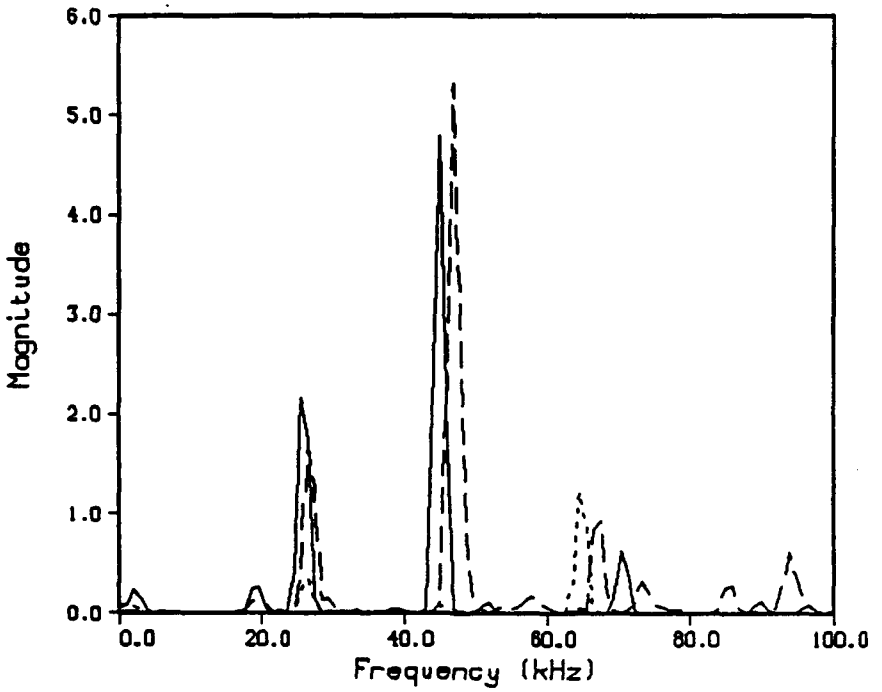

Figure 24. Chamber With Outflow. Injection Through a 0.25-cm-Radius Hole. Turbulence. Fourier Transform of Wall Pressure. 20 × 20 Grid (line). 40 × 40 Grid (dot). 60 × 60 Grid (dash).

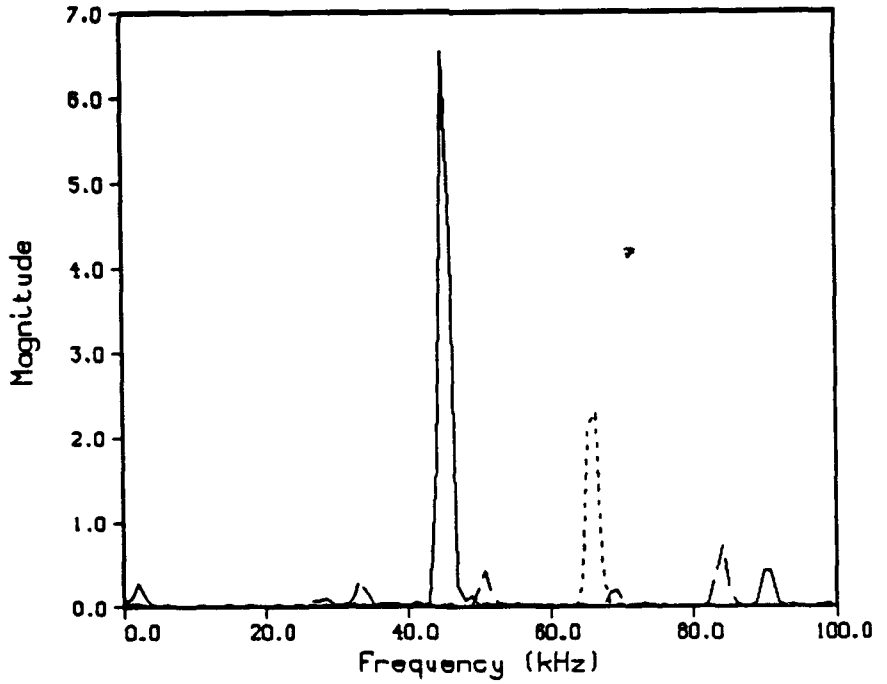

Figure 25. Chamber With Choked Outflow. Injection Through a 0.25-cm-Radius Hole. Turbulence. Fourier Transform of Wall Pressure. 20 × 20 Grid (line). 40 × 40 Grid (dot). 60 × 60 Grid (dash).

To take a time step, the pressure and viscosity terms are computed in the chamber and then in the tube. The boundary conditions are updated. Then the combustion terms are computed in the chamber and tube. Note that droplets can enter into the tube and combust, although the amount of liquid in the tube is generally small. Again the boundary conditions are updated. Finally, the convection terms in the chamber and then the tube are computed, the new pressures are computed, and the boundary conditions are updated. If necessary, a new grid point is added to the tube.

To test the procedure, some simple test problems were set up and comparisons made with the lumped parameter gun code. The chamber was filled with hot gas, which expands and pushes the projectile down tube. For the first case, the chamber and gun tube were given the same diameter. For a laminar simulation (slip boundary conditions) the problem did reduce to one dimension (no radial variation). The chamber pressure and projectile velocity were identical for the lumped parameter code and for the two-dimensional simulation.

Next, the chamber was made larger than the gun tube. The chamber radius was 3 cm, and the tube radius was 1.5 cm (30-mm gun). The gas was set to an initial pressure of 100 MPa. The integration was carried out to 6 ms, at which point the projectile was just over 100 cm down tube. The chamber grid was 20 × 20. At the end of the integration, the gun tube grid was 400 × 10. Again, the chamber pressure and projectile velocity were identical to the lumped parameter code. Figure 26 shows the gun tube velocity profiles at the end of the integration. The solid line is the lumped parameter code, using a modified Lagrange pressure distribution. The dotted line is flow along the centerline, and the dashed line is flow along the wall. The flow was laminar with a slip boundary condition. The flow is more rapid along the centerline. In fact, there is a small recirculation region at the wall where the flow enters the tube. However, the flow does become more one-dimensional farther down tube. Figure 27 shows the same curves for turbulent flow. The behavior is very different. The boundary layer makes the flow much slower along the tube wall. However, there is a singularity where the tube wall meets the projectile, since the gas at the projectile must move axially at the speed of the projectile. At this corner, the fluid velocity must match the projectile speed. That means that gas flows more rapidly down the centerline and then moves radially up near the projectile to fill the space left as the projectile moves. However, the pressure equilibrates even though

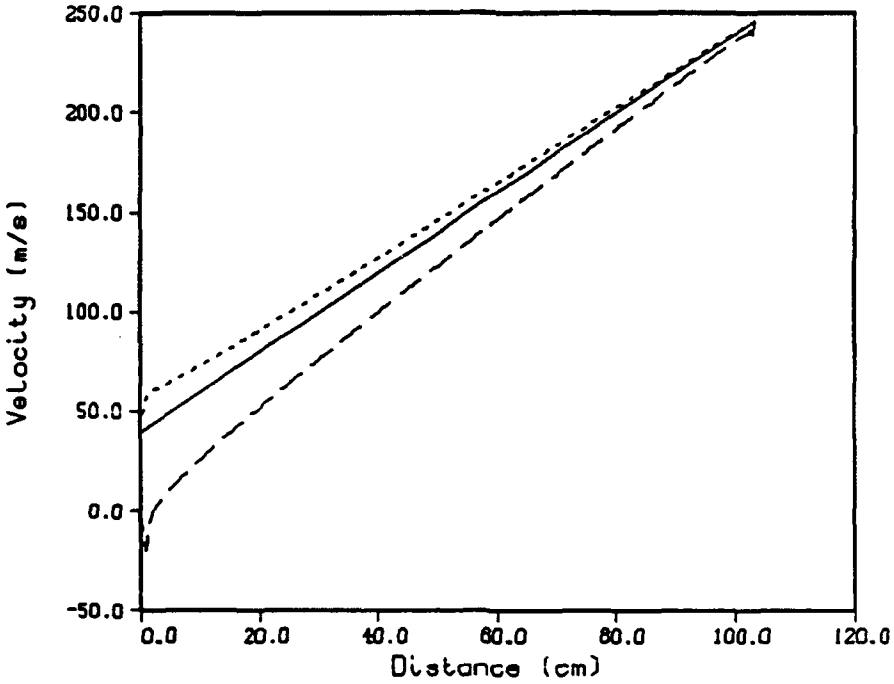

Figure 26. Gun Tube Test Problem - Laminar. Velocity. Lumped Parameter Model (line). Two-Dimensional Model. Centerline (dot). Wall (dash).

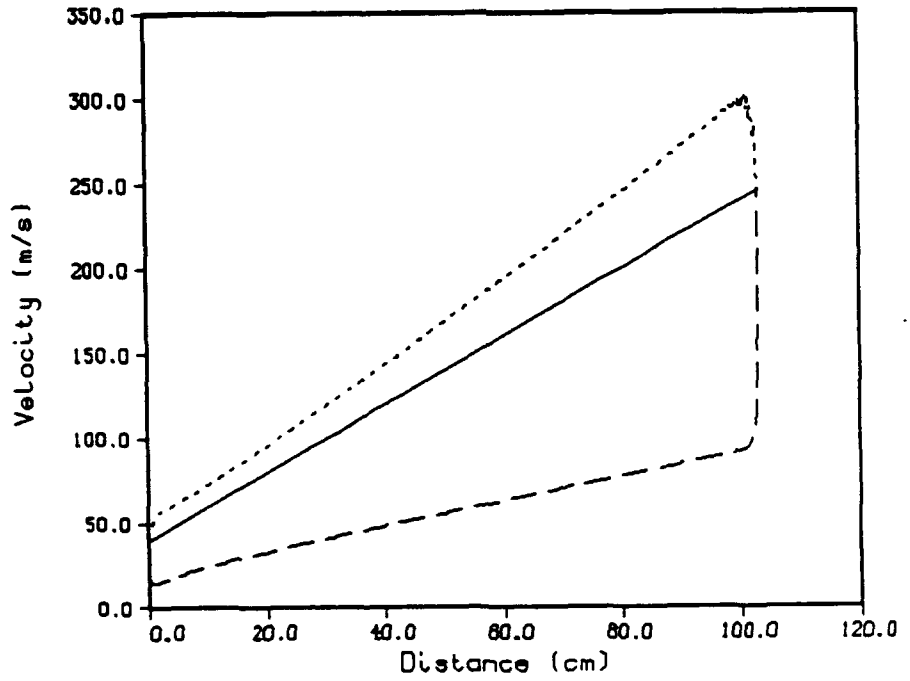

Figure 27. Gun Tube Test Problem - Turbulent. Velocity. Lumped Parameter Model (line). Two-Dimensional Model. Centerline (dot). Wall (dash).

the velocity does not (Figure 28). There is some oscillation near the projectile due to the flow disturbance.

7. SANDIA TEST FIXTURE

A simplified test fixture has been developed at Sandia National Laboratories to study pressure oscillations. Figure 29 shows a picture of the combustion chamber of the fixture. Liquid propellant is injected through the circular opening at the left by a differential piston. The liquid combusts and burns. Hot gas and possibly some liquid flow through the converging orifice at the right into atmospheric pressure. There is a burst disc at the end of the injection orifice to prevent liquid propellant from leaking into the chamber prematurely. There is also a burst disc at the end of the converging orifice so outflow does not start until the combustion is started. A primer initially prepressurizes the combustion chamber.

In the model, the chamber is represented by a cylinder. The radius is taken to be the radius of the body of the chamber (one inch). The length is chosen to obtain the proper chamber volume (volume between the two burst discs). A choked flow boundary condition is applied at the right boundary.

The chamber is initially given a uniform pressure of 22.0 MPa due to the igniter. The differential piston is driven by pressurized helium. The piston motion can be calculated from the recorded helium pressure. The point at which the burst disc breaks can be found from the sudden dip in the liquid pressure. This is taken as the zero time in the calculation. In the experiment, 65 cm^3 of propellant is injected, followed by water. From the liquid pressure, the density of the water and the propellant can be calculated. The amount of liquid in the reservoir is then calculated, which gives the amount of liquid injected. The derivative of the amount of liquid injected gives the rate of injection required by the code. The code does not presently allow two different kinds of liquid. So at the point where the propellant is computed to be exhausted, the size of the injected droplets is increased by several orders of magnitude. This makes the rate of combustion negligible.

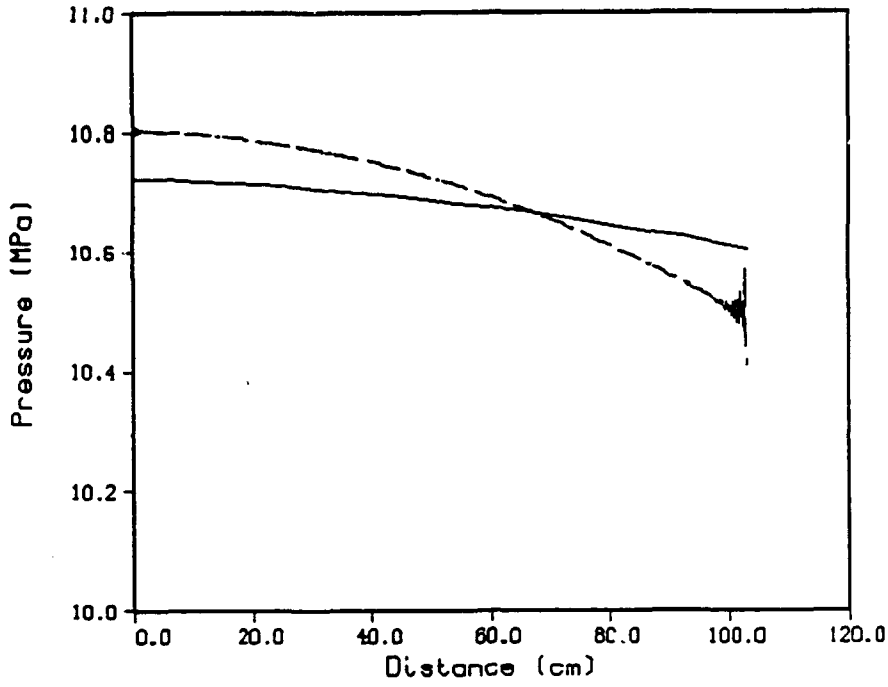

Figure 28. Gun Tube Test Problem - Turbulent. Pressure. Lumped Parameter Model (line). Two-Dimensional Model. Centerline (dot). Wall (dash).

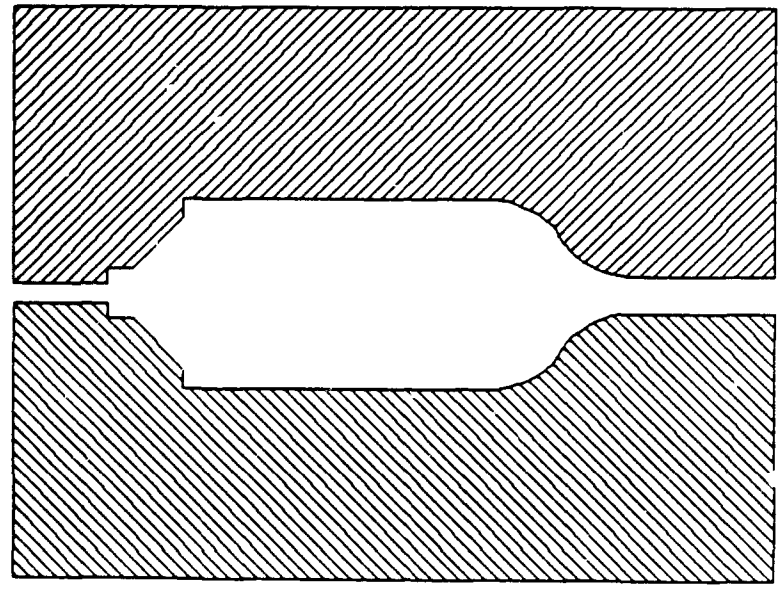

Figure 29. Sandia Test Fixture - Combustion Chamber.

The right-hand boundary is treated as a solid wall before the burst disc breaks. When the disc breaks (41.4 MPa), the boundary condition for the exit orifice becomes that of choked outflow.

Data were obtained for a typical test (CT-48). There are four pressure gauges in the same plane 3.5 inches from the injector. Figure 30 shows the recorded pressures. All the gauges show large pressure oscillations, but some gauges consistently show a higher oscillation level. Experimentation has shown that if the holes in which the pressure gauges are mounted are enlarged, the magnitude of the oscillations increases. So it is felt that the higher level of oscillations is closer to what occurs in the chamber and that the lower levels are caused by damping in the gauge hole (Griffiths 1991).

Figure 31 shows the filtered chamber pressures. There is some variation. All of the pressure gauges eventually record negative pressures. Pressure gauges do tend to record low when they become hot (thermal drift), so the actual chamber pressure may be slightly higher than the recorded pressures.

In Figure 32, the Fourier transforms are given for a 1-ms time window. There is a wide range in the magnitudes. However, all of the gauges show a fairly clean first radial mode. The higher frequencies are overtones due to the fact that the pressure oscillations are not pure sinusoidal waves. That is, the higher frequencies are multiples of the first radial mode, rather than the slightly different frequencies corresponding to the second and third radial modes.

A model was set up for this fixture. The liquid is assumed to enter as 200-μm drops. Figure 33 shows the filtered chamber pressure from the model measured at the wall for three different grids. The model pressure decreases substantially as the grid is refined. For a finer grid, the jet is less spread out, and more of the liquid exits the chamber unburnt. The sensitivity to the grid size is probably due in part to the simplification in the outflow condition. The actual fixture has a converging nozzle, which the model cannot presently duplicate. If the liquid is assumed to enter as smaller droplets, all the liquid burns in the chamber, and the filtered pressure is not very sensitive to the grid refinement.

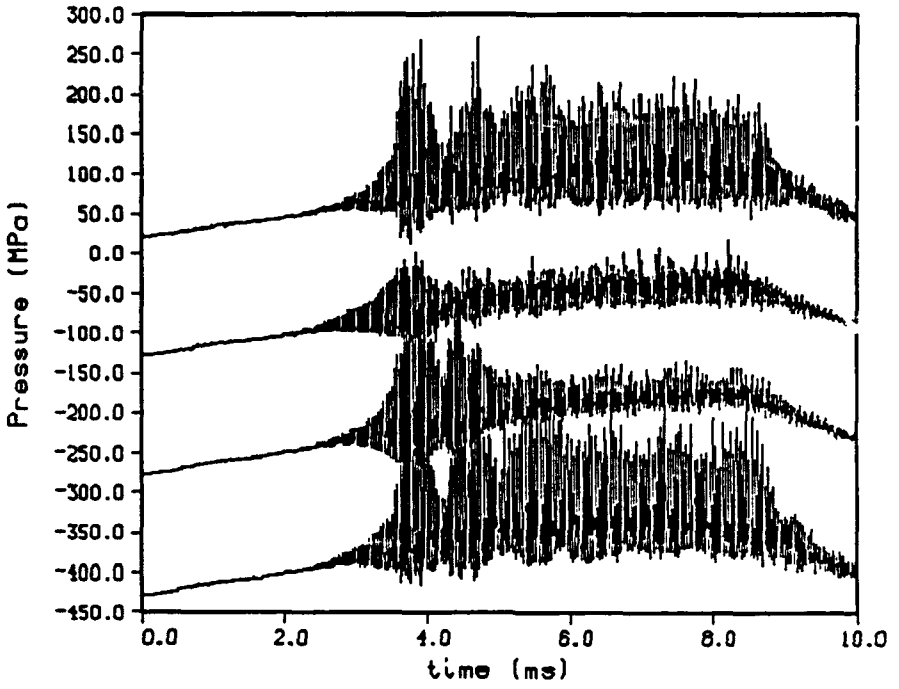

Figure 30. Sandia Test Fixture. Chamber Pressures. P32 (top). P33 (second from top). P34 (second from bottom). P35 (bottom).

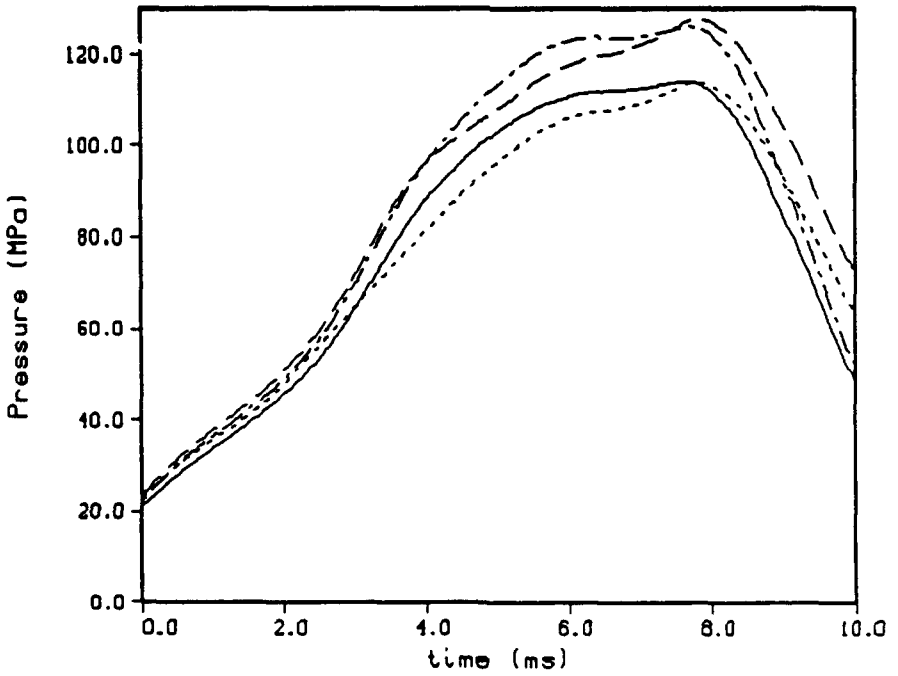

Figure 31. Sandia Test Fixture. Filtered Chamber Pressures. P32 (line). P33 (dot). P34 (dash). P35 (dot-dash).

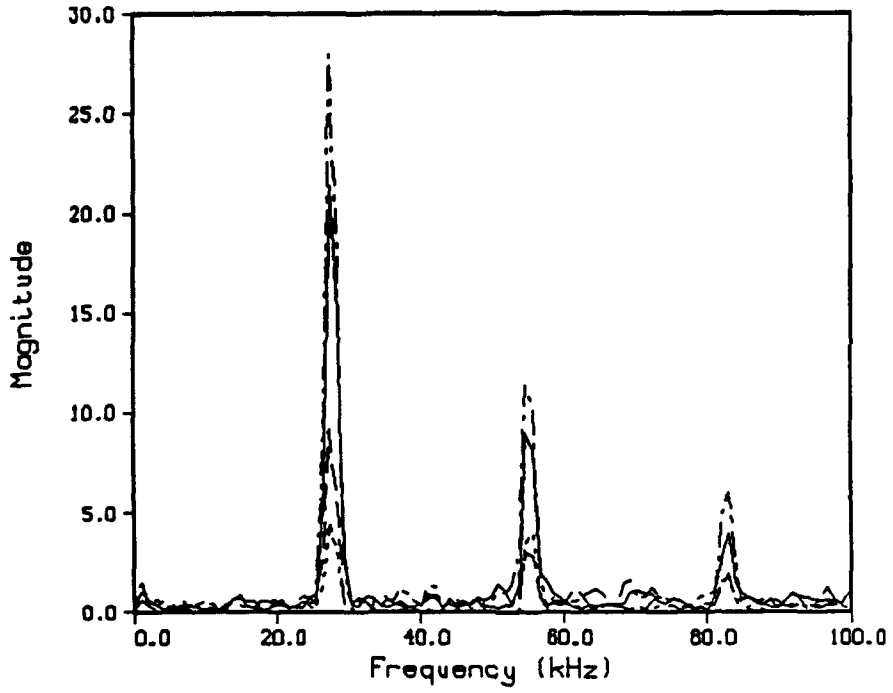

Figure 32. Sandia Test Fixture. Fourier Transforms - 5 to 6 ms. P32 (line). P33 (dot). P34 (dash). P35 (dot-dash).

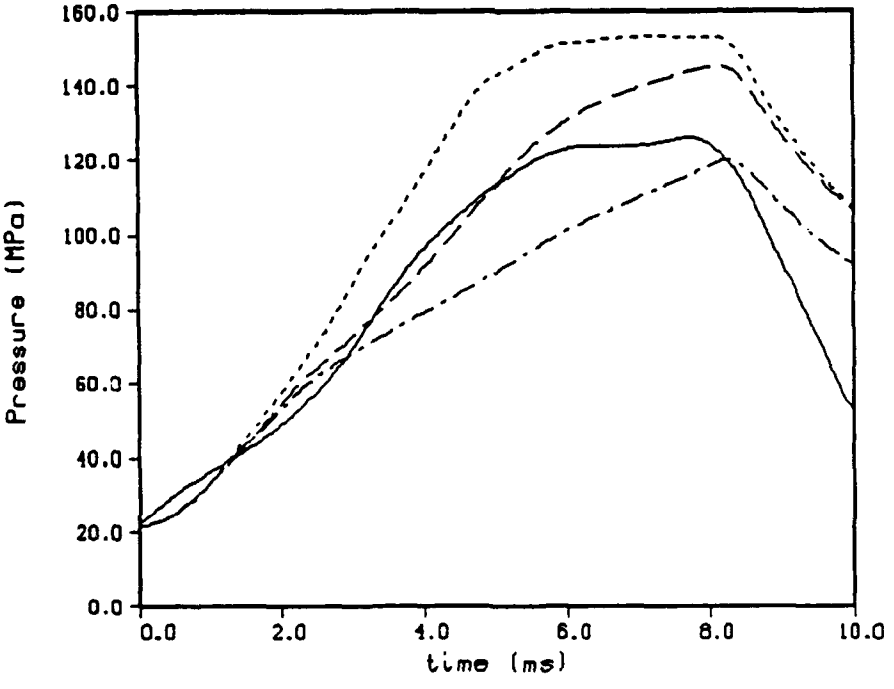

Figure 33. Sandia Test Fixture. Filtered Chamber Pressures. P35 (line). Model. 20 × 20 Grid (dot). 40 × 40 Grid (dash). 60 × 60 Grid (dot-dash).

In Figure 34, the unfiltered pressures are given for the three grids. For the coarse grid, the agreement with experiment is reasonable, although the oscillations are a little too regular. Unfortunately, for the finer grids, the oscillations decrease drastically. This effect has been seen in some of the test problems. When the liquid combusts in a very small volume, it can generate high frequency pressure oscillations which do not pump the first radial mode. Figure 35 shows the Fourier transforms for the three grids. With the finer grids, the higher radial modes are excited. A number of variations in the above model were implemented. In every case, when the grid became fine enough, the oscillations essentially disappeared.

This problem may be due in part to the simplified geometry in the model. However, it is probably related to the simplified combustion model. The breakup of the jet and the heat transfer to the liquid are ignored in the model. Also, the pressure-dependent burn rate used is not firmly established, especially at higher pressures. In the future, variations in the breakup and combustion models will be examined. Results here indicate that the liquid must combust as a unit in a reasonably sized volume to drive the first radial mode.

8. THE 155-mm GUN

Finally, a test case from the GE first generation 155-mm gun (Round 65) is modeled. This is a 7.2-liter charge. The gun fixture and this particular shot are discussed in detail in a previous report (Wren, Coffee, and Morrison 1990). The lumped parameter model was run using a jet breakup model developed at BRL (Coffee et al. 1991). The piston motion, injection rate, and injected droplet size from the lumped parameter model were used as input into the two-dimensional code.

Figure 36 compares the experimental and model chamber pressure. The model oscillations start a little later and die out much sooner. Analysis indicates that the oscillation die out because the injected droplets are very small. The liquid burns almost instantaneously, and there is no liquid accumulation to support the generation of oscillations.

The jet breakup model used was developed before the new burn rates were measured, and the slower McBratney rate was extrapolated to higher pressures. When the new burn rate is used at high pressures, much larger droplets can be injected with only a minor effect

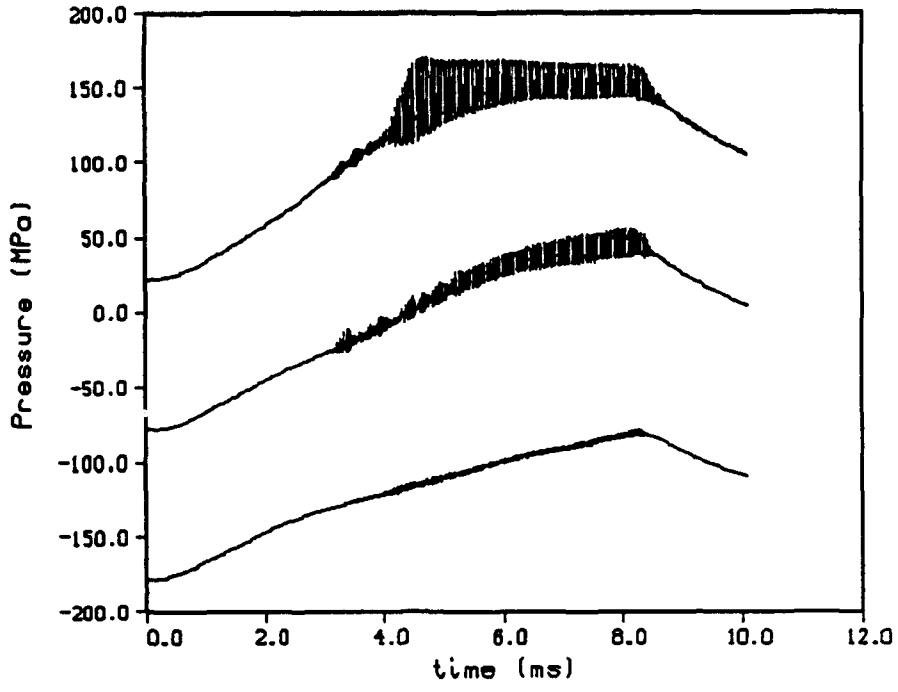

Figure 34. Sandia Test Fixture. Chamber Pressures. Model. 20 x 20 Grid (top). 40 x 40 Grid (middle). 60 x 60 Grid (bottom).

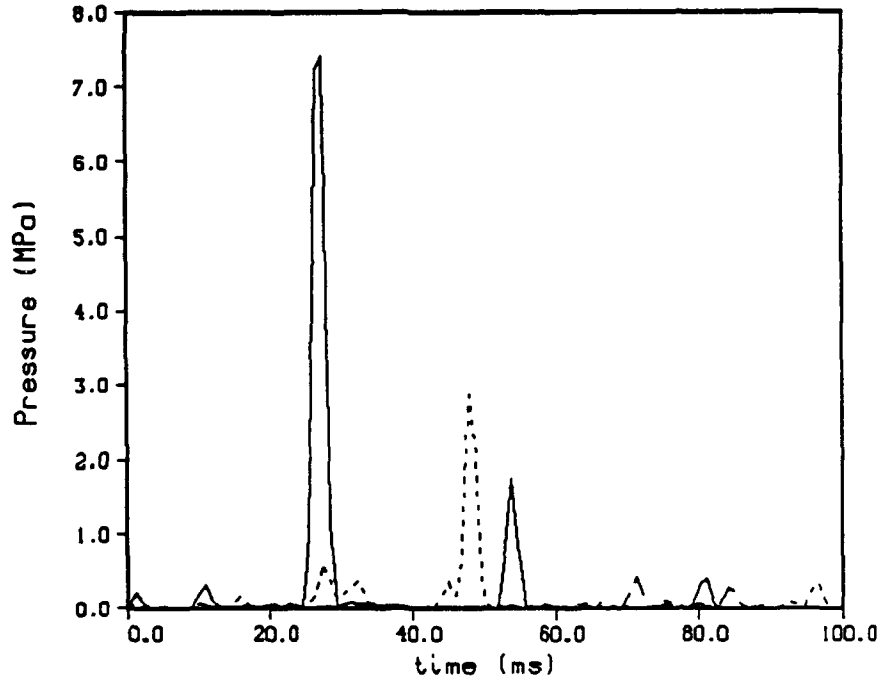

Figure 35. Sandia Text Fixture. Fourier Transforms - 5 to 6 ms. Model. 20 x 20 Grid (line). 40 x 40 Grid (dot). 60 x 60 Grid (dash).

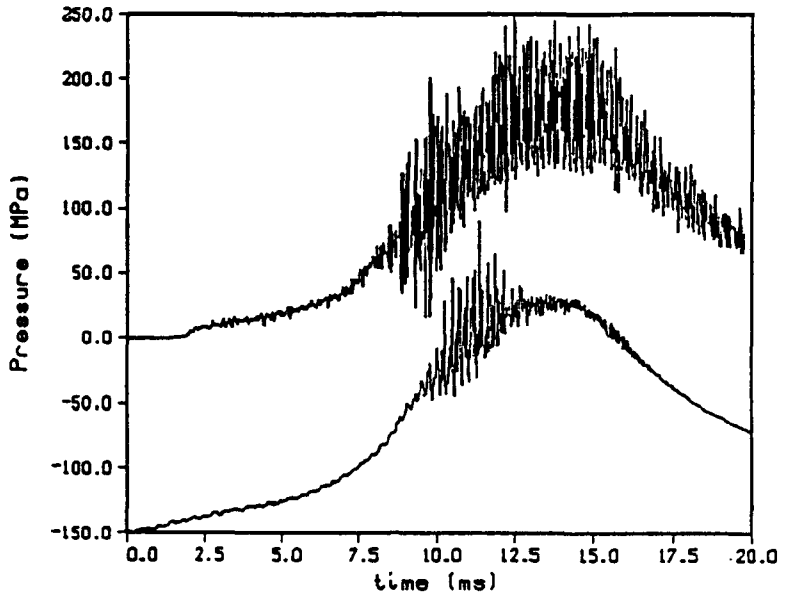

Figure 36. 155-mm Gun, Shot 65. Chamber Pressure. Experiment (top). Model - Small Drops (bottom).

on the lumped parameter model. So the lumped parameter model was modified so that the smallest droplets injected were 100 μm in diameter. The result is shown in Figure 37. In the model, the oscillations still start a little late and die out too rapidly. However, the magnitude of the oscillations is a very good match. Figure 38 compares the experiment and model at the barrel gauge, B3, which is uncovered after 79.5 cm of projectile travel. The model gauge is uncovered a little too soon, and the oscillations are noticeably smaller than in the experiment.

In Figure 39, the effect of refining the grid is considered. The top curve is from a 20 × 20 grid in the chamber and a 450 × 10 grid in the tube. The middle curve is from a 40 × 40 grid in the chamber and a 900 × 20 grid in the tube. The bottom curve is from a 60 × 60 grid in the chamber and a 1,000 × 30 grid in the tube. The oscillations are very similar regardless of the grid refinement. It is possible that, if the grid is made fine enough, the oscillations will diminish in magnitude. However, since the last case required about 8 hr of run time on the BRL Cray X-MP, further grid refinement is impractical.

The oscillations were filtered from the model chamber pressure, and the filtered pressure was compared with the lumped parameter model (Figure 40). The agreement is very good

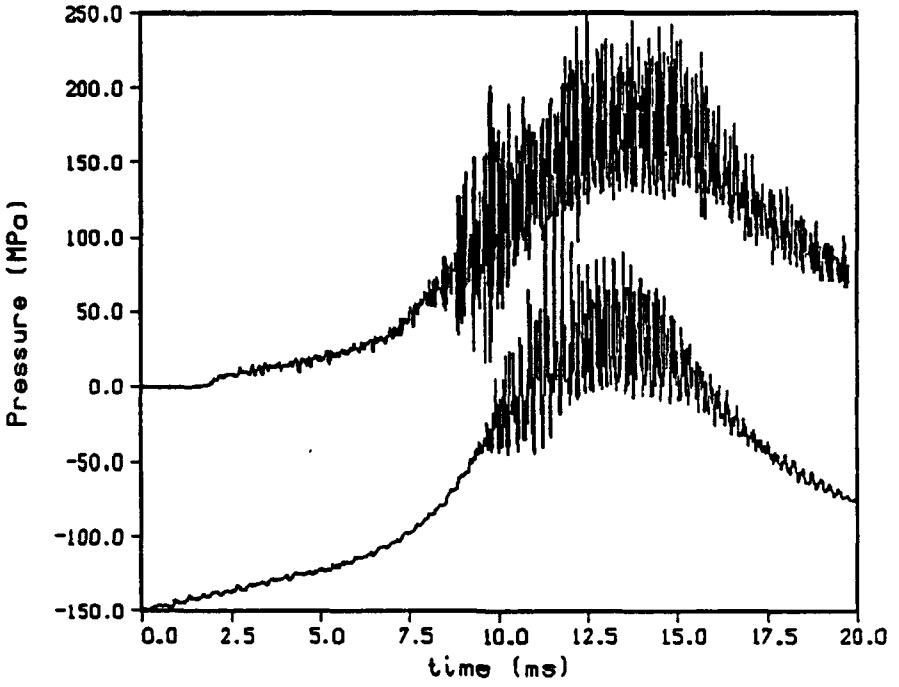

Figure 37. 155-mm Gun, Shot 65. Chamber Pressure. Experiment (top). Model - Large Drops (bottom).

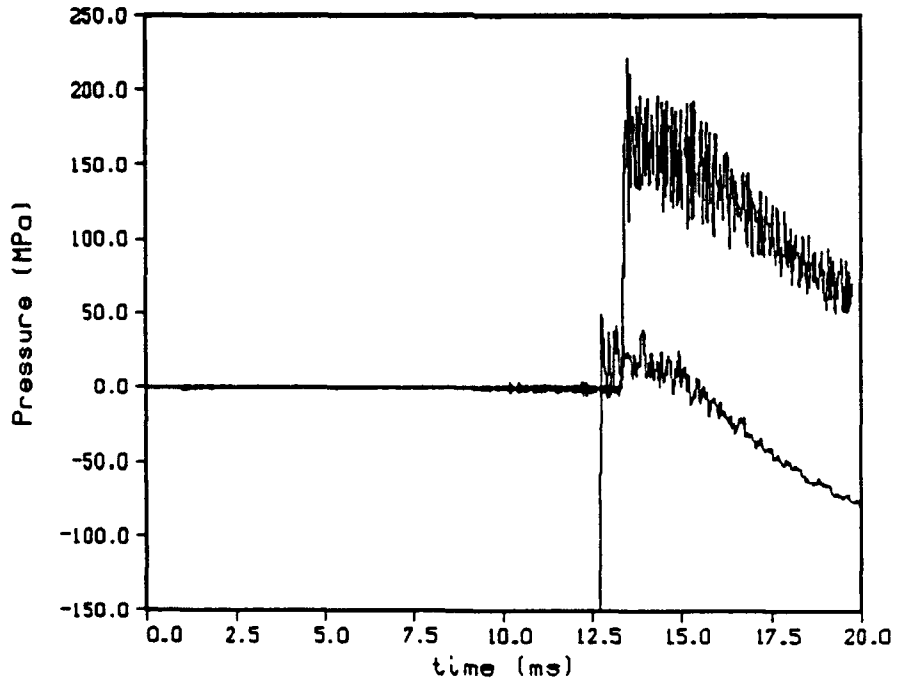

Figure 38. 155-mm Gun, Shot 65. Barrel Gauge. Experiment (top). Model (bottom).

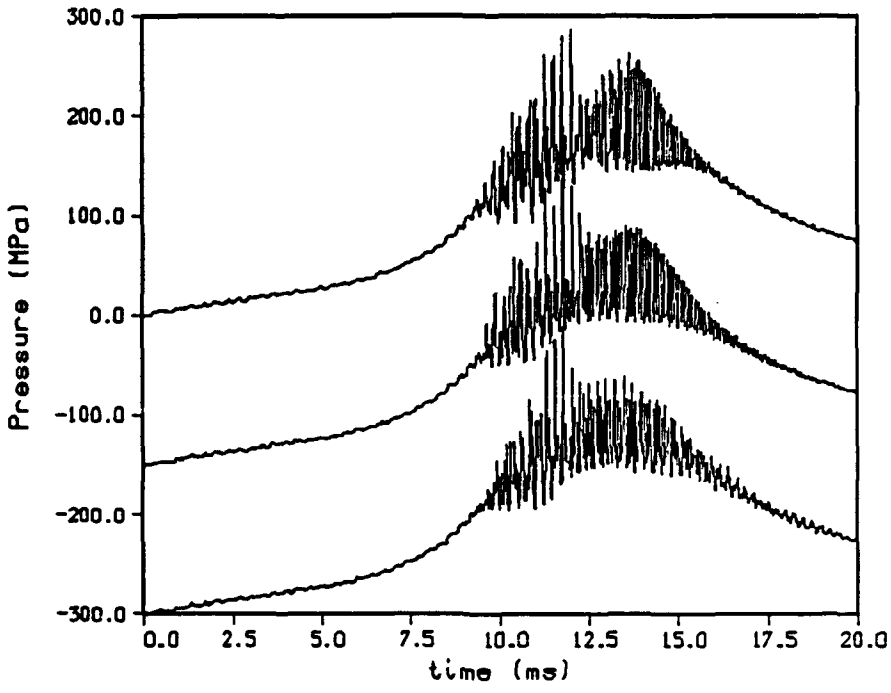

Figure 39. 155-mm Gun, Shot 65. Chamber Pressure. Model - Large Drops. 20 × 20 Grid (top). 40 × 40 Grid (middle). 60 × 60 Grid (bottom).

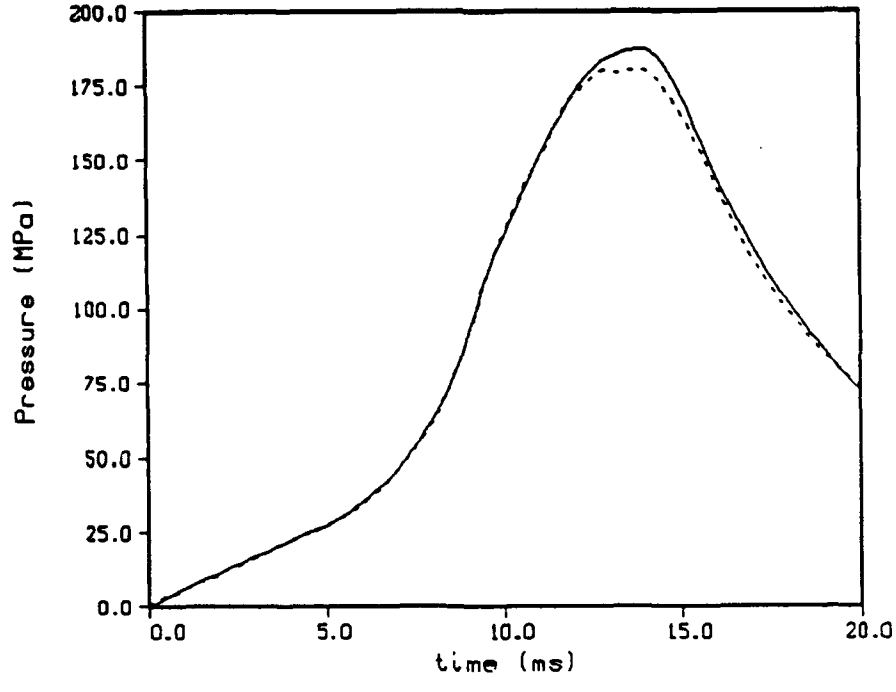

Figure 40. 155-mm Gun, Shot 65. Smoothed Chamber Pressure. Lumped Parameter Model (line). Two-Dimensional Model (dot).

until near the peak pressure, when the two-dimensional model shows a little lower pressure. Since the lumped parameter model has a simplified algorithm for flow into the gun tube and the pressure distribution in the tube, this minor disagreement is not surprising. However, the projectile velocity almost exactly matches the experimental data (Figure 41).

Figures 42–44 compare the Fourier transforms of the experiment and model for different time windows. The agreement is actually quite reasonable. Both the model and the experiment show a broad range of frequencies. The experiment shows higher peaks at the higher frequencies, especially at later times. At later times, the model tends to settle in at a third radial mode (at approximately 10.5 kHz), since the liquid is injected about a third of the way from the centerline to the wall. Figure 45 compares the transforms for the barrel gauge. The agreement is good for the lower frequencies, but the model totally fails to pick up the frequencies from 10 to 20 kHz.

One of the problems in analyzing the experimental data has been the unexpected wide range of frequencies. The expected acoustic modes of the chamber are fairly small (first radial is around 4 kHz). In liquid propellant rockets, if oscillations occur, they generally match the lower acoustic modes (Harrje 1972). However, the operating pressures for a gun are much higher than for a rocket. Large amounts of liquid have to be injected into a small volume. The energy density is much greater than for a rocket.

One proposed mechanism has been a random combustion model (Haberl and Pasko 1990). That is, a cloud of droplets in a small volume ignites and burns very rapidly, generating a pressure pulse. Since the liquid is injected rapidly, a dense cloud of liquid is expected to be formed, and combustion may not be immediate. Groups of droplets could be exposed to hot gas by vortex shedding, or combustion in a volume could be started by a previous pressure pulse. For a previous version of the two-dimensional code, in which the two-phase equations were not implemented, assuming random combustion was the only mechanism which was found to generate high frequencies (Coffee 1990).

However, with the present version of the model, higher frequencies are generated naturally, without the necessity of putting in a random element. The liquid is injected into a

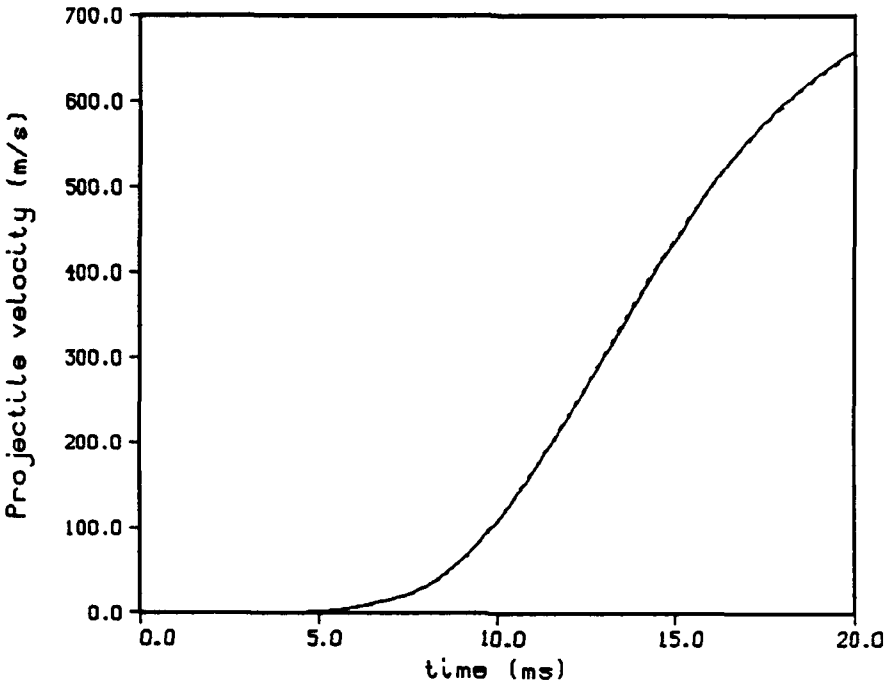

Figure 41. 155-mm Gun, Shot 65. Projectile Velocity. Lumped Parameter Model (line). Two-Dimensional Model (dot).

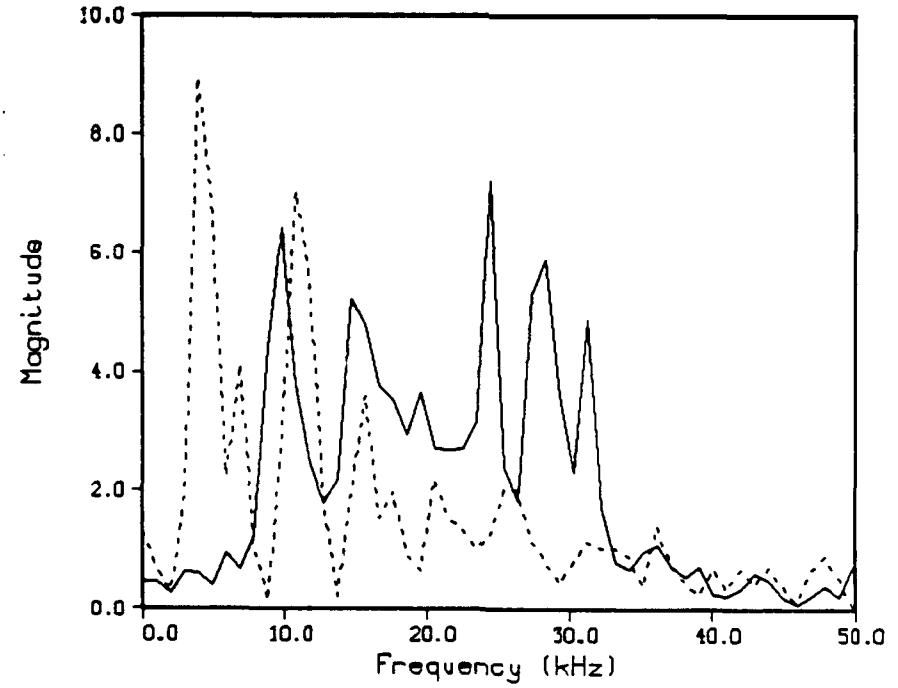

Figure 42. 155-mm Gun, Shot 65. Chamber Pressure. Fourier Transforms, 10 to 11 ms. Experiment (line). Model (dot).

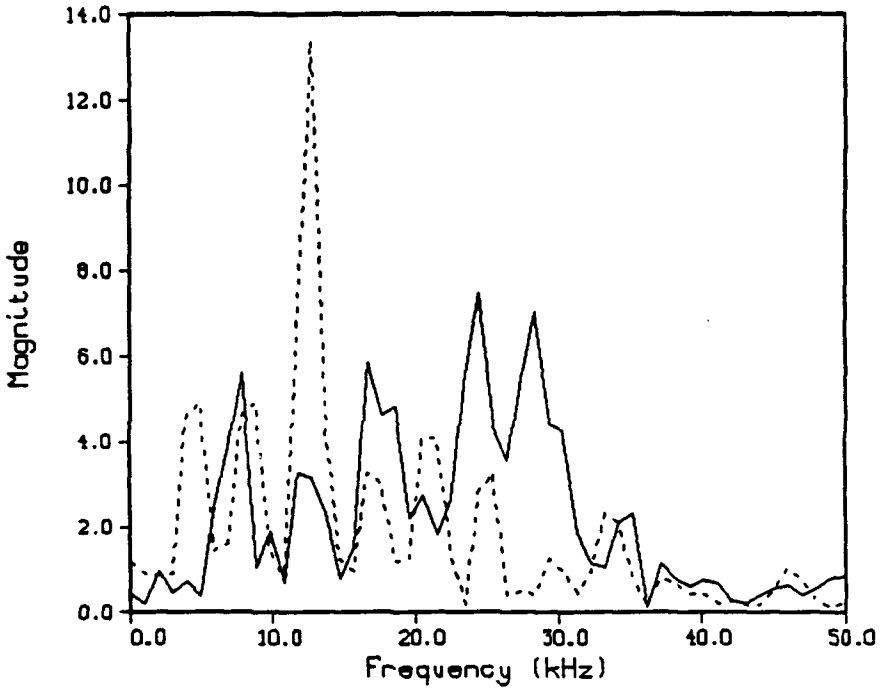

Figure 43. 155-mm Gun, Shot 65. Chamber Pressure. Fourier Transforms, 12 to 13 ms. Experiment (line). Model (dot).

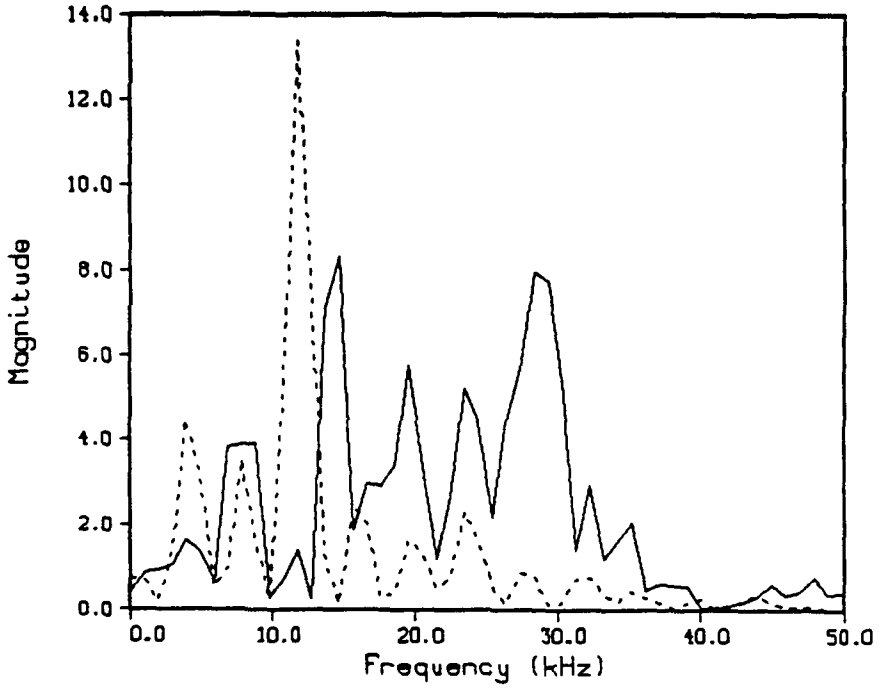

Figure 44. 155-mm Gun, Shot 65. Chamber Pressure. Fourier Transforms, 14 to 15 ms. Experiment (line). Model (dot).

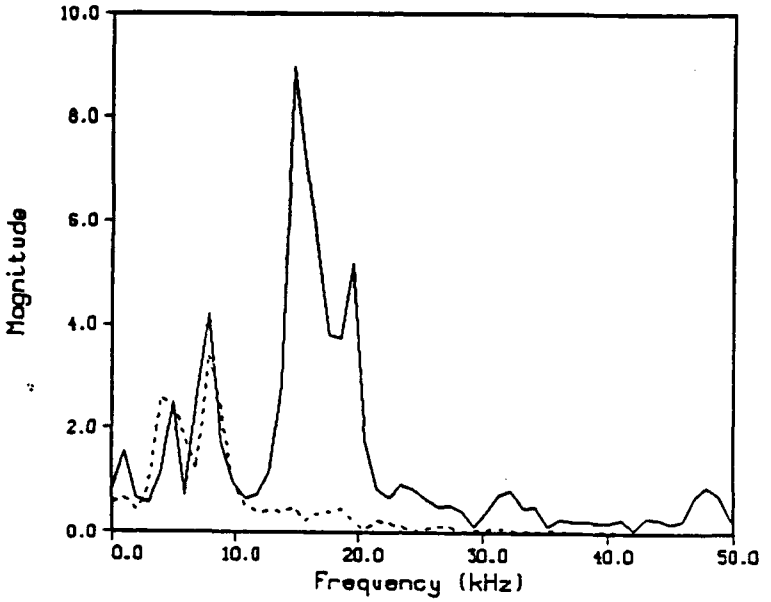

Figure 45. 155-mm Gun, Shot 65. Gun Tube Pressure. Fourier Transforms, 14 to 15 ms. Experiment (line). Model (dot).

small volume. This small volume combusts rapidly and generates a high pressure region. The pressure is kept high for a short period by inertial confinement, and a pressure pulse is generated. These pressure pulses bounce off the walls and interact with the accumulated liquid.

The complicated frequency structure is probably due in part to the complicated geometry of the chamber. The two-dimensional model was also run without the gun tube model. That is, outflow conditions were implemented at the entrance to the gun tube, with the pressure just outside the chamber obtained from the lumped parameter code. Figure 46 compares the early frequencies from the model with and without the gun tube. Without the gun tube, the frequencies correspond to a third radial mode with overtones. With the gun tube, the structure is more complicated. The tentative conclusion is that the more complicated geometry causes more structure in the frequencies. In the actual gun, the control piston extends into the chamber, and there is chambrage from the chamber to the tube.

The presence of oscillations in the gun tube has been taken as evidence that liquid must enter the tube and combust there. While the agreement between model and experiment at

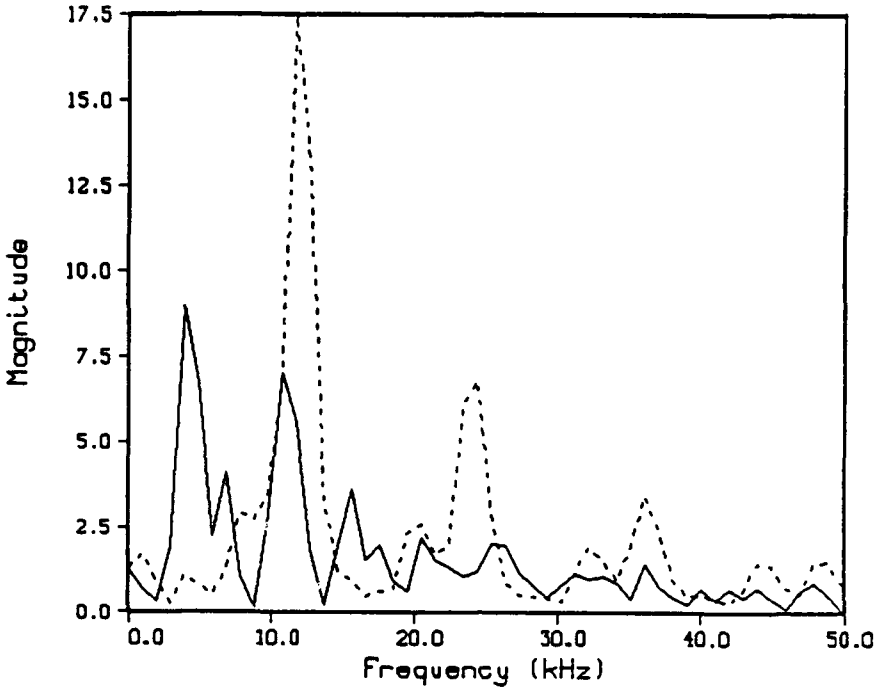

Figure 46. 155-mm Gun, Shot 65. Chamber Pressure. Fourier Transforms, 10 to 11 ms. Model With Tube (line). Model Without Tube (dot).

the barrel gauge is less impressive, the model does show that pressure oscillations can reach far down tube. Figure 47 shows the liquid volume fraction in the chamber (volume of liquid over total control volume). The graphs shows the chamber from centerline to wall. The liquid combusts well before the entrance to the gun tube. Figure 48 shows the corresponding pressure.

Of course, the model greatly simplifies the injection process. The model does not include the actual jet breakup, the heat transfer to the liquid, and the ignition process. Nevertheless, the model demonstrates that even if the combustion is confined to the chamber, pressure waves can still propagate down tube.

9. CONCLUSIONS

A two-dimensional model of the combustion chamber/gun tube of a regenerative liquid propellant gun has been developed. The code has been extensively checked over a series of test problems. The code has been compared with experimental data for two cases—a Sandia

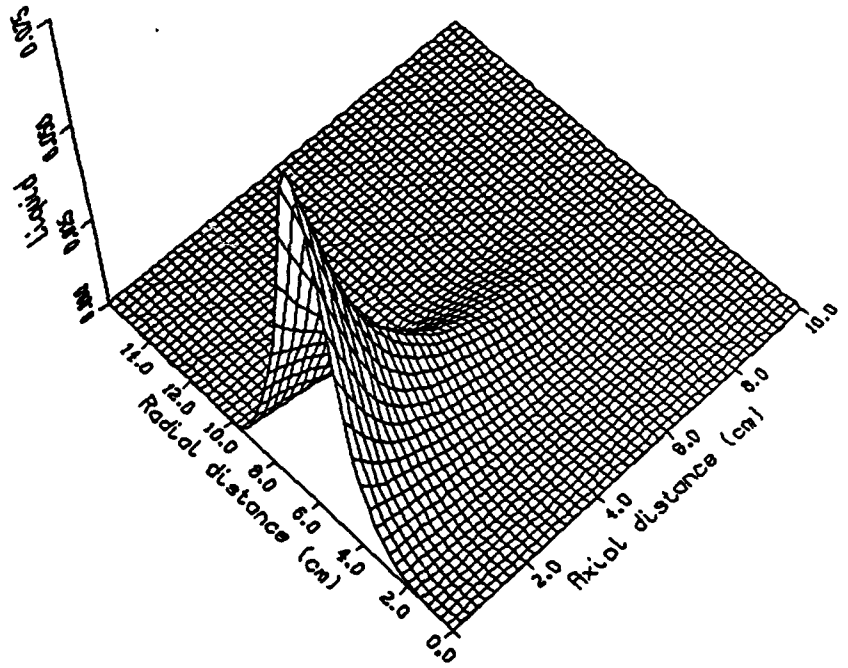

Figure 47. 155-mm Gun, Shot 65. Chamber Liquid Volume Fraction. Time = 10 ms.

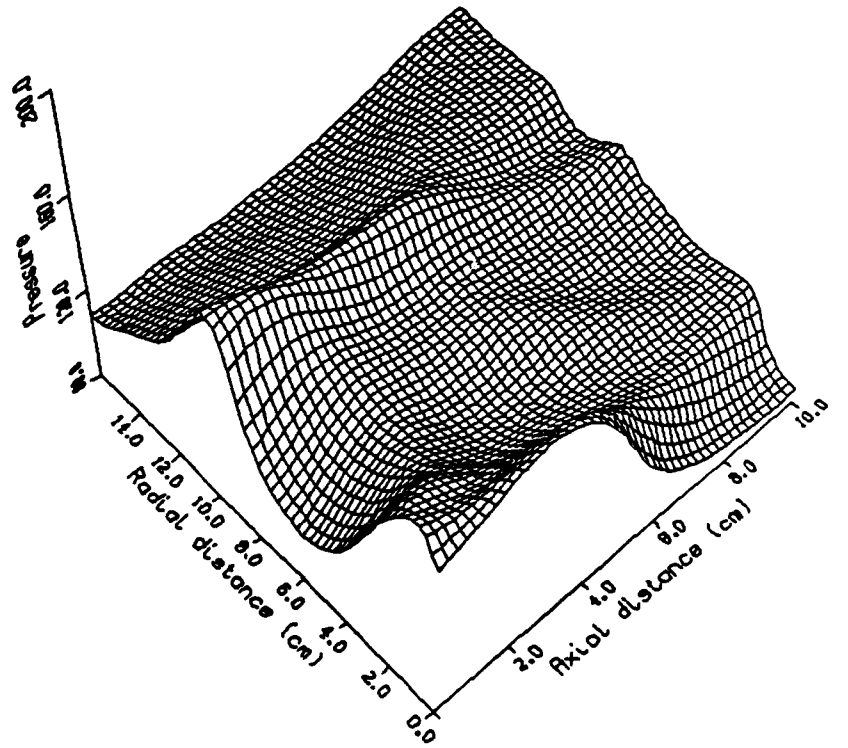

Figure 48. 155-mm Gun, Shot 65. Chamber Pressure. Time = 10 ms.

test chamber and an actual 155-mm gun firing. While agreement between model and experiment is not exact, the qualitative features of the experimental data are reproduced.

There are some known weaknesses in the model. The geometry is restricted to simple cylinders. The liquid and gas always move at the same velocity (infinite drag). The actual injection process is greatly simplified (that is, the jet breakup, heat transfer, and ignition process is not included). The first two weaknesses can be fixed. However, the details of the injection process are not well understood.

It has long been a puzzle why high frequency oscillations are generated in large caliber liquid propellant guns. The present model indicates this is related to the rapid injection of large amounts of liquid propellant into a small volume. Due to the large pressure sensitivity of the burning rate, large pressure pulses are generated just by inertial confinement. These pressure pulses bounce off the walls of the chamber and further interact with the unburned liquid. In liquid propellant rockets, the rate of injection of liquid per unit volume is much smaller.

There are several possibilities for reducing or eliminating the oscillations. If the burning rate exponent was smaller, oscillations would not be generated because the combustion would not be sensitive to pressure. However, no known reasonable propellant has a small enough exponent. Alternately, the burning rate could be increased, so that the liquid combusts almost as soon as it enters the chamber. If there is no liquid accumulation, there is no way to generate a local high pressure pulse. This can be done mechanically, by breaking up the jet into small droplets. There has been some success in the Sandia test fixture using a splitter plate just inside the chamber (Rychnovsky 1991). Alternately, the propellant could be chemically changed to burn more rapidly. A propellant with these properties is about to be tested (Klein, Coffee, and Leveritt, to be published). Also, there are devices to damp out oscillations used in liquid propellant rockets, such as liners, quarter-wave chambers, and Helmholtz resonators. The model presented here indicates that the mechanisms that create the oscillations are the same as in liquid rockets, and the same damping methods should work. Again, work with the Sandia test fixture shows some success, especially with liners. However, the moving pistons make it difficult to implement these designs in an actual gun.

10. REFERENCES

Amsden, A. A., J. D. Ramshaw, P. J. O'Rourke, and J. K. Dukowicz. "KIVA: A Computer Program for Two- and Three-Dimensional Fluid Flows with Chemical Reactions and Fuel Spray." LA-10245-MS, UC-32, and UC-34, Los Alamos National Laboratory, Los Alamos, NM, February 1985.

Band, W. Introduction to Mathematical Physics. Princeton, NJ: D. Van Nostrand Co. Inc., 1960.

Bird, R. B., W. E. Stewart, and E. N. Lightfoot. Transport Phenomena. New York, NY: John Wiley & Sons, Inc., 1960.

Boris, J. P., and D. L. Book. Methods in Computational Physics. Vol. 16, pp. 85–129, New York: Academic Press, 1976.

Bradshaw, P. Turbulence, Topics in Applied Physics. Vol. 12, New York: Springer-Verlag, 1978.

Cloutman, L. D., J. K. Dukowicz, J. D. Ramshaw, and A. A. Amsden. "Conchas-Spray: A Computer Code for Reactive Flows with Fuel Spray." LA-9294-MS, UC-32, Los Alamos National Laboratory, Los Alamos, NM, May 1982.

Coffee, T. P. "A Lumped Parameter Code for Regenerative Liquid Propellant Guns." BRL-TR-2703, U.S. Army Ballistic Research Laboratory, Aberdeen Proving Ground, MD, December 1985.

Coffee, T. P. "An Updated Lumped Parameter Code for Regenerative Liquid Propellant In-Line Guns." BRL-TR-2974, U.S. Army Ballistic Research Laboratory, Aberdeen Proving Ground, MD, December 1988.

Coffee, T. P. "A Two-Dimensional Model for the Combustion Chamber/Gun Tube of a Concept VIC Regenerative Liquid Propellant Gun." 27th JANNAF Combustion Meeting, Cheyenne, WY, November 1990.

Coffee, T. P., P. G. Baer, W. F. Morrison, and G. P. Wren. "Jet Breakup and Combustion Modeling for the Regenerative Liquid Propellant Gun." BRL-TR-3223, U.S. Army Ballistic Research Laboratory, Aberdeen Proving Ground, MD, April 1991.

Coffee, T. P., G. P. Wren, and W. F. Morrison. "A Comparison Between Experiment and Simulation for Concept VIC Regenerative Liquid Propellant Guns. I. 30 mm." BRL-TR-3072, U.S. Army Ballistic Research Laboratory, Aberdeen Proving Ground, MD, December 1989.

Coffee, T. P., G. P. Wren, and W. F. Morrison. "A Comparison Between Experiment and Simulation for Concept VIC Regenerative Liquid Propellant Guns. II. 105 mm." BRL-TR-3093, U.S. Army Ballistic Research Laboratory, Aberdeen Proving Ground, MD, April 1990.

Decker, M. M., N. Klein, E. Freedman, C. S. Leveritt, and J. Q. Wojciechowski. "Han-Based Liquid Gun Propellants: Physical Properties." BRL-TR-2864, U.S. Army Ballistic Research Laboratory, Aberdeen Proving Ground, MD, November 1987.

Fox, R. W., and A. T. McDonald. Introduction to Fluid Mechanics. Third Edition, New York, NY: John Wiley and Sons, 1985.

Gough, P. S. "A Model of the Interior Ballistics of Hybrid Liquid-Propellant Guns." Final Report, Contract DAAK11-82-C-0154, PGA-TR-83-4, Portsmouth, NH, September 1983.

Griffiths, S. Private communication. Sandia National Laboratories, Albuquerque, NM, 1991.

Haberl, J. B., and W. J. Pasko. "Combustion Noise in Liquid Propellant Guns." 27th JANNAF Combustion Meeting, Cheyenne, WY, November 1990.

Harrje, D. T. "Liquid Propellant Rocket Combustion Instability." NASA SP-194, Washington, DC, 1972.

Hinze, J.O. Turbulence. New York: McGraw-Hill, 1975.

Hirt, C. W., A. A. Amsden, and J. L. Cook. "An Arbitrary Lagrangian-Eulerian Computing Method for All Flow Speeds." Journal of Computational Physics, vol. 14, pp. 227–253, 1974.

Hughes, W. F., and J. A. Brighton. Schaum's Outline of Theory and Problems of Fluid Dynamics. New York: McGraw-Hill, 1967.

Jones W. P., and B. E. Launder. "The Prediction of Laminarization with a Two-Equation Model of Turbulence." International Journal of Heat Mass Transfer, vol. 15, pp. 301–314, 1972.

Jones, W. P., and J. H. Whitelaw. "Calculation Methods for Reacting Turbulent Flows: A Review." Combustion and Flame, vol. 48, pp. 1–26, 1982.

Klein, N., T. P. Coffee, and C. S. Leveritt. "Pressure Oscillations in a Liquid Propellant Gun - Possible Dependence on Propellant Burning Rate." U.S. Army Ballistic Research Laboratory, Aberdeen Proving Ground, MD, to be published.

Kollmann, W. Prediction Methods for Turbulent Flows. Von Karman Institute for Fluid Dynamics, New York: McGraw-Hill, 1980.

McBratney, W. F. "Windowed Chamber Investigation of the Burning Rate of Liquid Monopropellant for Guns." BRL-MR-03018, U.S. Army Ballistic Research Laboratory, Aberdeen Proving Ground, MD, April 1980.

McBratney, W. F. "Burning Rate Data, LPG 1845." BRL-MR-03128, U.S. Army Ballistic Research Laboratory, Aberdeen Proving Ground, MD, August 1981.

Monchick, L., and E. A. Mason. "Transport Properties of Polar Gases." Journal of Chemical Physics, vol. 33, pp. 1676–1697, 1981.

Morrison W. F., and T. P. Coffee. "A Modified Lagrange Pressure Gradient for the Regenerative Liquid Propellant Gun." BRL-TR-3073, U.S. Army Ballistic Research Laboratory, Aberdeen Proving Ground, MD, January 1990.

Ng, K. H., and D. B. Spalding. "Turbulence Model for Boundary Layers near Walls." Physics of Fluids, vol. 13, pp. 20–30, 1972.

Oberle, W., and G. Wren. "Closed Chamber Combustion Rates of Liquid Propellant 1846 Conditioned Ambient, Hot, and Cold." 27th JANNAF Combustion Meeting, Cheyenne, WY, November 1990.

Peyret, R., and T. D. Taylor. Computational Methods for Fluid Flow. New York: Springer-Verlag, 1983.

Reid, D. C., and T. K. Sherwood. The Properties of Gases and Liquids. Second Edition, New York: McGraw-Hill, 1966.

Rychnovsky, R. Private communication. Sandia National Laboratories, Albuquerque, NM, 1991.

Wren, G. P., T. P. Coffee, and W. F. Morrison. "A Comparison Between Experiment and Simulation for Concept VIC Regenerative Liquid Propellant Guns. III. 155 mm." BRL-TR-3151, U.S. Army Ballistic Research Laboratory, Aberdeen Proving Ground, MD, September 1990.

INTENTIONALLY LEFT BLANK.

LIST OF SYMBOLS

- b - covolume, cm^3/g
- c_L - liquid sound speed, cm/s
- c_G - gas sound speed, cm/s
- c - mixture sound speed, cm/s
- c_p - specific heat at constant pressure, J/g-K
- c_v - specific heat at constant volume, J/g-K
- e_L - chemical energy of the propellant, J/g
- g_o - conversion constant = 10^7 g/MPa-cm-s^2
- h_L - enthalpy of the liquid, J/g
- h_G - enthalpy of the gas, J/g
- k - turbulent kinetic energy, cm^2/s^2
- K_1 - bulk modulus at zero pressure, MPa
- K_2 - derivative of the bulk modulus
- m - combustion rate, g/s
- M_L - liquid mass, g
- M_G - gas mass, g
- M - mixture mass, g
- p - pressure, MPa
- P_k - rate of production of kinetic energy, cm^2/s^3
- R_s - specific gas constant, J/g-K
- S - surface area, cm^2
- t - time, s
- T - gas temperature, K
- u^* - wall friction velocity, cm/s
- v_x - axial velocity, cm/s
- v_y - radial velocity, cm/s
- VL - liquid volume, cm^3
- V_G - gas volume, cm^3
- V - volume, cm^3
- V' - Lagrangian volume, cm^3
- x - axial distance, cm

y - radial distance, cm

ε - turbulent dissipation, cm^2/s^3

ε_G - gas volume fraction

γ - ratio of specific heats

ρ_L - liquid density, g/cm^3

ρ_G - gas density, g/cm^3

ρ - mixture density, g/cm^3

τ_{xx} - normal stress, $g/cm\text{-}s^2$

τ_{yy} - normal stress, $g/cm\text{-}s^2$

τ_{xy} - shear stress, $g/cm\text{-}s^2$

μ - dynamic viscosity, poise = g/cm-s

μ_t - turbulent viscosity, poise = g/cm-s

ν - kinematic viscosity, cm^2/s

No. of Copies | Organization

2 Administrator
Defense Technical Info Center
ATTN: DTIC-DDA
Cameron Station
Alexandria, VA 22304-6145

1 Commander
U.S. Army Materiel Command
ATTN: AMCAM
5001 Eisenhower Ave.
Alexandria, VA 22333-0001

1 Commander
U.S. Army Laboratory Command
ATTN: AMSLC-DL
2800 Powder Mill Rd.
Adelphi, MD 20783-1145

2 Commander
U.S. Army Armament Research, Development, and Engineering Center
ATTN: SMCAR-IMI-I
Picatinny Arsenal, NJ 07806-5000

2 Commander
U.S. Army Armament Research, Development, and Engineering Center
ATTN: SMCAR-TDC
Picatinny Arsenal, NJ 07806-5000

1 Director
Benet Weapons Laboratory
U.S. Army Armament Research, Development, and Engineering Center
ATTN: SMCAR-CCB-TL
Watervliet, NY 12189-4050

(Unclass. only)1 Commander
U.S. Army Armament, Munitions, and Chemical Command
ATTN: AMSMC-IMF-L
Rock Island, IL 61299-5000

1 Director
U.S. Army Aviation Research and Technology Activity
ATTN: SAVRT-R (Library)
M/S 219-3
Ames Research Center
Moffett Field, CA 94035-1000

1 Commander
U.S. Army Missile Command
ATTN: AMSMI-RD-CS-R (DOC)
Redstone Arsenal, AL 35898-5010

No. of Copies | Organization

1 Commander
U.S. Army Tank-Automotive Command
ATTN: ASQNC-TAC-DIT (Technical Information Center)
Warren, MI 48397-5000

1 Director
U.S. Army TRADOC Analysis Command
ATTN: ATRC-WSR
White Sands Missile Range, NM 88002-5502

1 Commandant
U.S. Army Field Artillery School
ATTN: ATSF-CSI
Ft. Sill, OK 73503-5000

2 Commandant
U.S. Army Infantry School
ATTN: ATZB-SC, System Safety
Fort Benning, GA 31903-5000

(Class. only)1 Commandant
U.S. Army Infantry School
ATTN: ATSH-CD (Security Mgr.)
Fort Benning, GA 31905-5660

(Unclass. only)1 Commandant
U.S. Army Infantry School
ATTN: ATSH-CD-CSO-OR
Fort Benning, GA 31905-5660

1 WL/MNOI
Eglin AFB, FL 32542-5000

Aberdeen Proving Ground

2 Dir, USAMSAA
ATTN: AMXSY-D
AMXSY-MP, H. Cohen

1 Cdr, USATECOM
ATTN: AMSTE-TC

3 Cdr, CRDEC, AMCCOM
ATTN: SMCCR-RSP-A
SMCCR-MU
SMCCR-MSI

1 Dir, VLAMO
ATTN: AMSLC-VL-D

10 Dir, USABRL
ATTN: SLCBR-DD-T

No. of Copies Organization

1 OSD/SDIO/IST
ATTN: Dr. Len Caveny
Pentagon
Washington, DC 20301-7100

1 Commander
U.S. Army Belvoir R&D Center
ATTN: STRBE-WC,
Tech Library (Vault) B-315
Fort Belvoir, VA 22060-5606

1 Commander
U.S. Army Research Office
ATTN: Technical Library
P.O. Box 12211
Research Triangle Park, NC 27709-2211

1 Director
Benet Weapons Laboratory
U.S. Army Armament Research,
Development, and Engineering Center
ATTN: SMCAR-CCB-RA, Julius Frankel
Watervliet, NY 12189-4050

1 Commander
U.S. Army Armament Research,
Development, and Engineering Center
ATTN: SMCAR-CCS-C, T. Hung
Picatinny Arsenal, NJ 07806-5000

2 Commandant
U.S. Army Field Artillery School
ATTN: ATSF-CMW
ATSF-TSM-CN, J. Spicer
Ft. Sill, OK 73503

1 Commandant
U.S. Army Armor Center
ATTN: ATSB-CD-MLD
Ft. Knox, KY 40121

3 Commander
U.S. Armament Research,
Development, and Engineering Center
ATTN: SMCAR-FSS-DA, Bldg 94,
J. Feneck
R. Kopmann
J. Irizarry
Picatinny Arsenal, NJ 07806-5000

No. of Copies Organization

1 Commander
U.S. Army Armament Research,
Development, and Engineering Center
ATTN: SMCAR-TSS
Picatinny Arsenal, NJ 07806-5000

8 Commander
U.S. Army Armament Research,
Development, and Engineering Center
SMCAR-AEE-B, *D. Downs*
SMCAR-AEE-BR,
W. Seals
A. Beardell
B. Brodman
SMCAR-AEE-W, N. Slagg
SMCAR-AEE,
A. Bracuti
D. Chieu
J. Salo
Picatinny Arsenal, NJ 07806-5000

2 Commander
U.S. Army Armament Research,
Development, and Engineering Center
SMCAR-FSS-D, L. Frauen
SMCAR-FSA-S, H. Liberman
Picatinny Arsenal, NJ 07806-5000

1 Commander
Naval Surface Warfare Center
ATTN: D. A. Wilson, Code G31
Dahlgren, VA 22448-5000

1 Commander
Naval Surface Warfare Center
ATTN: Code G33, J. East
Dahlgren, VA 22448-5000

2 Commander
Naval Surface Warfare Center
ATTN: O. Dengel
K. Thorsted
Silver Spring, MD 20902-5000

1 Commander
Naval Weapons Center
China Lake, CA 93555-6001

No. of
Copies Organization

1 Superintendent
Naval Postgraduate School
Dept. of Mechanical Engineering
ATTN: Code 1424, Library
Monterey, CA 93943

1 Commandant
USAFAS
ATTN: ATSF-TSM-CN
Ft. Sill, OK 73503-5600

1 Director
Jet Propulsion Laboratory
ATTN: Technical Library
4800 Oak Grove Dr.
Pasadena, CA 91109

2 Director
National Aeronautics and
Space Administration
ATTN: MS-603, Technical Library
MS-86, Dr. Povinelli
21000 Brookpark Rd.
Lewis Research Center
Cleveland, OH 44135

1 Director
National Aeronautics and
Space Administration
Manned Spacecraft Center
Houston, TX 77058

1 Director
Sandia National Laboratories
ATTN: Dr. Ray Rychnovsky, Div. 8152
P.O. Box 969
Livermore, CA 94551-0969

1 Director
Sandia National Laboratories
ATTN: Dr. Stuart Griffiths, Div. 8244
P.O. Box 969
Livermore, CA 94551-0969

1 Director
Applied Physics Laboratory
The Johns Hopkins University
Johns Hopkins Rd.
Laurel, MD 20707

No. of
Copies Organization

1 University of Illinois at Chicago
Dept. of Chemical Engineering
ATTN: Professor Sohail Murad
Box 4348
Chicago, IL 60680

1 University of Maryland at College Park
Dept. of Chemistry
ATTN: Professor Franz Kasler
College Park, MD 20742

1 University of Missouri at Columbia
Dept. of Chemistry
ATTN: Professor R. Thompson
Columbia, MO 65211

1 University of Michigan
Dept. of Aerospace Engineering
ATTN: Prof. Gerard M. Faeth
Ann Arbor, MI 48109-3796

1 University of Missouri at Kansas City
Dept. of Physics
ATTN: Prof. R. D. Murphy
1110 East 48th St.
Kansas City, MO 64110-2499

1 Pennsylvania State University
Dept. of Mechanical Engineering
ATTN: Prof. K. Kuo
University Park, PA 16802

2 Princeton Combustion Research
Laboratories, Inc.
ATTN: N. A. Messina
M. Summerfield
4275 U.S. Highway One North
Monmouth Junction, NJ 08852

1 University of Arkansas
Dept. of Chemical Engineering
ATTN: J. Havens
227 Engineering Bldg.
Fayetteville, AR 72701

2 University of Delaware
Dept. of Chemistry
ATTN: Mr. James Cronin
Professor Thomas Brill
Newark, DE 19711

No. of Copies | Organization

1 University of Texas at Austin
Bureau of Engineering Research
ATTN: BRC EME133, Room 1.100
H. Fair
10100 Burnet Rd.
Austin, TX 78758

1 California State University, Sacramento
School of Engineering & Computer Science
ATTN: Dr. Frederick Reardon
6000 J St.
Sacramento, CA 95819-2694

1 University of Colorado at Boulder
Dept. of Mechanical Engineering
ATTN: Dr. John Daily
Engineering Center ME 1-13
Campus Box 427
Boulder, CO 80309-0427

1 Calspan Corporation
ATTN: Technical Library
P.O. Box 400
Buffalo, NY 14225

7 General Electric Ord Sys Div.
ATTN: J. Mandzy, OP43-220
R. E. Mayer
W. Pasko
R. Pate
I. Magoon
Lou Ann Walker
J. McCaleb
100 Plastics Avenue
Pittsfield, MA 01201-3698

1 IITRI
ATTN: Library
10 W. 35th St.
Chicago, IL 60616

1 Paul Gough Associates, Inc.
ATTN: Dr. Paul Gough
1048 South St.
Portsmouth, NH 03801-5423

No. of Copies | Organization

1 Science Applications International Corporation
ATTN: Norman Banks
4900 Waters Edge Dr.
Suite 255
Raleigh, NC 27606

1 Sundstrand Aviation Operations
ATTN: Mr. Owen Briles
P.O. Box 7202
Rockford, IL 61125

1 Veritay Technology, Inc.
ATTN: E. B. Fisher
4845 Millersport Highway
P.O. Box 305
East Amherst, NY 14051-0305

1 Conway Enterprises
ATTN: Professor Alistair MacPherson
499 Pine Top Trail
Bethlehem, PA 18017-1828

1 CFD Research Corporation
ATTN: Dr. Andrzej J. Przekwas
3325-D Triana Blvd.
Huntsville, AL 35805

1 Mr. Paul Baer
2514 Strathmore Ave.
Baltimore, MD 21214

No. of
Copies Organization

1 RARDE
GS2 Division
Bldg. R31
ATTN: Dr. Clive Woodley
Ft. Halstead
Sevenoaks, Kent TN14 7BT
England

1 Imperial College of Science and Medicine
ATTN: Prof. J. H. Whitelaw
Exhibition Rd., London SW7 2BX
England

INTENTIONALLY LEFT BLANK.

USER EVALUATION SHEET/CHANGE OF ADDRESS

This laboratory undertakes a continuing effort to improve the quality of the reports it publishes. Your comments/answers below will aid us in our efforts.

1. Does this report satisfy a need? (Comment on purpose, related project, or other area of interest for which the report will be used.) _____

2. How, specifically, is the report being used? (Information source, design data, procedure, source of ideas, etc.) _____

3. Has the information in this report led to any quantitative savings as far as man-hours or dollars saved, operating costs avoided, or efficiencies achieved, etc? If so, please elaborate. _____

4. General Comments. What do you think should be changed to improve future reports? (Indicate changes to organization, technical content, format, etc.) _____

BRL Report Number BRL-TR-3341 Division Symbol _____

Check here if desire to be removed from distribution list. ____

Check here for address change. ____

Current address: Organization _____
Address _____

DEPARTMENT OF THE ARMY
Director
U.S. Army Ballistic Research Laboratory
ATTN: SLCBR-DD-T
Aberdeen Proving Ground, MD 21005-5066

OFFICIAL BUSINESS

BUSINESS REPLY MAIL
FIRST CLASS PERMIT No 0001, APG, MD

Postage will be paid by addressee.

Director
U.S. Army Ballistic Research Laboratory
ATTN: SLCBR-DD-T
Aberdeen Proving Ground, MD 21005-5066

NO POSTAGE
NECESSARY
IF MAILED
IN THE
UNITED STATES